DSA Report
June 2025, Number 3

Three Decades of UV-monitoring in Norway: Trends and Drivers

DSA

Norwegian Radiation and Nuclear Safety Authority

Referanse

Johnsen, B, Hansen, EL, Nilsen, LT, Saxebøl, G, Hoftuft, J, Svendby, TM, Dahlback, A, Kjeldstad, B, Berge, E, Hannevik, M. Tre tiår med overvåking av naturlig UV-stråling i Norge: trender og drivere. DSA-rapport 2025:03. Østerås, Direktoratet for strålevern og atomsikkerhet, 2025. Språk: engelsk.

Emneord

Ultrafiolett stråling, UV, UV-dose, effektiv skytransmittans, UV overvåking, flerkanals filter radiometer, GUV, langtids-trender, globale klimasystemer.

Resymé

Overvåking av naturlig UV-stråling ved ni steder i landet, inkl. Svalbard, viser statistisk signifikante endringer over tid og fra nord til sør i landet i løpet av de snart 30 siste årene. Endringene er størst på vårparten. Års- og månedsdoser indikerer innvirkninger fra storskala klimasystemer gjennom påvirkning av skydannelse, ozon og bakkealbedo. Data er fritt tilgjengelige for informasjons og forskningsformål.

Reference

Johnsen, B, Hansen, EL, Nilsen, LT, Saxebøl, G, Hoftuft, J, Svendby, TM, Dahlback, A, Kjeldstad, B, Berge, E, Hannevik, M. Three Decades of UV-monitoring in Norway: Trends and Drivers. DSA Report 2025:03. Østerås: Norwegian Radiation and Nuclear Safety Authority, 2025.

Key words

Ultraviolet radiation, UV, UV-dose, effective cloud transmittance, UV-monitoring, multiband filter radiometer, GUV, long-term trends, global climate systems.

Abstract

UV-monitoring at nine sites in Norway, including Svalbard reveal significant trends and meridional patterns in surface UV doses over the past three decades. Increases are largest during spring. Correlation studies indicate associations with global circulation systems. Data is publicly available for information and research purposes.

Prosjektleder: Bjørn Johnsen.

Godkjent:

Kjetil Longva, avdelingsdirektør, avdeling atomberedskap

Publisert Juni 2025
Sider 85

DSA,
Postboks 329,
0213 Oslo
Norge.

Telefon 67 16 25 00
Faks 67 14 74 07
Email dsa@dsa.no
dsa.no

ISSN 2535-7339

Three Decades of UV-monitoring in Norway: Trends and Drivers

Bjørn Johnsen[1], Elisabeth L. Hansen[1], Lill T Nilsen[1], Gunnar Saxebøl[1], Jostein Hoftuft[1], Tove Svendby[2], Arne Dahlback[3], Berit Kjeldstad[4], Erik Berge[5], Merete Hannevik[1]

DSA[1], NTNU[2], NILU[3], UIO[4], METno[5]

Frontpage photo: Monitoring solar UV at the Finse (60°N) Research Station. Photo: B. Johnsen

1 Summary

The UV-monitoring network was established in the mid-1990s in response to a concerning increase in skin cancer cases in Norway and the other Nordic countries, along with anticipated rises in natural UV radiation due to long-term emissions of ozone-depleting substances. Norway was then and is still ranked among the countries with the highest rates of melanoma incidence and mortality worldwide. Estimates from Oslo Economics (2018) indicate that the societal costs of skin cancer in Norway amounts to 6.5 billion NOK per year, with 5.3 billion NOK attributed to the burden of disease, including both years of life lost and years lived with disability. More than 90% of new melanoma cases can be attributed to UV exposure from natural sunlight and cosmetic sunbeds (Keim et al. 2021), and many cases could likely have been prevented with careful sun behavior. Additionally, excessive UV exposure to unprotected eyes contributes to common vision impairments, such as cataracts (often requiring surgical intervention) and photokeratitis (snow blindness).

UV data on GitHub

Data products from the Norwegian UV monitoring network are publicly available on https://github.com/uvnrpa. These data products are weighted sums of spectral irradiances recorded by individual detector channels of network instruments (GUV-541/GUV-511, Biospherical Instruments). Different data products use different weights and reflect different endpoints. The E-UV data product and the associated dimensionless UV index (UVI) for instance tells us how effective measured sunlight is at causing erythema, or sunburn. On GitHub, there are eleven different data products that can be retrieved as minute-by-minute dose rates or as hourly mean dose rates. These dose rates, or effective irradiances, are reported in units of W/m^2. The data products are also available as integrated daily, monthly, and yearly doses, so-called effective radiant exposures, reported in J/m^2. The current report is chiefly concerned with the UVI and the E-UV and UV-A data products. These data products are highly relevant for evaluating health effects, e.g., from acute and chronic UV exposure to the skin, eyes, and immune system (Neale et al., 2023), as well as for evaluating influences on the radiation climate from variations in total ozone, clouds and aerosols, and surface albedo.

This report provides a retrospective look at the 30-years period since the network was founded, including the goals that were set at the time (see below), new knowledge gained from the data regarding seasonal and geographical variations in UV radiation, long-term changes in the radiation environment and underlaying drivers, and signs of possible links to global warming. The report discusses how the data and information about the UV radiation climate have benefited the public in sun protection and how data has served research activities related to health, environment, and the climate.

Goal 1. Provide high-quality long-term UV data for Norway, relevant to health, environmental assessments, and scientific research

- UV monitoring data from nine network locations in Norway including Svalbard have been used in studies examining the effects of UV radiation on human health and ecosystems.
- The measurements support the national skin cancer prevention strategy and related risk assessments.
- The data set enables research on interactions between UV radiation and global climate change.
- Nearly 30 years of surface UV radiation data are now publicly available on GitHub—a web-based platform for sharing data.

Goal 2. Map geographical and topographical distributions of UV radiation

- The data show that yearly E-UV doses vary significantly across locations, with Svalbard receiving about 50% of the E-UV dose compared to the southernmost station at Landvik.
- The summer-noon UVI is low/moderate at Svalbard, high in lowland areas, and very high in the mountains of southern Norway.
- Coastal Bergen receives about 85% of the yearly E-UV dose found in southeastern Norway, while the Finse mountain plateau experiences about 135% of the yearly E-UV dose in lowland southeastern Norway.

Goal 3. Detect long-term trends in surface UV radiation

- Southern Norway shows an upward trend in yearly E-UV dose by +2% to +4% per decade, while Svalbard shows a downward trend of -1.5% per decade.
- Over the 30 years period, surface E-UV and UV-A doses in April and June exhibit statistically significant increases by +20% to +30% in southern Norway and decreases of -15% in spring at Svalbard.
- August in southern Norway shows significant decreases in surface E-UV and UV-A doses by -10% to -15% and Svalbard a significant increase by +15% for the same period.
- Changes in E-UV and UV-A are driven by cloud conditions, including cloud cover, cloud thickness, cloud occurrence rate (relative sunshine duration) and possibly aerosols, as well as surface albedo.
- Variations and trends in cloud cover, including aerosol loads, is the dominating factor influencing yearly E-UV.
- Interannual variations in total ozone have a minor influence on trends in yearly E-UV, suggesting that the Montreal Protocol on Substances that Deplete the Ozone Layer has helped stabilize ozone layer depletion.
- Daily E-UV levels remain strongly affected by ozone fluctuations, especially in spring during the seasonal breakdown of the polar vortex.

Goal 4. Document yearly and seasonal variations in surface UV radiation

- Interannual variations in yearly E-UV and UV-A doses are typically within 6% but can exceed 10% due to persistent weather conditions.
- Monthly variations and trends in E-UV, effective cloud transmittance, and total ozone show greater interannual variations compared to yearly averages.
- Initial investigations of how surface UV varies with indirect drivers like major climate systems, including the El Niño-Southern Oscillation (ENSO), the Quasi-Biennial Oscillation (QBO), Atlantic and Arctic climate indicators (NAO and AO), the solar cycle, and Arctic sea-ice extent, reveal varying degrees of correlations.
- The strongest and most consistent correlations are found with NAO and AO, which are key indicators of cyclonic activity in the Atlantic and the Arctic.

Goal 5. Offer public information on sun protection based on UV measurements

- Nine stations across Norway continuously measure UVI in near real time.
- The UV data is actively shared with the public to support sun safety and preventive actions.
- Early warnings and sun protection advice are regularly issued, especially when the UVI rises unexpectedly.

Goal 6. Validate UV-forecasts with real-time UV data

- UVI forecasts are occasionally validated against ground-based measurements to improve accuracy of forecasts.
- Ground-based UV data are used to verify and support the quality of satellite-derived UV data products.

Over the 30-year period, surface UV measurements reveal significant and seasonally distinct trends—particularly in spring, with increasing UV levels in southern Norway and decreasing levels at Svalbard. These pronounced changes may have health implications, such as increased risk of sunburn, especially in spring, when people spend more time outdoors during holidays and public events. Trends in springtime UV radiation may also affect timing and functioning in terrestrial and aquatic ecosystems. This is particularly important in Arctic marine environments, where spring is a critical period for early life stages, influencing ice melt, access to food sources, and various developmental stages in the marine food chain.

While 30 years is a relatively short span in the context of solar and climate variability—which often operates on decadal to centennial timescales—the trends and interannual variations in surface UV radiation observed so far highlight the importance of continued UV monitoring. The trends in surface UV radiation, their underlaying drivers and projected changes in circulation systems affirm that the ongoing monitoring will be relevant for many more decades to come.

New instruments are being gradually introduced at the Norwegian network stations to operate alongside the existing ones, enabling an overlap period for continuity and comparison. These newer instruments also measure in the visible and near-infrared parts of the solar spectrum. The extended spectral range may support a more comprehensive understanding of the processes influencing surface solar radiation and the health and environmental implications from these variations.

Contents

2 Three decades of UV monitoring in Norway

2025 marks the 30th anniversary of the establishment of the UV-monitoring network in Norway, including Svalbard. The first stations started regular UV-monitoring in the summer of 1995. In the fall of 1996, seven additional stations were brought online, reporting measurements publicly on the internet. Since then, more than a hundred million data points of surface UV dose rates have been gathered from nine network stations between 58°N and 79°N, spanning almost a quarter of the latitudinal angle between the Equator and the North Pole. Today we can look back and retrieve UV dose rates measured on the ground with minute-by-minute resolution. Using ancillary data and modelling to fill in for sporadic downtime, we can form daily, monthly, and yearly integrated doses. Through these data, we can study features and trends of the Norwegian UV climate over the past three decades.

The establishment of the UV-monitoring network took place in the context of widespread uncertainty that existed in the early 1990s about future UV levels in response to ozone depletion. Ozone is one of the direct drivers of surface UV levels. At the same time, a rising skin cancer incidence was observed (Magnus 1973).

Some 20 years earlier, Molina and Rowland first predicted (Molina and Rowland, 1974) the destruction of stratospheric ozone catalyzed by chlorofluorocarbons (CFCs) drifting into the atmosphere from products like refrigerants, fire extinguishers and aerosol propellants. By the mid-1980s, decreasing stratospheric ozone concentrations were reported over Antarctica (Farman et al., 1985). The observed dramatic depletion, in this geographic region and on such scale, was unexpected by the scientific community at the time (Douglass et al., 2014).

Subsequent reports of a thinning ozone layer and the presence of 'ozone holes' over polar regions brought solar UV radiation into both widespread public as well as political awareness. In 1987, the Montreal Protocol on Substances that Deplete the Ozone Layer opened for signature. As this landmark treaty entered into force in 1989, concurrently the late 1980s and early 1990s saw the establishment of new or extended national as well as regional ozone monitoring and UV-monitoring programs (DeLuisi et al., 2013; Schmalwieser et al., 2017).

In 1992, the United Nations Framework Convention on Climate Change (UNFCCC) was established at the Earth Summit in Rio de Janeiro among growing global awareness and concern about climate change. The rising global temperatures associated to climate change have the potential to affect both direct and indirect drivers of surface UV levels, through changes to for example cloudiness and snow and ice cover.

Before introducing the implementation and specific objectives of a network in Norway, we therefore first provide a brief overview of how solar radiation reaches Earth's surface and introduce the direct and indirect drivers that determine the surface irradiance, or surface dose rate. Direct drivers of surface UV are total ozone (TOC), clouds and aerosols, and surface albedo. Indirect drivers are circulations in the middle atmosphere, stratosphere, troposphere, and in the oceans, that affect the climate and weather systems that in turn influence the direct drivers. Our main aim with the current report is to investigate how surface UV levels over Norway have developed over the last three decades in response to features and trends of these direct and indirect drivers.

Glossary

Radiant energy (in J) is a quantitative measure of the energy emitted, transferred, or received in the form of electromagnetic radiation.

Irradiance (in W/m^2) is a quantitative measure of the radiant energy incident per area of a surface per unit of time.

Radiant exposure (in J/m^2) is a quantitative measure of the radiant energy incident per area of a surface.

UV radiation is optical radiation with wavelengths roughly in the range from 100 nm to 400 nm, commonly subdivided into UV-C (100 nm to 280 nm), UV-B (280 nm to 315 nm) and UV-A (315 nm to 400 nm).

The *E-UV dose rate* (in W/m^2) and *E-UV dose* (in J/m^2) are quantitative measures formed by weighting respectively the spectral irradiance or the spectral radiant exposure with the action spectrum for erythema. E-UV is responsive for causing sunburn (erythema) in human skin. Approximately 80% of the E-UV dose rate or dose comes from wavelengths in the UV-B part of the solar spectrum. The E-UV dose rate and dose are sensitive to variations in total ozone.

UV index, or UVI, is a dimensionless quantitative measure formed by multiplying the E-UV dose rate expressed in units of W/m^2 with 40 m^2/W. It is used for communicating UV levels to the public. The UVI scale ranges from low (0-2), to moderate (3-5), high (6-7), very high (8-10), and extreme (11+).

The *UV-A dose rate* (in W/m^2) and *UV-A dose* (in J/m^2) are quantitative measures formed by integrating the spectral irradiance or the spectral radiant exposure across the UV-A region. 100% of the UV-A dose rate or dose comes from wavelengths in the UV-A part of the solar spectrum. The UV-A dose rate and dose are almost insensitive to variations in total ozone.

Effective cloud transmittance (eCLT) is the ratio of measured surface irradiance in a specified UV-A region divided by the corresponding radiative transfer modelled irradiance in this region for a cloudless and aerosol-free atmosphere and a non-reflecting surface.

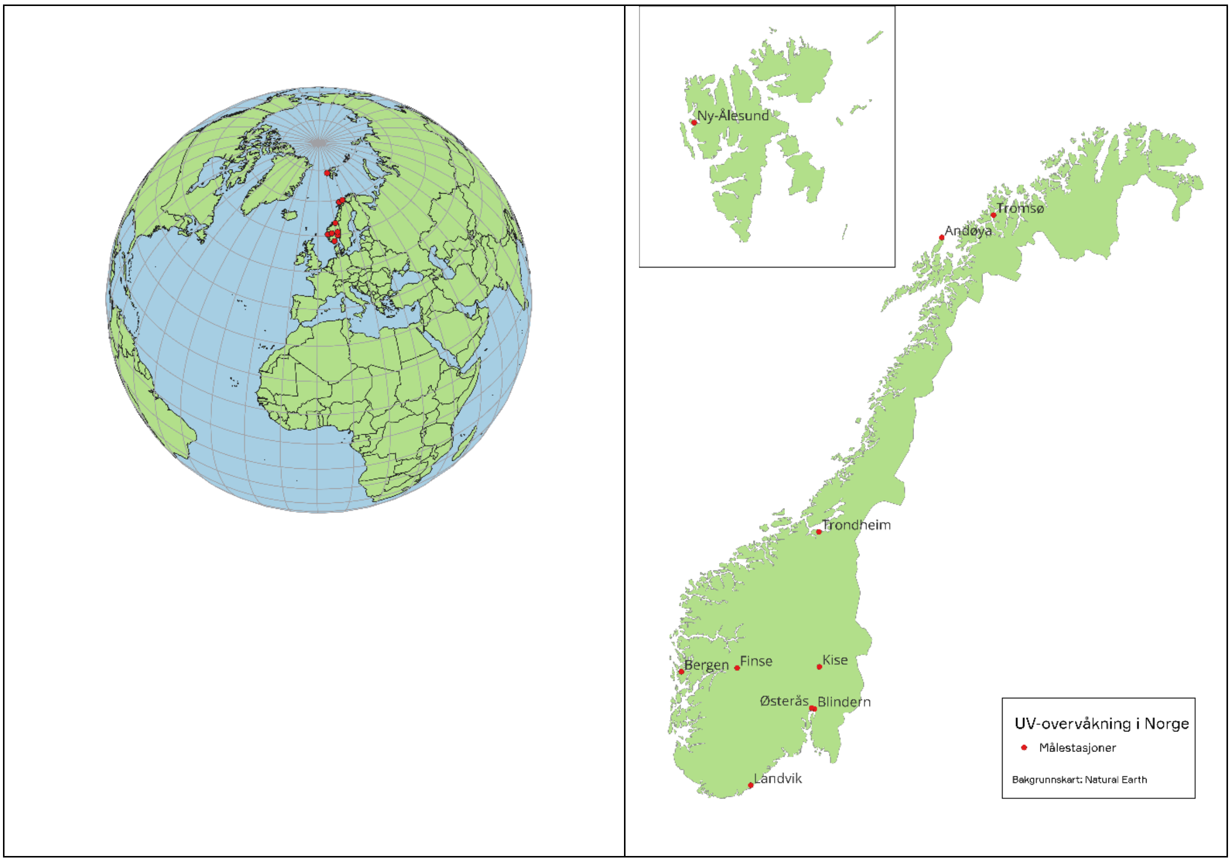

Figure 1 The geographical extent of the Norwegian UV-monitoring network. Image credit: Lene Valle.

2.1 Direct drivers: total ozone, clouds and aerosols, and surface albedo

The GUV instruments of the Norwegian UV-monitoring network measure surface irradiance, or surface dose rate (see definitions and abbreviations in Glossary info-boxes). Without an atmosphere, the irradiance over Earth's surface would be determined by the distance to the sun and the solar elevation angle over the horizon, resulting in the well-known day-night and summer-winter cycles. Some of this incident radiant energy would be reflected from the ground depending on the ground reflectivity, or albedo. The albedo of Earth's surface is typically in the range of 0.02 to 0.05 in the UV-B and UV-A for natural vegetation and around 0.18 for dry sand (Feister & Grewe, 1995) but may exceed 0.90 for fresh and dry snow (Turner et al., 2018). Albedo is one of the direct drivers for surface UV irradiance.

Because Earth does have an atmosphere, radiant energy from the sun interacts with matter in the atmosphere to undergo absorption as well as Rayleigh scattering on gas molecules and Mie scattering on aerosols and on water droplets in clouds. Surface UV is therefore made up of a direct beam component and a scattered diffuse sky component. On a clear summer day in Norway, the direct beam and diffuse sky components contribute about equally to both the UV-B and UV-A irradiance at noon. The direct contribution gradually diminishes as the Sun approaches the horizon. On a completely overcast summer day with thick clouds, the direct component also approaches zero. Clouds and aerosols are thus direct drivers for surface UV irradiance.

Under conditions with broken clouds, the surface irradiance can surpass that of a cloud-free sky. This phenomenon is referred to as cloud enhancement. The enhancement may be explained by the redirection of the direct beam through reflections and refractions by water droplets in the cloud boundaries surrounding the sun disc along with an increase in the diffuse component from Mie scattering.

Ozone is the third direct driver for surface UV irradiance. Ozone is produced by interactions of UV-C with oxygen molecules in the stratosphere. The main production occurs around the equator, where the irradiance on top of the atmosphere is largest. Ozone is transported towards the extratropics via the Dobson-Brewer circulation which creates a higher total ozone concentration at higher latitudes. Ozone absorbs radiant energy in the UV-C and UV-B and marginally in the UV-A. Longer path lengths through the atmosphere (e.g., at higher latitudes, during winter, or near sunrise and sunset) cause a spectral shift towards longer wavelengths due to the much stronger absorption of short wavelengths by stratospheric ozone. Since the cross section for Rayleigh scattering decreases as the fourth power of the wavelength, a longer path length through the atmosphere also shifts the spectral distribution towards longer wavelengths due to scattering.

All three direct drivers of surface UV levels (total ozone, clouds and aerosols, and surface albedo) are wavelength dependent and connected. This means that the effect on UV levels from e.g. a change in albedo will depend also on the cloudiness and on total ozone, as well as on the time of day and time of year. Radiative transfer models can simulate the transport of radiant energy through the atmosphere. Surface UV levels can then be simulated under different conditions of the direct drivers. In a later chapter we compare real-sky measurements with modelled clear-sky data, taking into account measured ozone and surface albedo values. We use the output of these analyses as a simplified way of estimating trends in the direct drivers of UV levels over the monitoring period from 1995/96 to 2024.

The Montreal Protocol

The Montreal Protocol on Substances that Deplete the Ozone Layer is an environmental agreement that regulates production and use of nearly a hundred man-made chemicals. When these so-called ozone depleting substances (ODSs) are released to the atmosphere, they damage the stratospheric ozone layer that protects Earth from harmful UV radiation from the sun. The Protocol is to date the only United Nations (UN) treaty ratified by all 198 UN Member States. Norway ratified the protocol in 1988. The initial agreement focused on phasing out chlorofluorocarbons (CFCs). Later, the Montreal amendment added phasing out of hydrochlorofluorocarbons (HCFCs). Both CFCs and HCFCs have ozone depleting potential (OPD) and global warming potential (GWP). The most recent Kigali amendments to the Montreal protocol are now phasing down hydrofluorocarbons (HFCs). HFCs have been used as replacements for CFCs and HCFCs. HFCs do not harm the ozone layer as much, but they have a high GWP and therefore impact climate change. See Q&A 17 in https://ozone.unep.org/20-questions-and-answers

2.2 Indirect drivers: circulation systems in the atmosphere and in the oceans

The direct drivers of surface irradiance (total ozone, clouds and aerosols, and surface albedo) are influenced by atmospheric circulation systems, coupled with ocean systems, that modulate wind, temperature, relative humidity, cloud and precipitation patterns, with a period that may differ from the yearly solar cycle. In a later section we will explore linear correlations between monthly variations in surface UV-doses and a few of these climate systems (see info box).

Glossary of indirect surface UV drivers

QBO The Quasi-Biennial Oscillation is a wind system in the tropical stratosphere, shifting between easterly and westerly winds, with a characteristic average 28 to 29 months cycle (Baldwin 2001). The shifting QBO-phases affect the strength of the stratospheric polar vortex and the strength and location of tropospheric jet streams differently and influence both global ozone dynamics and chemistry and weather systems. Due to its regular rhythm, it is commonly called the pacemaker or the heartbeat of the atmosphere.

ENSO The El Niño Southern Oscillation (ENSO) is a climate pattern, originating in the tropical Pacific Ocean, that affects cloud formation, rainfall and temperature patterns around the world. ENSO alternates between a warm phase (El Niño), a cool phase (La Niña) and a neutral phase, with a cycle of 2-7 years (Paek et al., 2017).

Solar Cycle Sun's magnetic activity fluctuates between periods of low and high activity, with an approximately 11-year cycle. Additionally, there are centennial cycles (100 years). The fluctuations affect solar energetic particles (like protons and electrons) and modulates cosmic rays reaching the Earth. Some studies indicate an influence from solar variations on clouds and climate, see e.g., Carslaw et al. (2002) and Seppälä et al. (2014).

AO The Arctic Oscillation is a climate pattern representing variations in surface atmospheric pressure between the Arctic and mid-latitudes. It influences weather patterns, such as cold air outbreaks in the Northern Hemisphere (Thompson and Wallace 1998).

NAO The North Atlantic Oscillation is a similar pattern to the AO but focuses on surface pressure differences between the Azores High and the Icelandic Low. It affects wind, storms, and precipitation in the North Atlantic region and adjacent continents. NAO exerts also a strong control on the pollution transport from northern hemisphere continents into the Arctic, particularly in winter and spring (Eckhardt et al. 2003).

Variations in Area of Arctic Sea-Ice Arctic sea-ice has declined markedly over the past 40 years (https://climate.copernicus.eu/climate-indicators/sea-ice). Reduced ice cover and volume leads to more solar energy absorption by the Arctic Ocean, warming the Arctic, which promotes further ice-loss and warming. Changes in the temperature gradient between the Arctic and Equator may affect ocean and atmospheric circulations and thereby affect regional weather systems.

3 Objectives and implementation of a network in Norway

The several political, organizational, and scientific steps that eventually led to the establishment of the Norwegian UV-monitoring network were initiated at a Nordic meeting in Stockholm in 1989 (Saxebøl, 1990). The meeting discussed the by then apparent rise in skin cancers and the need for real-sky UV data to inform the public about careless tanning. Shortly after, a Norwegian working group was formed with representatives from Statens institutt for strålehygiene (SIS, later the Norwegian Radiation and Nuclear Safety Authority, DSA), Institutt for kreftforskning at Radiumhospitalet, Norsk institutt for luftforskning (NILU), Meteorologisk institutt (MET), Statens forurensningstilsyn (SFT, later Miljødirektoratet), Helsedirektoratet (HDir), the University of Oslo (UiO), the University of Trondheim (NTNU), and the University of Tromsø (UiT). Its mandate was to elaborate on the rationale for establishing a national UV-monitoring network also in Norway.

In 1992, Miljøverndepartementet (now Klima- og miljødepartementet, KLD) and Sosialdepartementet (now Helse- og omsorgsdepartementet, HOD) established a second working group with representatives from Strålevernet (later DSA), SFT and HDir. Its mandate was to consider short- and long-term effects of UV on human health and the environment and to present to the ministries detailed strategy for the implementation of a UV monitoring network. The working group was also asked to consider the need for UV forecasting.

In 1994 the ministries formally made the decision to establish the Norwegian UV-monitoring network as a joint program between the health and environmental authorities, represented by Strålevernet (later DSA) and SFT. The long-term perspective of the UV-monitoring program was stated in the Allocation Letter of HOD for 1994: 'This is a long-term project that must continue for many decades to come.' NILU, which already conducted ozone monitoring on behalf of SFT, was contracted to perform UV-monitoring at the three existing stations of Ny-Ålesund (NYA, 79N), Tromsø (TSO, 69N)/Andøya (AND, 69N) and Blindern (BLI, 60N)/Kjeller (KJE, 60N). In addition to reporting UV and ozone from these stations, other environmental parameters were also included. Funding for this ongoing program is provided by Miljødirektoratet on behalf of KLD.

Five more network stations were to be under the administrative care of Strålevernet (later DSA). These stations should span a large range in latitudes and climate zones (such as inland and coastal) and reflect population dense areas or areas of crop production. They were therefore established respectively in Trondheim (TRH, 63N), Bergen (BRG, 60N), Kise (KIS, 60N), Østerås (OST, 60N, near Oslo) and Landvik (LAN, 58N). In 2003, the network was extended to Finse (FIN, 60N), representing a mountainous site. In addition to being responsible for the operation and maintenance at these six stations, DSA is also responsible for the calibration of all UV-instruments in the network. DSA furthermore retains the overall administrative and scientific responsibility for the network, with funding provided by HOD and KLD.

GUV instruments

The main instruments of the Norwegian UV monitoring network are multiband, moderate bandwidth filter radiometers, so-called Ground-based UV Radiometer Systems (GUV-541/511, Biospherical Instruments Inc.). GUV instruments have two separate parts. An electronic box residing indoors, connected to a PC, running a data logger program, and an outdoor detector unit coupled to the electronic box via a long detector cable. The detector unit has a set of internal photodiodes, preamplifiers and analogue-to-digital-converters that transform electrical signals generated by solar radiation to digital signals, which next is recorded by the logger software. Each photodiode ('detector channel') has a stack of optical filters that transmit a narrow part of the solar spectrum, while effectively blocking the rest. Moreover, the detector unit has a front optic that is designed to obtain a good angular responsivity to radiation from all parts of the sky. Electronics and optics are housed in a temperature stabilized and watertight cylinder to ensure stable performance under all weather conditions. To avoid ice and snow buildup, the front optic is heated and fitted with water drainage holes.

A GUV-511 has been operating at Blindern (BLI, 60N)/Kjeller (KJE, 60N) since 1994, being the first GUV instrument installed in Norway. Later, newer instruments purchased for the UV-network were of type GUV-541. Both instrument models have four channels with nominal wavelengths at 305, 320, 340 and 380 nm. The full width at half maximum of the channels is about 10 nm, which means the detector channels record a moderately wide slice of the solar spectrum. The GUV-511 also has a fifth channel in the visible part of the spectrum, recording photosynthetically active radiation, whereas this channel has been replaced with a channel at 313 nm in GUV-541s. The new generation GUV-instruments (GUVis-3511, Biospherical Instruments, Witthun et al., 2017) with a total of 19 detector channels, offer an extended wavelength range that also includes the visible and near-infrared. Currently, there are four such 19-channel models in operation in the network at monitoring stations Trondheim (TRH, 63N), Finse (FIN, 60N), Østerås (OST, 60N) and Kjeller (KJE, 60N), recording solar radiation side-by-side with the older instruments to avoid step changes in the time series. Since the network was established, measurements from both old and new GUV/GUVis instruments have been recorded as one-minute averages for each detector channel.

3.1 Quality of data products and gap filling

Applications of the Norwegian UV-monitoring data, from validations of satellite-based data products (ground truthing) to analyses of direct and indirect drivers of UV levels, place firm quality requirements on data products. Ensuring this quality has been a major contribution of DSA to the network. The three main components that ensure metrological quality of data products are drift corrections, traceability and intercomparisons.

Drift corrections involve quantifying the drift in responsivity over time of each channel of each GUV instrument against a travelling reference GUV. The drift in the channels of the travelling reference itself is monitored through laboratory measurements with calibration lamps and verified by shipping the reference instrument for an independent lamp calibration at the laboratory of the instrument manufacturer (Biospherical Instruments Inc.). Correcting for drift ensures that all instruments in the network across all years have measurements that can be compared to each other. In other words, it ensures a common scale for all instruments in the network and maintains this scale over time.

This scale is also linked to a common scale for UV measurements worldwide. Currently, this so-called metrological traceability for data products from the Norwegian network comes from the FARIN campaign

(‘Factors Affecting UV Radiation In Norway’, Johnsen et al., 2008), in which instruments from many countries made simultaneous measurements on the roof-platform of the DSA-building at station Østerås (OST, 60N). All data products from the Norwegian network that are presently available on GitHub are traceable through results from this campaign to the QASUME world travelling reference spectroradiometer (Quality Assurance of Spectral Ultraviolet Measurements in Europe) operated by the Physical Meteorological Observatory in Davos, the World Radiation Center (PMOD/WRC) (Gröbner et al., 2005; Hülsen et al., 2016). Through this instrument, the Norwegian UV measurements are ultimately traceable to a primary standard for spectral irradiance at the Physikalisch-Technische Bundesanstalt (PTB).

In addition to the GUV instruments, the network includes a spectroradiometer that is co-located with the permanently installed GUV instrument operating at station Østerås (OST, 60N). The travelling reference GUV is periodically intercompared to this instrument for validations. The spectroradiometer, as well as some of the GUV instruments in the network, have participated in intercomparisons against QASUME in respectively 2003, 2005, 2010, 2014 and 2019. The agreement in UVIs between the Norwegian spectroradiometer and QASUME has been “good” to “excellent” (see Annex 11.1). The protocol from the latest intercomparison in Oslo in 2019 states that the mean ratio of the Norwegian network’s spectroradiometer UVIs to those measured by QASUME is -1 % and that this result is consistent to all previous intercomparisons (ref: Protocol Qasume Site Audit (pmodwrc.ch). This means that the Norwegian spectroradiometer performs absolute measurements of spectral irradiance in the solar UV region consistently, thus being useful for validations of e.g., UVI measurements performed with the travelling reference GUV.

Intercomparisons of the travelling reference GUV with QASUME

The travelling reference GUV9273 is regularly intercompared with the DSA spectroradiometer at stations Østerås (OST, 60N) for validations (Figure 45). The travelling reference and some of the other GUV instruments in the network have also participated in several QASUME campaigns. As reported by the QASUME team, the agreement in UVI measured with the GUV instruments and QASUME has been: an average ratio of GUV9275 (NYA, 79N) to QASUME of 1.00, variability of +/- 2.4% [2009, NYA]; average ratio of GUV9273 (travelling reference) to QASUME of 1.005, standard deviation <2%, rated “excellent” [2010, Oslo]; average ratio of GUV9273 (travelling reference) to QASUME of 0.98, standard deviation <5%, rated “good” [2014, Jokioinen]. No results were reported for the travelling reference GUV instrument in the official QASUME2019 report, however, validations by DSA, applying reference spectra from the QASUME instrument, indicates mean daily differences between measurements with the GUV and QASUME of -2.6%, 2.0% and -2.1% for UVI, UV-B and UV-A, respectively. In summary, the differences in UVI scales for the DSA spectroradiometer and the travelling reference GUV have stayed within a few percent relative to QASUME in the period of intercomparisons. A compilation of ratios between UVI from QASUME and UVI for the groups of GUV instruments operating co-located with QASUME (Figure 38) shows interquartile ranges within ±4% for each campaign period.

Most of the data from the Norwegian UV-monitoring network results directly from GUV measurements. GUV up-times, defined as the percentage of one-minute dose rates successfully acquired from sunrise to sunset over the span of a monitoring period (see Annex 11.2), have been consistently high. In the GitHub datasets, gaps in GUV measurements have been filled using modeling to provide complete series of hourly mean dose rates, as well as integrated daily, monthly, and yearly doses. The gap filling method is based on the libRadtran radiative transfer model (Embde et al., 2016). The model provides clear-sky dose rates based on the location of a station and the solar elevation angle that is given by the date and time. It also incorporates total ozone concentrations (TOC) obtained from the Total Ozone Mapping Spectrometer

(TOMS) on NASA's Earth Probe satellite and the Ozone Monitoring Instrument (OMI) on NASA's AURA satellite (NASA Goddard Space Flight Center), as well as ground-based measurements retrieved from the World Ozone and UV Radiation Data Centre (WOUDC) for periods when satellite data were unavailable. Subsequently, a seasonal correction is applied that matches modelled clear-sky dose rates with averages of measured real-sky dose rates from the same station at the same date and time, obtained from years without gaps in the GUV data. The resulting dose rates thus account for average seasonal variations in aerosol amount and surface albedo. Finally, the modelled clear-sky dose rates are multiplied with cloud modification factors (CMFs). These factors are primarily based on local pyranometer instruments measuring total solar radiation, but also on observations of cloud cover in okta. At station Finse (FIN, 60N), cloud modification factors have also been retrieved from a broadband UV instrument.

3.2 Dissemination and use of UV-data

Complete, gap-filled, and quality-controlled data, aggregated as hourly mean UV dose rates, and as daily, monthly, and yearly integrated doses, are freely accessible for public and non-commercial use at https://github.com/uvnrpa. The repository is administered by DSA and NILU. UV-index measurements and guidance for sun protection are presented online at https://uvnett.dsa.no.

The current report is chiefly concerned with the UVI and the E-UV and UV-A data products that are relevant for evaluating health effects, e.g., from acute and chronic UV exposure to the skin, eyes, and immune system (Neale et al., 2023). The repository also has data products that address effects on plants, microorganisms, and on aquatic life. Climate-relevant data products that can be retried are total ozone concentrations (TOC) and effective cloud transmittance (eCLT). Through these parameters we begin in this report to assess how the indirect drivers of surface UV levels such as circulations in the atmosphere and in the oceans, in turn influence the direct drivers of surface UV levels.

Since the establishment of the network, DSA has published five summary reports covering UV radiation at all network locations (Hannevik 1998; Norvang 2000; Johnsen 2002; Aalerud 2006; Johnsen 2011). NILU is reporting both atmospheric ozone and UV-radiation for the stations Oslo, Andøya and Ny-Ålesund on a yearly basis, the latest from 2024 (Svendby et al., 2024).

Data and insights from the UV-monitoring network also support Norway's UV and skin cancer strategy, initiated by DSA in 2019 (Nilsen et al., 2019). Norway is among the countries with the highest incidence and mortality rates of melanoma skin cancer (IARC 2024, Cancer Today, https://gco.iarc.who.int). More than 90% of new melanoma cases can be attributed to UV exposure from natural sunlight and cosmetic sunbeds (Keim et al. 2021), and many cases could likely have been prevented with careful sun behavior. The UV and skin cancer strategy aims to reduce the increase in new skin cancer cases by 25% within 2040 compared with 2018. Data from the UV-monitoring network supports this strategy through estimations of UV doses to the Norwegian population (Nilsen et al., 2015) and through its potential for issuing public alerts on high UV levels.

Since 2011, UVI data from the Norwegian UV-monitoring network has been featured every year in the so-called State of the Climate-series, published as an annual supplement to the Bulletin of the American Meteorological Society (BAMS). Here UVI data from stations Ny-Ålesund (NYA, 79N), Andøya (AND, 69N), Trondheim (TRH, 63N), Finse (FIN, 60N) and Østerås (OST, 60N), together with measurements from stations belonging to networks in Finland and Canada, form the ground-based counterpart to UVI values derived from satellite data for sub-Arctic and Arctic areas.

A list of major topics where UV-monitoring data have been utilized is listed below:

- Public guidance on sun protection: Support for light-sensitive patients, efficacy of UV-shading structures, sun protection factor of sunglasses and textiles, preparation of sun protection guidelines.
- Early warnings for the public during periods of elevated sunburn risk.
- International UV-monitoring efforts (Schmalwieser et al., 2017).
- Validation of national UV forecasts from the Norwegian Meteorological Institute, featured on the Yr platform (Yr app and www.yr.no).
- Validation of UV forecasts and UV satellite data products (Lakkala et al., 2020; Kosmopoulos et al., 2021; Bernhard et al., 2015; Bernhard et al., 2013; Staiger et al., 2008; Koepke et al., 2007).
- Studies on exceptional UV and Ozone conditions (Petkov et al., 2022, 2023; Bernhard et al.,2013,2015,2020; Karpechko et al., 2013; Knudsen et al., 2005).
- Input for yearly State of the Climate in the Arctic reports by the American Meteorological Society since 2011, with recent reports in 2023 and 2024 (Bernhard et al., 2023; Butler et al., 2024).
- Research on UV Effects in marine microalgae (Xie et al., 2020).
- Research on sunlight and health effects: Epidemiological studies on skin cancer, studies on vitamin D, photoallergic reactions, and jaundice in infants (Stenehjem et al., 2018A,B, 2020,2022; Nedrebø, 2017; Rønneberg 2016).
- Methods developments for UV-monitoring (Svendby et al., 2021; Seckmeyer et al., 2010; Johnsen et al., 2008; Lindfors et al., 2007; WMO 2008).
- UV-monitoring data for academic research: Data use in master’s and doctoral theses at the Norwegian universities (University of Oslo, University of Bergen, Norwegian University of Science and Technology, and Norwegian University of Life Sciences).

4 Measured UVI, E-UV and UV-A doses

The following chapters present the UV dataset gathered over the past three decades in terms of the UVI and the E-UV and UV-A data products, as featured and publicly available on GitHub. The data from station Østerås (OST, 60N) has large gaps up to 1999, as this station initially was established for calibration purposes only and therefore did not have a permanently installed GUV instrument before that year. Measurements at Finse (FIN, 60N) were performed with a Solar Light broadband meter that frequently suffered data losses until 2002, when a GUV instrument was permanently installed. Additionally, two network instruments have been transferred between locations, respectively from Tromsø (TSO, 69N) to Andøya (AND, 69N) in 2000 and from Blindern (BLI, 60N) to Kjeller (KJE, 60N) in 2019.

4.1 The Global Solar UV index (UVI)

The Global Solar UV index (UVI) is a measure of the UV radiation level at the Earth's surface weighted by its wavelength dependent ability to cause erythema, or sunburn (WHO 2002). The UVI is the internationally recognized standard for communicating UV levels to the public, with higher values indicating shorter exposure times needed to cause sunburn.

The UVI ranges in categories from low (0-2), to moderate (3-5), high (6-7), very high (8-10), and extreme (11+). During cloud-free conditions, the summer noon UVI in southern Norway is typically 5.5 (moderate/high) for lowland stations like Landvik (LAN, 58N) but has occasionally reached 7 (high) when the sky has been partly covered by clouds and the total ozone amount low (Figure 2, lower panel). Corresponding numbers for the mountain station at Finse (FIN, 60N) is 6.5 (high) and 8 (very high). In Norway, the highest instantaneous UVI value recorded is 10.0 (very high), measured at Finse on 12 June 2020 (Figure 2, mid panel). Two other instances of very high UVI occurred at Finse in June 2005 and June 2015. Common to these events of very high UVI is the concurrence of mixed cloud conditions (giving a strong diffuse sky component) while the sun disk is unobstructed (giving also a strong direct beam component, Calbo ́et al., 2005) along with late onset of snow melt (high albedo). Snow distribution maps reveal snow cover lasting till late June these years (https://www.senorge.no/).

Comparing daily max UVI levels to monitoring period mean daily max levels, the largest percentage differences have been recorded at the northernmost station of Ny-Ålesund (NYA, 79N) (Figure 2, upper panel). Increases by 70% above the period mean were observed in March/April 2020 due to a massive ozone depletion in the Arctic, resulting from an exceptional strong, cold, and persistent stratospheric polar vortex, favoring chemical destruction of stratospheric ozone (Bernhard et al., 2020; Petkov et al., 2023). There is evidence that strong anomalous springtime ozone depletions in the Arctic, like in 2011, may persist from spring to summer, leading to increased clear-sky summer UVI values (Karpechko et al., 2013).

Data products

Time series data for effective doses in J/m^2 and dose rates in W/m^2 at the UV-monitoring network stations can be freely accessed at https://github.com/uvnrpa. Currently, eleven dose products are offered, including several that are particularly relevant for assessing health and environmental impacts from solar UV exposure. These include:

CIE1998 (E-UV): Represents the erythema-weighted effective dose or dose rate. Like the Global Solar UV Index, the weighing function is the standard erythema action spectrum, which measures the susceptibility of Caucasian skin to erythema, commonly referred to as sunburn (CIE, 1998).

CIE1987: Closely related to CIE1998 but based on an earlier erythema action spectrum proposed by McKinlay and Diffey (CIE, 1987).

NMSC: The effective dose or dose rate using the action spectrum for photo-carcinogenesis of non-melanoma skin cancers (ISO/CIE 28077:2016).

VITD: The effective dose or dose rate using the action spectrum for the conversion of 7-DH7 to previtamin D_3 in human skin (CIE 2006).

DNA: The effective dose or dose rate, based on the generalized DNA-damage action spectrum determined by Setlow (1974) and normalized at 300 nm according to Bernhard and Seckmeyer (1997). This spectrum is important for assessing the effectiveness of UV radiation in causing DNA damage, which can inactivate microorganisms, including viruses.

ANCHOVY: The effective dose or dose rate using the action spectrum for damage to eggs and larvae of northern anchovy (Hunter et al., 1979), relevant for understanding UV-B effects on aquatic primary productivity.

FLINTPLANT: The effective dose or dose rate using the generalized plant damage action spectrum for higher plants, by Flint and Caldwell (2003).

HEP: The effective dose or dose rate using the proposed action spectrum for hematopoetic porphyria hypersensitivity to UV-A and visible.

PAR: Refers to photosynthetically active radiation within the wavelength range of 400-700 nm. The measurements of PAR are provided in units of mol/s/m^2 or mol/m^2, whereas all other dose products at the github site are J/m^2 and W/m^2.

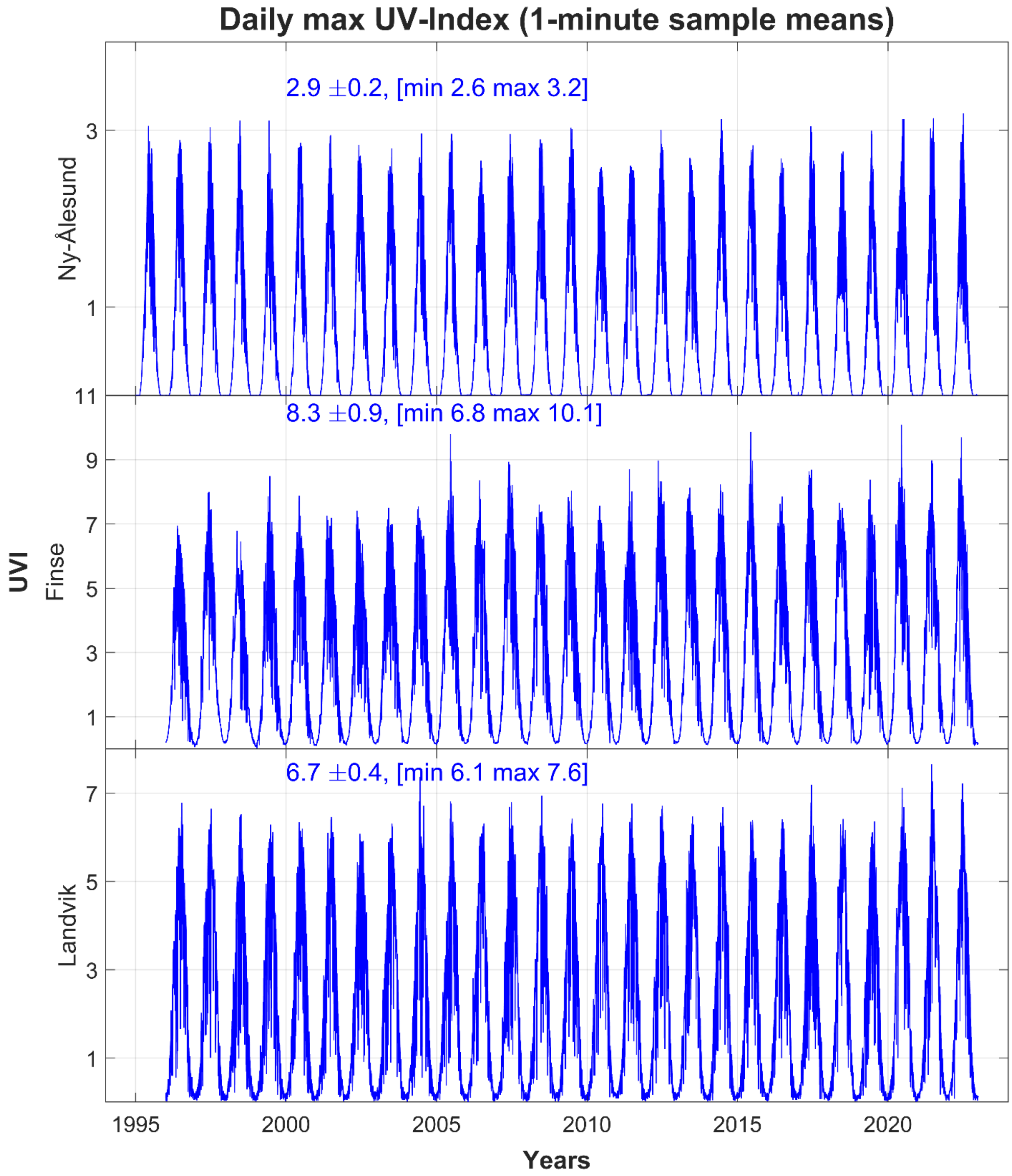

Figure 2 Daily max UVI for stations Ny-Ålesund (NYA, 79N), Finse (FIN, 60N)/Hardangervidda and Landvik (LAN, 58N). Legends denote period means, std, max and min. Note different scales on the Y-axis.

4.2 UV Index hour and daily E-UV doses

The daily E-UV dose is the E-UV dose rate integrated over a full day during all the shifting sun and sky conditions of that period. A related unit is the UV Index hour (UVH), which is the E-UV dose rate corresponding to one unit UVI integrated over one hour (Saxebøl 2000). One unit UVH equals 90 J/m^2, which is 0.9 Standard Erythema Dose (SED) (Schmalwieser 2020, CIE 1997). The Australian Radiation Protection and Nuclear Safety Agency (ARPANSA) recommends taking sun protective measures if you have fair skin and expect receiving a dose exceeding 1 SED a day. The UVH expressed in units of SED per hour provides an intuitive connection between instantaneous UVI and hourly accumulated E-UV dose and has been adopted by ARPANSA for public information (Ultraviolet radiation dose | ARPANSA). Figure 44 in Annex 11.6 illustrates the relation between UVI and UVH at station Østerås (OST 60N).

In Norway, daily E-UV doses may reach a summertime maximum of about 3.0 kJ/m² (30 SED) in Ny-Ålesund (NYA, 79N) and 4.5 kJ/m² (45 SED) in Landvik (LAN, 58N) whereas the mountain station Finse (FIN, 60N) may reach a peak of more than 6.0 kJ/m² (60 SED) in early summer, just before the disappearance of the snow. For comparison, the maximum daily E-UV dose reported for the Malaysian peninsula (latitude 1-7 °N) in April 2015 is 7.7 kJ/m² (77 SED) (Tan et al., 2018).

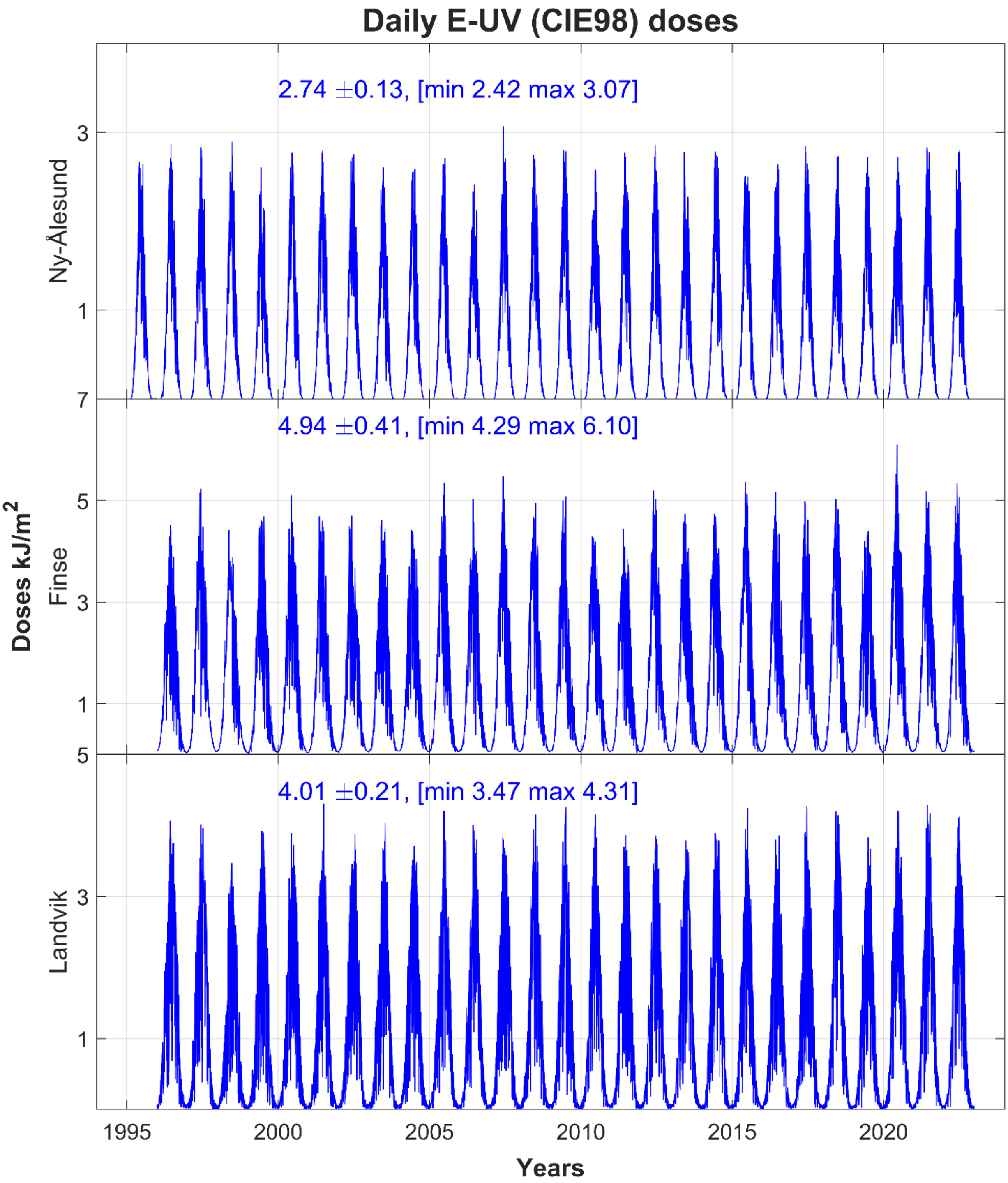

Figure 3 Daily erythemal (E-UV) UV doses at three stations (kJ/m²). Legends denote period means, std, max and min. Note different scales on the Y-axis.

4.3 Yearly E-UV and UV-A doses

Yearly E-UV and UV-A doses (Figure 4 and Figure 5) are E-UV and UV-A dose rates integrated over a year. Finse (FIN, 60N) displays higher yearly doses than any of the lowland stations. Located 1200 meters above sea level and adjacent to the Hardangerjøkulen glacier, the station experiences reduced atmospheric scattering, higher surface albedo, and a longer snow season compared to other stations. For lowland stations, UV doses decrease with increasing latitude due to the lower angle of the sun above the horizon at higher latitudes. However, doses are also influenced by differences in local climate and cloud circulation patterns, which despite the difference in latitude between Trondheim (TRH, 63N) and Bergen (BRG, 60N) results in almost equal mean yearly doses due to the sunnier conditions in Trondheim. Furthermore, minor differences in UV doses between geographically close stations, such as Østerås (OST, 60N) and Blindern (BLI, 60N), may be attributed to local variations in cloud cover and microclimatic conditions. When comparing E-UV and UV-A doses, latitude has a smaller impact on UV-A than on E-UV doses.

Comparing the two arctic stations, Ny-Ålesund (NYA, 79N) and Andøya (AND, 69N), the mean yearly UV-A doses are nearly equal (Figure 5). The presence of nearby glaciers in Ny-Ålesund (NYA, 79N) and late snowmelt provides high surface albedo and enhanced surface irradiance, which partially compensates for the lower solar elevation. Additionally, Ny-Ålesund provides a two month longer midnight sun period (https://www.timeanddate.no/astronomi/sol/norge), where the sun remains above the horizon 24 hours a day. Yearly UV-A doses in Ny-Ålesund may even surpass UV-A doses in Bergen (BRG, 60N) in years with sunny conditions in the north and rainy late spring and summer months in Bergen (1998, 2011, 2015).

Mean yearly E-UV doses generally exhibit larger variations than UV-A doses (Table 1). Although both are strongly influenced by variations in cloud cover, aerosols, and surface albedo, variations in total ozone comes as an additional parameter, affecting E-UV much more than UV-A. Comparing variability between stations, arctic and coastal locations exhibit larger variations than inland stations like Østerås (OST, 60N), Blindern (BLI, 60N) and Kise (KIS, 60N). Trondheim is an exception and displays the smallest variability among stations.

Comparing the mean yearly E-UV and UV-A doses across various geographic locations reveals clear influences from differences in latitude and climate (Table 2). For example, the northernmost station at Ny-Ålesund (NYA, 79N) receives only 52% of the average yearly E-UV dose and 75% of the UV-A dose compared to the southernmost station at Landvik (LAN, 58N). The smaller north-south fraction for E-UV doses, compared to UV-A doses, is largely due to the stronger attenuation of E-UV with decreasing solar elevation.

Comparing the coastal station Bergen (BRG, 60N) with the inland, more continental station Kise (KIS, 60N), the influence from mild and humid westerlies crossing the Atlantic is stronger at the windward side of the mountains in western Norway compared with the leeward, eastern side, as reflected by the larger standard deviation and lower dose fractions (86%) compared with Kise (KIS, 60N). This applies also to the mountain site Finse (FIN, 60N). Still, yearly doses are 138% of those at lowland Kise (KIS, 60N). The prolonged snow cover at Finse compared with Kise likely contributes to the higher yearly UV doses observed there.

Additionally, Finse (FIN, 60N) benefits from a pristine location with a wider horizon compared to most lowland stations, likely experiencing less influence from local air pollution due to the absence of roads and industrial activities. These factors may further enhance UV levels at Finse. However, the area is occasionally affected by long-distance transport of atmospheric particles, such as Saharan dust. For example, in late March 2022, a yellowish layer of dust was visible on the snow fields around the research station. (https://atmosphere.copernicus.eu/historical-saharan-dust-episode-western-europe-cams-predictions-accurate). Cases of Saharan desert has likely no significance for the yearly UV doses at Finse.

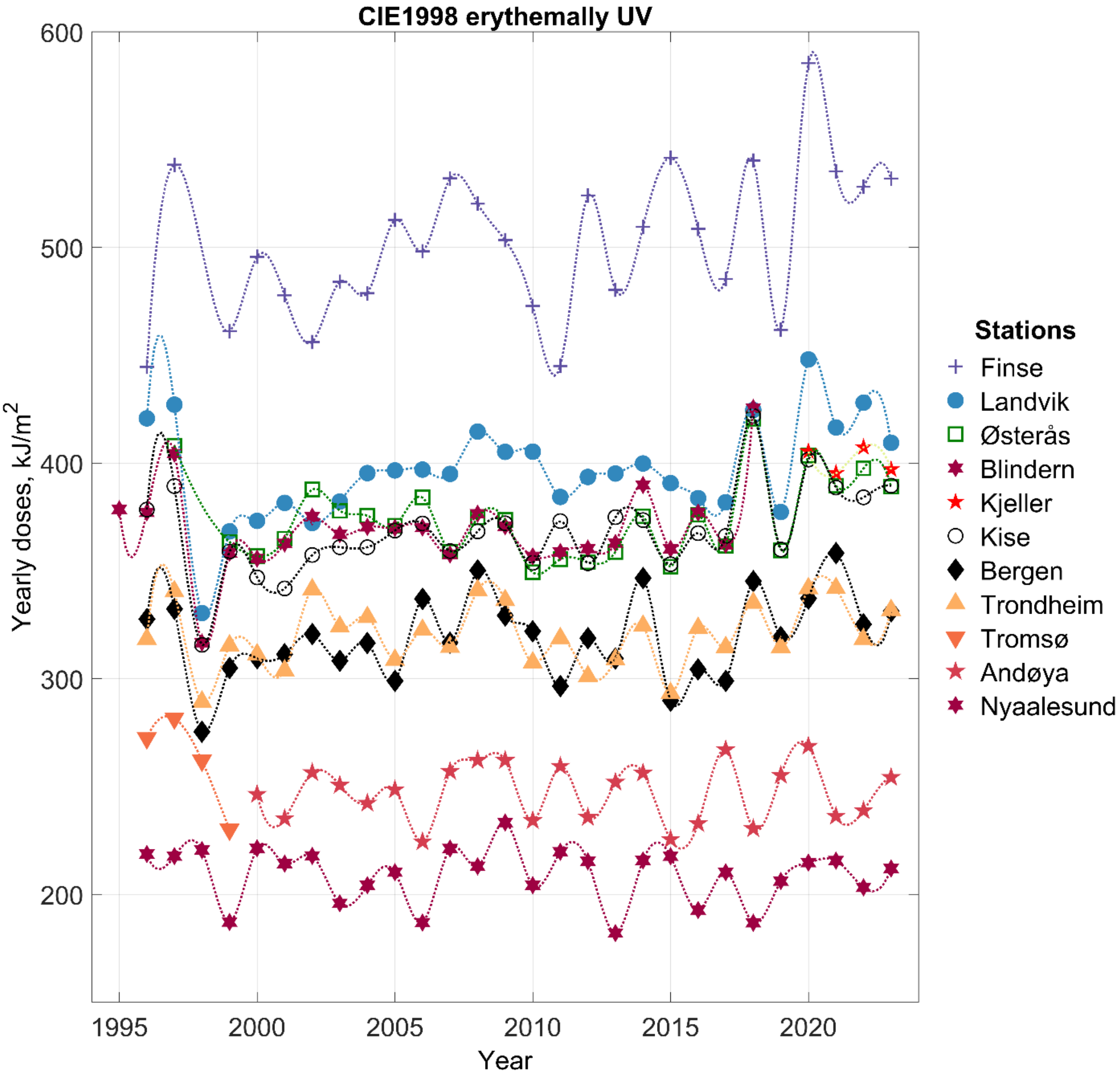

Figure 4 Yearly E-UV-weighted UV-doses at the UV-monitoring stations.

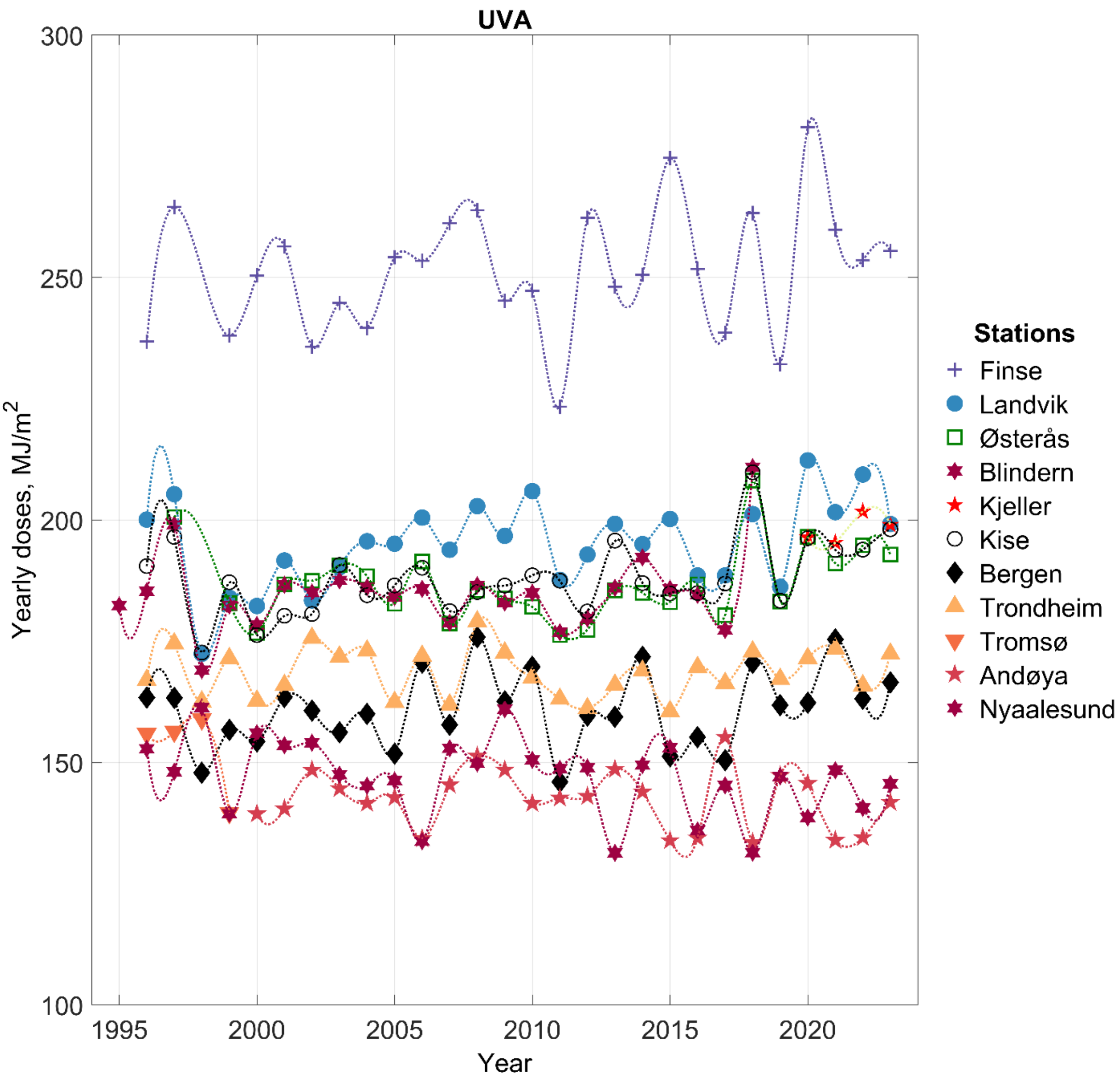

Figure 5 Yearly UV-A doses at the UV-monitoring stations.

4.4 Variations in yearly E-UV doses: exceptional years

Variations in yearly E-UV doses at the respective stations are in this chapter expressed as relative deviations from the period mean, (D_y/D_M – 1). Here D_y is the yearly E-UV dose at year y and D_M is the period mean yearly E-UV dose for all years of measurements at the specific station (see Figure 8, graphs labelled Sum).

Some successive years display a large span in the relative deviation of E-UV doses, as is seen for the southern lowland stations in the years 1997 (up to about +10% at BLI, 60N) and 1998 (down to about -20% at LAN, 58N). The winter 1997/98 had an exceptionally strong transition in El Niño/La Niña phases, collectively called El Niño Southern Oscillation (ENSO) (Paek et al., 2017). Other years of such exceptionally strong ENSO transitions were 2015/16. However, these years do not show a similarly large span in relative deviations of yearly E-UV doses at the southern lowland stations.

Some years show consistent relative deviations of E-UV doses across most stations in the network except for the arctic locations. The year 2011 for example shows consistently large interannual negative deviations (down to about -12% at FIN, 60N). According to WMO (2011), this was the wettest year on record in Norway since 1900 (start of registrations). The year 2018 shows large positive interannual deviations (up to about +15% at BLI, 60N) for particularly at the southeastern inland stations Østerås (OST, 60N), Blindern (BLI, 60N) and Kise (KIS, 60N). May and July of 2018 brought exceptionally hot and dry conditions in southeastern Norway and Scandinavia. The anomalously high yearly E-UV doses were due to a persistent high-pressure system providing exceptional sunny conditions during summer months, starting in Scandinavia and progressing southwards to the Iberian Peninsula (Rousi et al., 2023; Skaland et al., 2019).

Year 2020 is another year with E-UV doses above the period average for most of the stations. The winter and spring brought a record strong and cold polar vortex and record strong chemical depletion of ozone (Lawrence et al., 2020). The largest increase in yearly dose was seen for the mountain station Finse (FIN, 60N) (+13%). Monitoring data show that the spring period, from April to June, also experienced prolonged periods of clear-sky conditions.

Table 1 Mean yearly E-UV and UV-A doses, standard deviations, and relative standard deviations.

	E-UV			UV-A		
	Mean [kJ/m²]	**Std [kJ/m²]**	**Rel. Std [%]**	**Mean [MJ/m²]**	**Std [MJ/m²]**	**Rel. Std [%]**
Finse (FIN, 60N)	500.9	34.3	6.9	251.6	12.9	5.1
Landvik (LAN, 58N)	397.2	23.3	5.9	195.1	8.8	4.5
Østerås (OST, 60N)	375.0	19.8	5.3	187.0	7.3	3.9
Blindern (BLI, 60N)	369.6	18.3	4.9	184.9	7.3	4.0
Kise (KIS, 60N)	368.1	19.7	5.3	187.5	7.7	4.1
Bergen (BRG, 60N)	320.3	19.5	6.1	161.0	7.7	4.8
Trondheim (TRH, 63N)	319.8	14.9	4.7	168.3	5.1	3.0
Andøya (AND, 69N)	250.0	14.8	5.9	145.1	8.5	5.9
Nyaalesund (NYA, 79N)	209.5	12.6	6.0	146.7	7.8	5.3

Table 2 Ratios in mean yearly doses for different climate regions.

Fraction	Fraction	E-UV	UV-A
North / South	Ny-Ålesund (NYA, 79N) / Landvik (LAN, 58N)	53 %	75 %
Coast / Inland	Bergen (BRG, 60N) / Kise (KIS, 60N)	87 %	86 %
Alpine / Lowland	Finse (FIN, 60N) / Kise (KIS, 60N)	136 %	134 %

4.5 Correlations of yearly doses between pairwise stations

In this section, we examine the strength of linear correlations in annual UV doses between stations representing different geographic locations (Figure 6 and Figure 7). Since winter months contribute minimally to the yearly integrated UV doses, the analysis applies primarily to the summertime cloud climate.

Strong correlations between station pairs may indicate consistent impacts on UV-levels from regional or large-scale circulation patterns or remote circulation systems. Examples of such large-scale circulation systems are the Quasi-Biennial Oscillation (QBO) in the tropical stratosphere, the El-Niño Southern Oscillation (ENSO) in the tropical Pacific Ocean, the North Atlantic Oscillation (NAO) and the Arctic Oscillation (AO) (see info box). These circulation systems are interconnected, see e.g., the conceptual model in figure 10a in Hall et al. (2015).

Weak correlations between station pairs may suggest weak correlations in cloudiness. In the atmosphere, the stratosphere and troposphere are distinct layers, and stratospheric circulation impacts E-UV doses more than UV-A doses due to variations in ozone concentration. Differences in the correlation coefficients for E-UV and UV-A doses may reflect the distinct geographical influences of respectively the stratosphere and the troposphere.

Comparing the E-UV correlation coefficients (Figure 6), the three south-eastern inland stations (KIS, OST, BLI, 60N) and the southernmost station Landvik (LAN, 58N) show strong positive pairwise correlations, with coefficients exceeding 0.80. A strong correlation in summertime cloud climate is probably the main driver.

Comparing the inland station Kise (KIS, 60N) with the coastal stations Trondheim (TRH, 63N) and Bergen (BRG, 60N), as well as the mountain station Finse (FIN, 60N), the correlations remain positive but more moderate, ranging from 0.55 to 0.69. For Trondheim and Bergen, their proximity to the ocean and position on the windward side of the Langfjella mountain ridge may result in a stronger influence from the Atlantic westerlies and orographic precipitation compared to the inland stations situated on the leeward side of the ridge. At the same time, these stations share impacts from overlapping large-scale circulation systems. When comparing UV-A correlation coefficients (Figure 7), the correlation declines more sharply with increasing distance between stations than in the E-UV. This can be because tropospheric circulation systems (e.g. clouds that affect both E-UV and UV-A doses) are more variable and have a more limited geographic extent compared to circulations in the stratosphere (that affect ozone and therefore primarily E-UV).

Turning to the arctic locations, the correlation in UV doses between Kise (KIS, 60N) and Andøya (AND, 69N, 1000 km to the north) is close to zero in the E-UV (0.09) and weakly negative in the UV-A (-0.27). Between Kise (KIS, 60N) and Ny-Ålesund (NYA, 79N, 2000 km to the north) the correlations are weakly negative in the E-UV (-0.25) and moderately negative in the UV-A (-0.66).

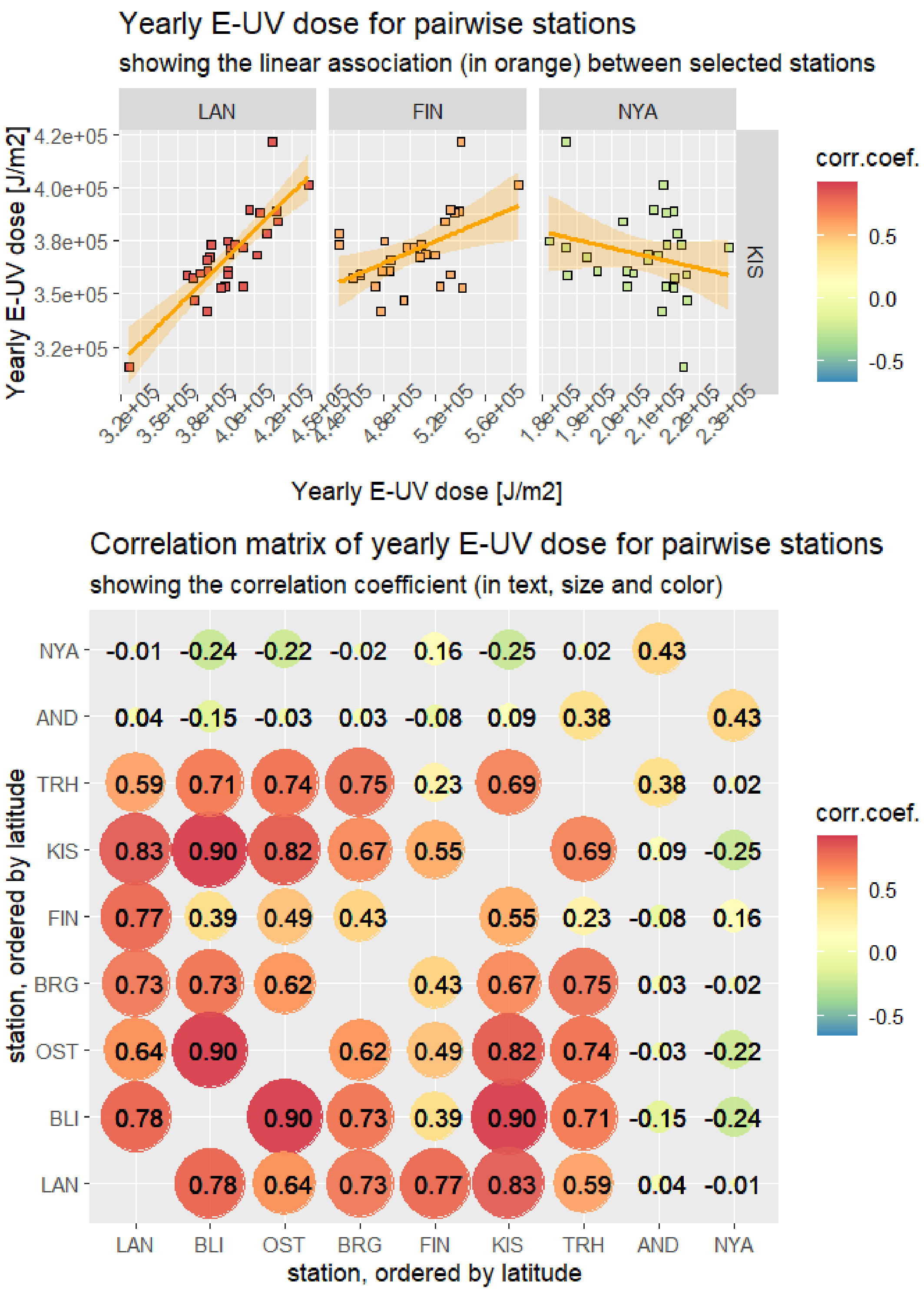

Figure 6 Correlations of yearly E-UV doses between pairwise stations. E-UV doses have a large UV-B component that is sensitive to stratospheric ozone. The three upper panels show yearly E-UV doses for station Kise (KIS, 60N) plotted against yearly E-UV doses for stations Landvik (LAN, 58N), Finse (FIN, 60N) and Ny-Ålesund (NYA, 79N). The straight lines in the upper panel show the fitted trends: KIS-LAN (TSLM(E-UV KIS ~ E-UV LAN): $R2 = 0.69$, adjusted $R2 = 0.68$, $F(1,26) = 59$, $p = 3.7e-8$), KIS-FIN (TSLM(E-UV KIS ~ E-UV FIN): $R2 = 0.25$, adjusted $R2 = 0.22$, $F(1,25) = 8.5$, $p = 7.3e-3$), KIS-NYA (TSLM(E-UV KIS ~ E-UV NYA): $R2 = 0.060$, adjusted $R2 = 0.024$, $F(1,26) = 1.7$, $p = 0.21$). The outlier of an unusually high yearly E-UV dose at Kise is from the 2018.The bottom panel shows the correlation coefficient (R2 is the square of this) between all the pairwise stations in the E-UV.

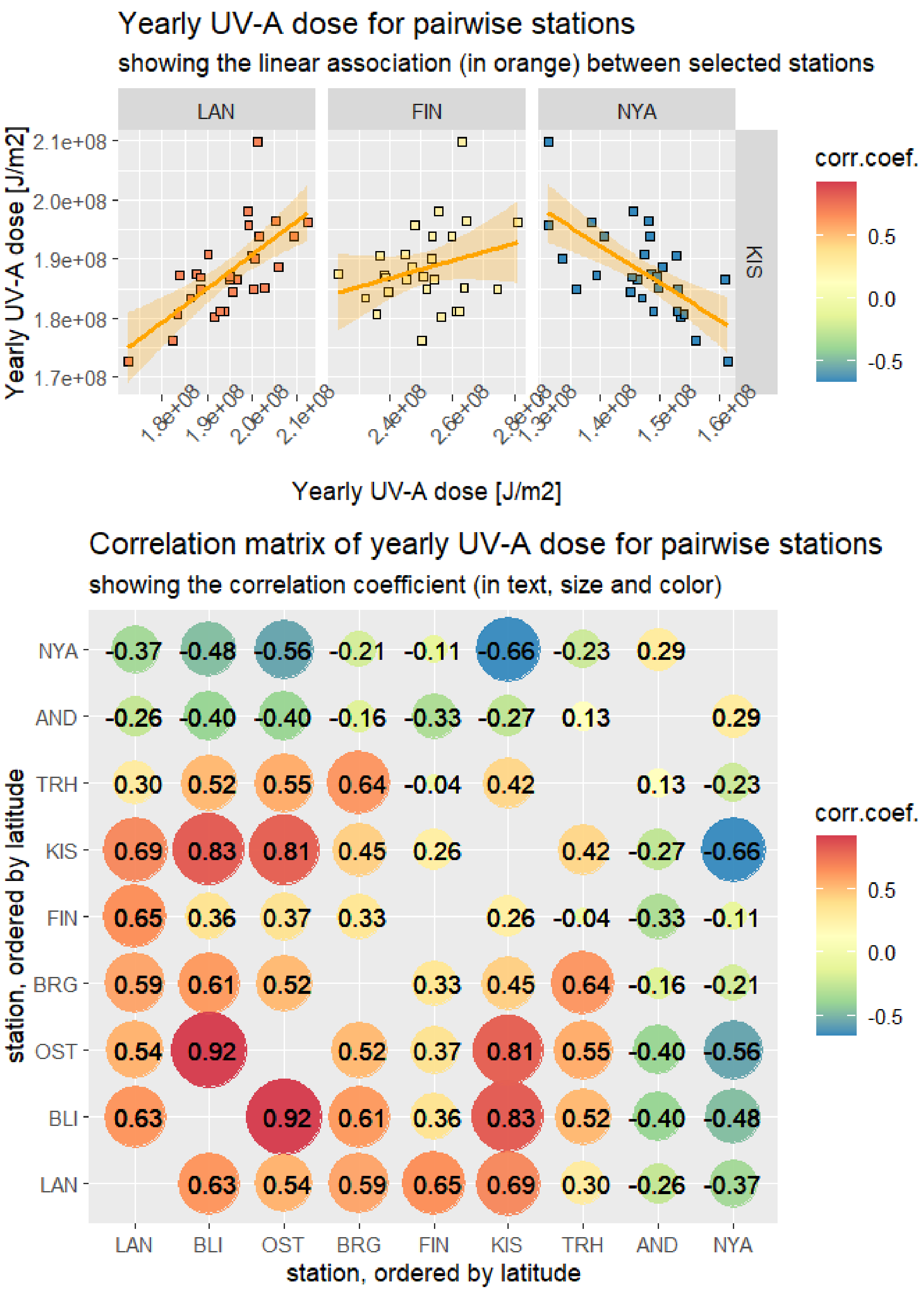

Figure 7 Correlations of yearly UV-A doses between pairwise stations. UV-A doses are sensitive to e.g., tropospheric clouds. The three upper panels show yearly UV-A doses for station Kise (KIS, 60N) plotted against yearly UV-A doses for stations Landvik (LAN, 58N), Finse (FIN, 60N) and Ny-Ålesund (NYA, 79N). The straight lines in the upper panels show the fitted trends: KIS-LAN (TSLM(UV-A KIS ~ UV-A LAN): $R2 = 0.47$, adjusted $R2 = 0.45$, $F(1,26) = 23$, $p = 5.4e-5$), KIS-FIN (TSLM(UV-A KIS ~ UV-A FIN): $R2 = 0.076$, adjusted $R2 = 0.039$, $F(1,25) = 2.0$, $p = 0.17$), KIS-NYA (TSLM(UV-A KIS ~ UV-A NYA): $R2 = 0.44$, adjusted $R2 = 0.42$, $F(1,26) = 21$, $p = 1.1e-4$). The outlier of an unusually high yearly UV-A dose at Kise is from the 2018. The bottom panel shows the correlation coefficient (R2 is the square of this) between all the pairwise stations in the UV-A.

5 Trends in the direct drivers of UV levels

The previous chapter summarized results from the Norwegian UV-monitoring network in terms of the UVI, daily E-UV doses and yearly E-UV and UV-A doses. Here, we further investigate the yearly data and explore any trends in the direct drivers of surface UV levels: total ozone (TOC), clouds and aerosols, and surface albedo. We also look at monthly trends in the effective cloud transmittance (eCLT), the E-UV and UV-A doses and TOC.

5.1 Exploring impacts from direct drivers on yearly E-UV and UV-A doses

Direct drivers of E-UV doses are total ozone, clouds and aerosols, and surface albedo, whereas the direct drivers of UV-A doses are primarily clouds, and aerosols and surface albedo. These drivers interact and it is therefore not possible to disentangle their individual impact on doses without considering the system as a whole (a priori knowing the ozone, clouds and aerosols, and surface albedo values).

However, as a simple first order approach to exploring the relative contributions of these drivers, we treat ozone and surface albedo independent of cloud cover. Ozone is retrieved from satellite data and surface albedo from an analysis of the levels of the 380-nm UV-A channel of the GUV instruments (Dahlback 1996), which is insensitive to ozone. Thereafter, we estimate the effect of clouds by comparing real-sky measurements with modelled clear-sky data, using the retrieved daily ozone and surface albedo value as input to the model. We use the output of these analyses as a simplified way of estimating trends in the direct drivers of UV levels.

We used the libRadtran radiative transfer model (Emde et al., 2016). Based on latitude, date and time we calculated the solar zenith angle (90° – solar elevation angle) as input to model. Aerosols were set to default. A pseudospherical solver, which considers the Earth's atmospheric curvature, along with a sub-arctic winter atmospheric height-profile, resulted in the closest agreement between modeled and observed UV doses at the locations of the stations.

Daily values for the total ozone concentration (TOC) were downloaded from the TOMS and OMI satellite overpasses for every station and every year of the monitoring period. A monitoring period mean TOC for every day of the year was obtained by taking the mean over the monitoring period and smoothing.

Daily values for the surface albedo were extracted from the GUV measurements using one of the UV-A-channels (380 nm) under clear-sky conditions. Gaps in daily surface albedo data were filled through interpolation. Finally, a monitoring period mean surface albedo for every day of the year was obtained by taking the mean over the monitoring period and smoothing.

To explore the impact of ozone on yearly E-UV and UV-A doses, the yearly doses at all stations was modelled in libRadtran using i) the daily TOC data and ii) the monitoring period mean daily TOC values, under cloud-free and snow-free conditions (albedo zero) with default aerosols. The year-by-year impact of variations in ozone on E-UV and UV-A doses is quantified as the relative deviation of the daily TOC derived data (i) to the monitoring period mean daily TOC derived data (ii) (Figure 8, TOC, E-UV). This analysis is independent of GUV measurements.

To explore the impact of surface albedo on yearly E-UV and UV-A doses, the yearly doses at all stations was modelled in libRadtran using iii) the daily surface albedo data and iv) the monitoring period mean daily surface albedo values, under cloud-free conditions and using the monitoring period mean daily TOC values. The year-by-year impact of variations in surface albedo on E-UV and UV-A doses is quantified as the relative deviation of the daily surface albedo derived data (iii) to the monitoring period mean daily surface derived data (iv) (Figure 8, albedo, E-UV). This analysis is dependent on the 380-nm UV-A channel of the

GUV instruments. It does not consider how clouds enhance the effect of albedo on the surface irradiance through multiple scattering between the cloud base and the ground.

Finally, the remaining impact of clouds and aerosols were estimated as the ratio of yearly measured E-UV and UV-A doses for real-sky-sky conditions to the doses modelled in libRadtran using the daily TOC data (i) and the daily surface albedo data (iii) under cloud-free conditions with default aerosols (Figure 8, clouds, E-UV). This analysis is dependent on both the 380-nm UV-A channel of the GUV instruments and the measured E-UV and UV-A doses.

The overall estimated impact on yearly E-UV and UV-A doses from the direct drivers of total ozone (Figure 8, ozone), surface albedo (Figure 8, albedo) and clouds including aerosols (Figure 8, clouds) are scaled to their period means to yield their relative contributions to the observed variations in measured E-UV and UV-A doses (Figure 8, sum).

Comparing the results across the different stations (Figure 8), impacts from variations in clouds are estimated to typically exert a stronger influence on yearly doses than variations in ozone and surface albedo alone. The cloud impacts are generally stronger at stations characterized by coastal or Arctic climates, such as Bergen (BRG, 60N), Finse (FIN, 60N), Andøya (AND, 69N), and Ny-Ålesund (NYA, 79N), in contrast to inland stations.

Interannual variations between dry and sunny or rainy summers like in 1997 and 1998, 2018, and 2020 however impacted inland stations to a comparable degree, if not more. An illustration of this is Landvik (LAN, 58N) during 1997 and 1998, where all three direct drivers interacted synergistically, leading to an additive effect that increased yearly doses in 1997 (+8%) and reduced them in 1998 (-17%).

The dry and sunny May and July 2018 was preceded by a winter with frequent cold spells, initiated by a Sudden Stratospheric Warming in late February (Knight et al., 2020). Surface albedo data retrieved from UV-measurements across Norwegian stations shows that the sunnier than normal conditions during spring caused a rapid fall in albedo. This had largest influence on the mountain station Finse (FIN, 60N). Effectively, the 18 days advancement in the timing of the snowmelt at Finse, as determined from surface albedo data retrieved from GUV-measurements, led to drop of -4% lesser in the yearly dose compared with a normal snow season. This was however more than compensated by the sunnier sky conditions, adding +10% to the yearly dose from reduced cloud conditions. Conversely, in 2020, the snow season was delayed 32 days (also based on retrieved surface albedo data), providing an albedo contribution to the yearly dose by +9% in addition to the +3% arising from the cloud contribution.

The impact of total ozone variations on yearly UV doses is generally within a few percent for most stations and years, as the period with the largest daily variations in total ozone and doses typically occur in early spring when the polar vortex is about to break up. The largest positive contribution to yearly E-UV doses was +6% in 2020 at Ny-Ålesund (NYA, 79N), attributed to the record cold and persistent polar vortex in spring 2020. Similarly, the years 1996, 1997, and 2011 showed positive anomalies of up to +3% at several stations. The most notable negative anomalies from yearly variations in TOC were observed in 1998, with the largest reduction in yearly E-UV doses of -6% at Landvik (LAN, 58N).

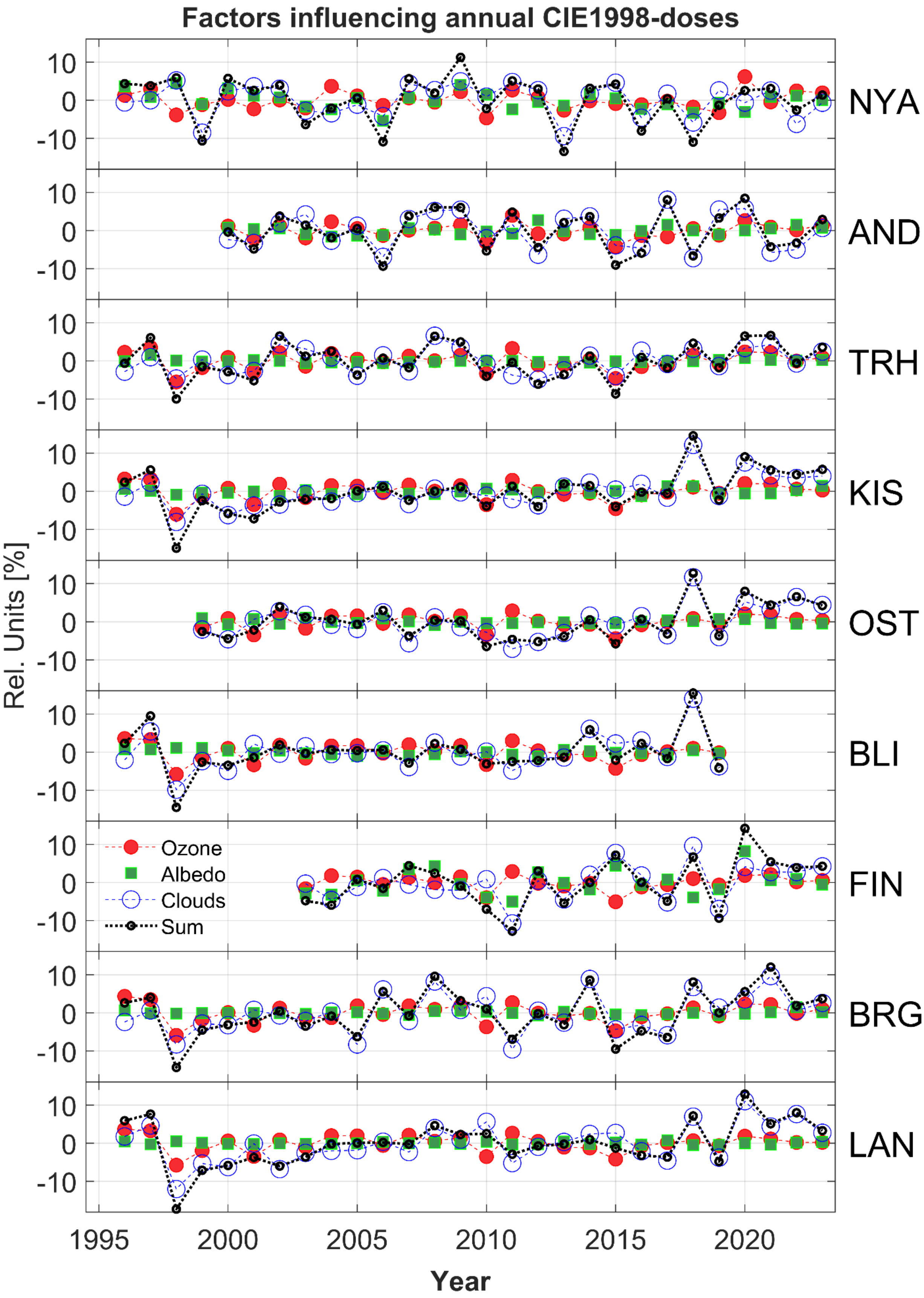

Figure 8 Variations in yearly E-UV doses (Sum) and contributions from yearly variations in total ozone, surface albedo and clouds, including aerosols. Analyses based on the libradtran radiative transfer model.

5.2 Yearly trends in direct drivers over the monitoring period

In the previous section we looked at variations in yearly E-UV doses and explored some estimated relative impacts from variations in total ozone, surface albedo, and clouds (Figure 8), without taking account of interactions of clouds with ozone and surface albedo. In the current section we will explore long-term trends in yearly E-UV and UV-A doses and accompanying trends in the direct drivers (Figure 9).

The linear trends in the estimated direct drivers of E-UV doses (Figure 9, ordinary least squares) show an overall picture where yearly E-UV doses for stations in the south increase by of +2% to +3% per decade in lowland areas, with the mountain station Finse (FIN, 60N) showing a higher increase of around +4% per decade. This trend diminishes as we move further north, with Trondheim (TRH, 63N) showing an increase in yearly E-UV dose of about +1% per decade. The trend continues to decrease with increasing latitude, becoming neutral at Andøya (69N) and finally reaching -1.5% per decade at Ny-Ålesund (NYA, 79N).

The linear trends in the estimated direct drivers of UV-A doses (Figure 10) present an overall pattern like that of the E-UV doses. However, positive trends in the south are less pronounced, while negative trends in the north are more substantial. UV-A trends are not influenced by trends in TOC because TOC has very low absorption in the UV-A part of the spectrum.

Confidence intervals (Figures 9 and 10) show statistically significant positive trends in E-UV and UV-A doses for stations Landvik (LAN 58N) and Kise (KIS 60N), while the negative trend in Ny-Ålesund (NYA 79N) is only statistically significant for UV-A doses. Because exceptional years have been more prevalent at the start of the monitoring period (e.g. 1997 and 1998) and towards the current day (e.g. 2018 and 2020), the ordinary least squares trend analysis is sensitive to these data points. The robust least squares analysis (Appendix 11.5 Fig 43) however shows similar features for most stations except Blindern (BLI, 60N) where the time series was terminated in 2019. This illustrates the impact of the special year 2018, but also the impact of the last 5-year period on the estimated trends in the direct drivers. The mean of yearly doses over the five-year period from 2019 to 2023 are up to +5% higher in the E-UV and up to +3% higher in the UV-A in southern Norway, compared to the means over the full monitoring period. In the Arctic, the mean over the last five-year period is +1% in the E-UV but -2% in the UV-A.

The ozone component (Figure 9) gives the smallest contribution of the direct drivers to trends in UV-doses, amounting to a change of less than 0.5% per decade for all stations, and often giving a negligible contribution. NILU (Svendby et al., 2023) has estimated annual trends in total ozone concentration per decade over Oslo (60N) to -5.9% (1.0% standard uncertainty) in the monitoring period from 1979-1997, and +0.4% (0.6% standard uncertainty) in the monitoring period from 1998-2023. The overall picture therefore suggests that the Montreal Protocol has been successful in stabilizing and gradually restoring stratospheric ozone levels over Norway.

The estimated impact of surface albedo trends on E-UV and UV-A doses is minimal for most stations. Some impact is observed at Finse (FIN, 60N) with a roughly +1% per decade increase in yearly E-UV and UV-A doses and Ny-Ålesund (NYA, 79N) with a roughly -1% decrease per decade. This is consistent with studies showing increased precipitation and higher temperatures in Svalbard (https://mosj.no/en/indikator/climate/atmosphere/air-temperature-and-precipitation/) and mainland Norway (Hanssen-Bauer et al., 2017), leading to delayed snow accumulation and earlier snowmelt. Surface albedo data from Ny-Ålesund, based on GUV-measurements, indicate a reduction in albedo and earlier spring melting, consistent with ongoing loss of Arctic sea-ice over the past 30-40 years and climate change projections for the 21st century (Zerefos, 2023).

The most pronounced factor influencing trends in yearly E-UV and UV-A doses is changing cloud conditions, including any possible trends in aerosol concentrations. Stations in the south show a net brightening of the sky (less clouds or aerosols), contributing +2% to +3% per decade to the yearly trends.

In contrast, northern stations like Ny-Ålesund (NYA, 79N) experience dimming from increased cloudiness (cloud thickening or increased cloud fraction and possibly also influence from aerosols), leading to a negative contribution to yearly E-UV doses of down to -0.5% per decade and to yearly UV-A doses of down to -2% per decade.

Bais et al. (2015) and Zerefos et al. (2023) provide a comprehensive review of global UVI trends and factors like ozone, aerosol amounts, clouds, and surface albedo for the periods 1955-1965 and 2010-2020. The findings for the Norwegian UV-network's sub-arctic/arctic locations generally align with these patterns, showing similar features such as meridional gradients in UVI trends, Arctic dimming from increased cloud attenuation and reduced surface albedo, and brightening at mid-latitudes in Europe due to less attenuation by clouds and aerosols.

A recent study by Dong et al. (2022) provides a physical explanation for the drivers and mechanisms behind these observed trends. They used atmospheric general circulation models (AGCMs) to simulate the effects of changes in sea surface temperature (SST), sea ice extent (SIE), greenhouse gas concentrations (GHG), and anthropogenic aerosol (AA) emissions on surface solar radiation (SSR) and cloud cover over the North Atlantic sector, including Europe. Their simulations indicate an increase in SSR and a decrease in cloud cover over Europe (35-60°N, 0-60°E), primarily attributed to reductions in anthropogenic aerosol emissions, with additional contributions from SST, SIE, and GHG changes.

The reduction in AA emissions has led to a decline in aerosol optical depth (AOD) and a shift in cloud microphysics, characterized by fewer but larger cloud droplets. This results in decreased cloud droplet number concentrations and increased droplet size, which effectively reduces cloud optical depth. Consequently, less solar radiation is scattered or absorbed by clouds and aerosols, enhancing surface solar radiation levels.

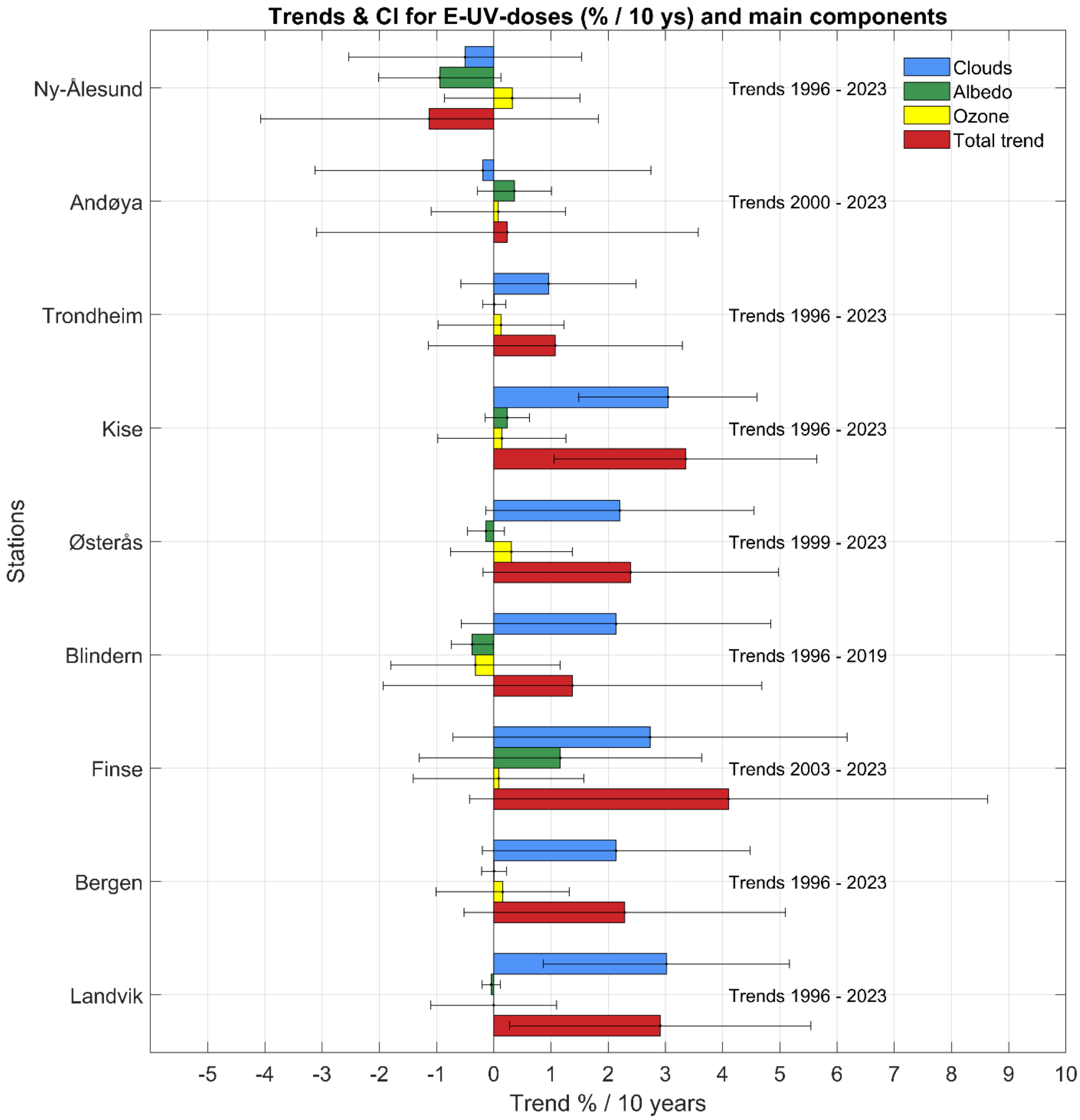

Figure 9 Linear trends in yearly E-UV UV-doses (% / 10 ys) for the UV-network locations, and their driving factors (total ozone, albedo, and clouds, including aerosols). Trends are based on linear regression. Error bars include 95% confidence intervals (CI). Note that trend periods differ for some stations due to shorter operation times. See also Figure 43 in Annex 11.5 for Robust regression fit.

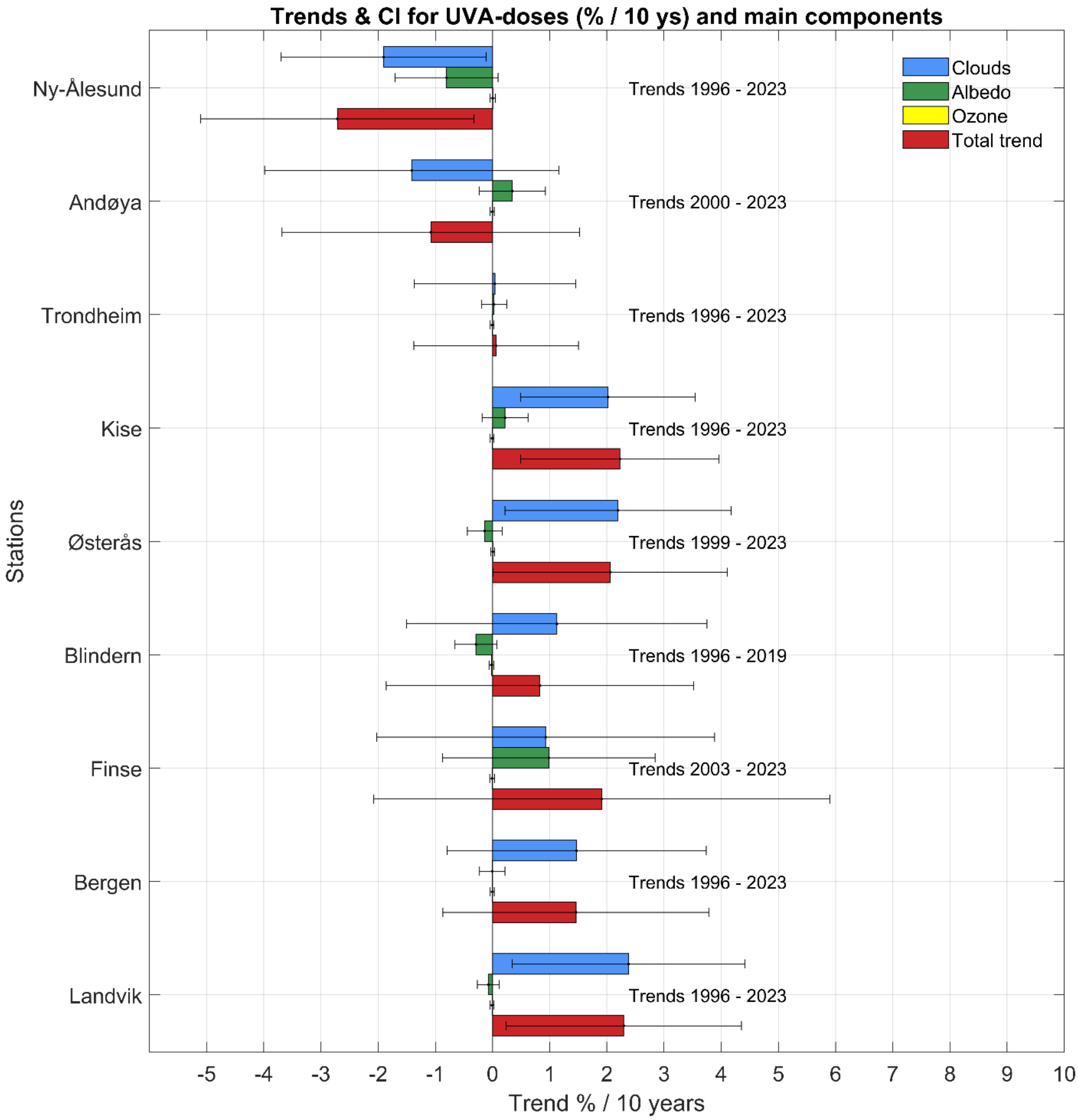

Figure 10 Linear trends in yearly UV-A UV-doses (% / 10 ys) for the UV-network locations, and their driving factors (total ozone, albedo, and clouds, including aerosols). Trends are based on linear regression. Error bars include 95% confidence intervals (CI). Note that trend periods differ for some stations due to shorter operation times.

5.3 Monthly trends: effective cloud transmittance (eCLT) at noon

Analyses of yearly E-UV and UV-A doses (Figures 9 and 10) show that clouds, including aerosols, are the most influential direct driver of surface UV levels, followed by surface albedo for stations experiencing a long winter season (NYA, 79N and FIN, 60N). Meridional gradients in long-term trends and drivers are also seen.

In the current section, we will examine the combined effects of variations in surface albedo, aerosols and cloud cover, expressed as the effective cloud transmittance (eCLT), to explore seasonal and meridional trends in more detail. The term eCLT, introduced by Dahlback (1996) and Svendby et al. (2021), is used as a measure of the cloud transmittance in the UV-A part of the solar spectrum, defined as the global irradiance under real-sky conditions, relative to the global irradiance under cloud-, aerosol- and snow-free conditions. Variations were assessed by analyzing anomalies in the monthly means of daily eCLT, centered one hour around local noon, relative to the period averages. The analysis utilizes real-sky measurements and simulated clear-sky measurements obtained with the 380-channel of GUV instruments.

Two examples are presented (Figures 11 and 12), illustrating anomalies in eCLT for the most geographically separate locations: Ny-Ålesund (NYA, 79N) and Landvik (LAN, 58N). Both locations exhibit biennial oscillations with characteristic 2–3-year periods, suggesting influences on weather systems from the well-known Quasi-Biennial Oscillation (QBO), a phenomenon where equatorial stratospheric winds shift between westerly and easterly phases and affects atmospheric circulation patterns globally. The amplitudes of monthly mean eCLT can vary notably, reaching up to ±50% during winter months and decreasing to approximately ±10% during summer months. The locations exhibit seasonal trends for the past 25-30 years, which far surpass long-term trends in yearly doses, e.g., April at Landvik (LAN, 58N), +10% per decade. Trends are downwards at both locations during winter months, but show distinct differences during the summer half, reflecting seasonal shifts in local climate patterns. In Ny-Ålesund (NYA, 79N), the downward trends make a temporal reversal in July and August, indicating a temporal brightening of the summer-sky, whereas Landvik (LAN, 58N) shows a marked brightening during spring- and autumn months which reverses to a slight dimming during July and August. Considering the cumulative influence of seasonal trends in eCLT on yearly doses, the net effect on yearly surface solar UV doses is a long-term brightening in the south and a long-term dimming in the north. The snow season is very short at Landvik (LAN, 58N) due to its milder winters, whereas in Ny-Ålesund (NYA, 79N), it lasts about nine months each year. A warmer climate, resulting in earlier snowmelt, as observed in the Arctic, may therefore intensify these meridional trends in eCLT and UV doses.

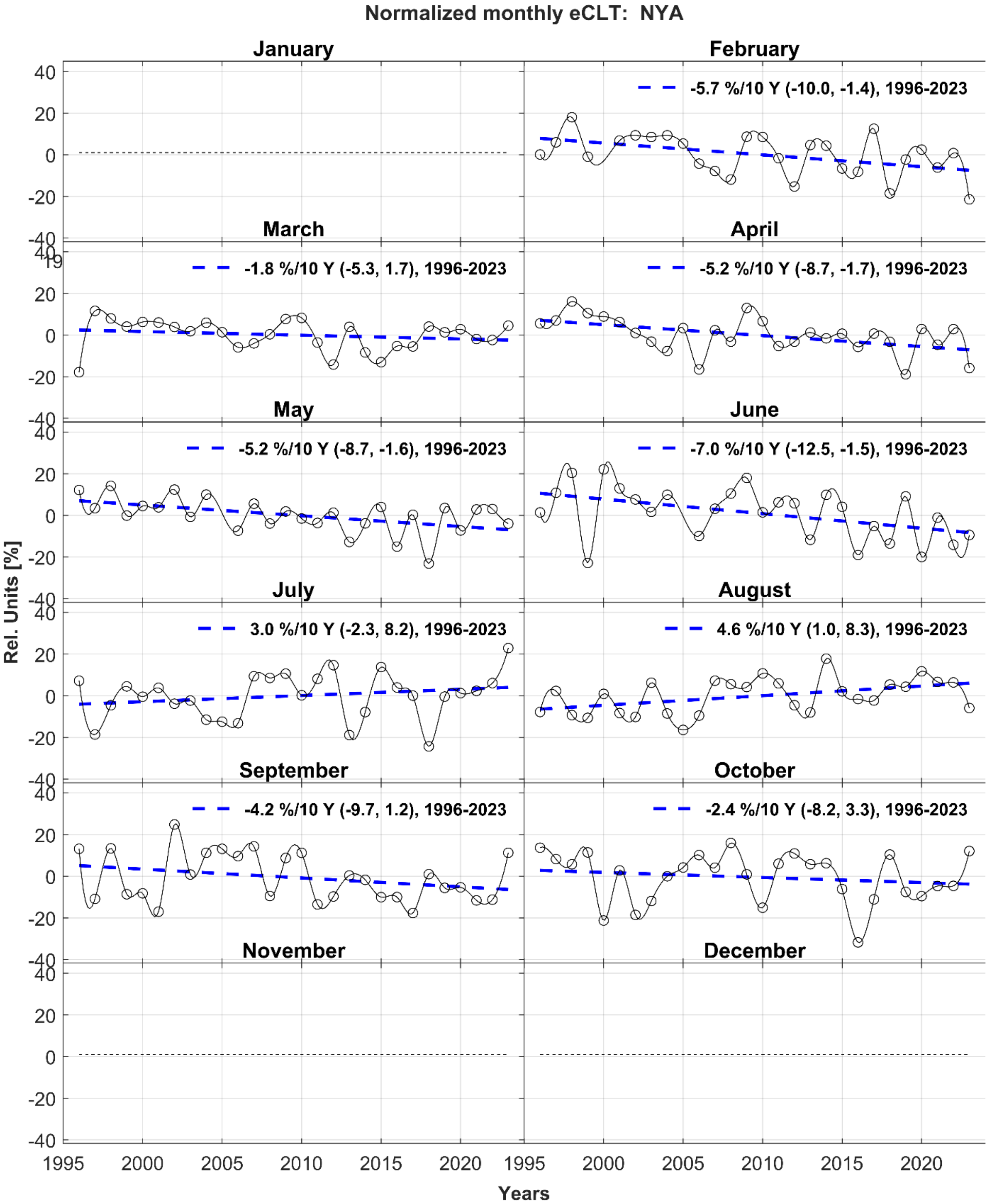

Figure 11 Variations in the monthly mean effective cloud transmittance (eCLT) at noon in Ny-Ålesund (NYA, 79N). The legend includes linear decadal trends, 95% confidence intervals in parenthesis, and the fitting period.

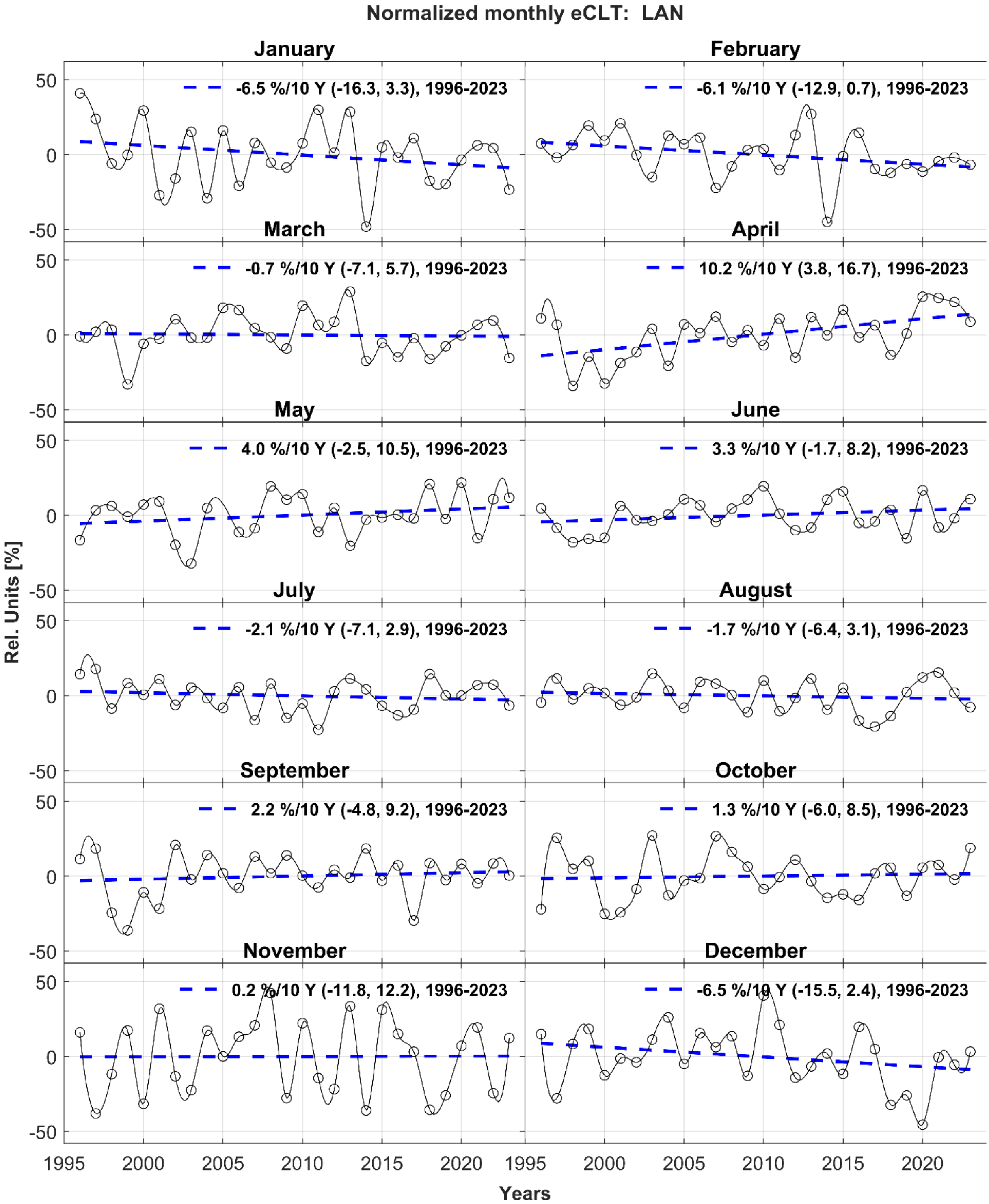

Figure 12 Variations in the monthly mean noon effective cloud transmittance (eCLT) at noon at Landvik (LAN, 58N). The legend includes linear decadal trends, 95% confidence intervals in parenthesis, and the fitting period.

5.4 Connecting monthly trends to direct drivers

This section investigates linear decadal trends (Figure 13) in monthly average E-UV and UV-A doses, effective cloud transmittance (eCLT) at noon, and total ozone (TOC), for the period the stations have been operating (approximately 1996-2023). UV doses and eCLT are based on GUV measurements, whereas total ozone (TOC) is based on TOMS/OMI satellite overpass data supplemented with ground-based ozone data (https://woudc.org/data/stations/) for the period in 1995-1996 where satellite observations are missing.

Trends in TOC (Figure 13) are positive (+1% to +3% per decade) from September to January and mixed during February to March. During the summer half, April to July, there is a shift towards smaller and generally negative numbers.

Comparing E-UV, UV-A, and eCLT (Figure 13), the seasonal trends are more pronounced than those observed for TOC, particularly during the early and late summer periods (April/June and August). Distinct seasonal and geographic patterns emerge across different locations, consistent with the earlier discussion in section 5.2. Stations in southern Norway show positive trends from April to June, linked to a decrease in cloudiness, including possible reductions in aerosol loads, while northern stations show negative trends, linked to enhanced cloud conditions, and reduced surface albedo due to earlier ice and snowmelt. These patterns begin to reverse in July, with a clear transition observed by August. During this period, Andøya (AND, 69N) and the southern stations experience increased cloudiness and/or aerosol loads, accompanied by higher precipitation (not shown here). In contrast, Ny-Ålesund (NYA, 79N) shows reduced cloudiness and/or aerosol loads, along with increased precipitation (also not shown here).

At Landvik (LAN, 58N) and Østerås (OST, 60N), eCLT increases by up to +10% per decade in April. In contrast, at the northernmost station, Ny-Ålesund (NYA, 79N), eCLT in April and May declines by -5% per decade, with the decrease intensifying to -10% per decade in June. During July and August, cloudier conditions dominate at all stations, except for Ny-Ålesund (NYA, 79N), which experiences a brightening trend. In contrast to the summer months, the winter period (DJF) exhibits greater variability in trends, likely reflecting the long-term changes in cloud cover and surface albedo.

Stations influenced by coastal climates, such as Bergen (BRG, 60N), Finse (FIN, 60N), Trondheim (TRH, 63N), and Andøya (AND, 69N), show distinct positive trends in January-February. In contrast, trends at inland stations are weaker or more variable. Notably, Landvik (LAN, 58N) stands out from the other stations, exhibiting distinct negative trends during these winter months.

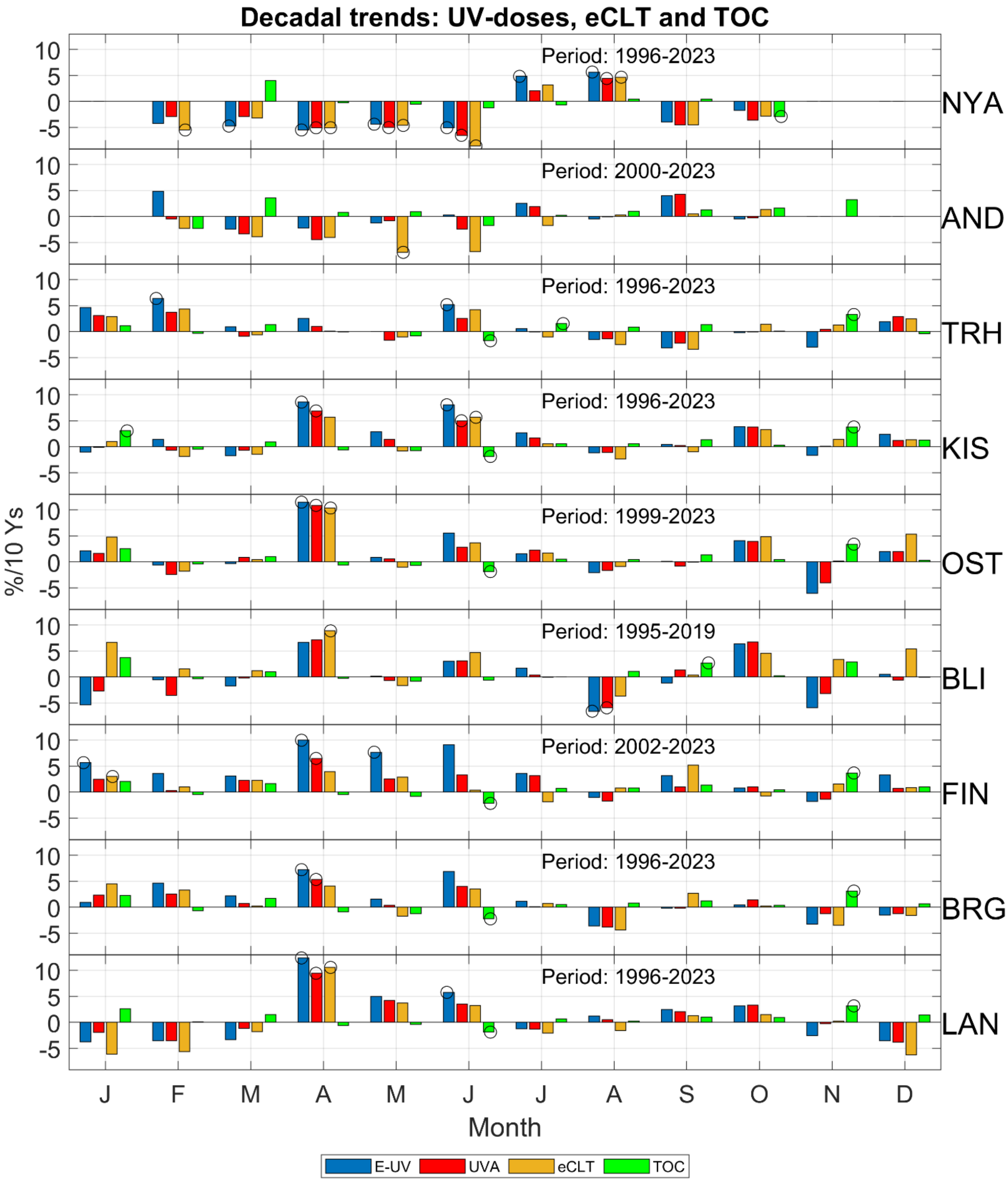

Figure 13 Decadal trends in monthly E-UV and UV-A doses, effective cloud transmittance (eCLT) and total ozone (TOC). Circles mark trends that are statistically significant at the 95% confidence level. Trends are based on robust linear regressions.

6 Interpreting trends in UV and environmental factors using histograms

The previous sections highlighted variations and trends in monthly mean eCLT (effective cloud transmittance) at noon. Interannual variations and seasonal trends were observed, along with a meridional (south-north) gradient. The eCLT includes the combined effects of clouds, aerosols, and surface albedo. Here we separate data gathered under cloud-free conditions from all-sky data to assess any long-term changes in cloud occurrence, surface albedo and transparency of the atmosphere. We explore whether changes may be related to general trends of brightening at mid-latitudes (Bais et al., 2015; Zerefos et al., 2023) and of milder and more precipitation-rich winters in Norway (Hanssen-Bauer et al., 2017).

6.1 Histograms of hourly mean eCLT grouped by month

Histograms of hourly mean eCLT grouped by month can clarify the contributions of these underlying factors to the observed trends in eCLT. An example is shown for July at Landvik (LAN 58N, Figure 14), comparing data from 1996, the initial year of operation, and 2023, the most recent year of operation. Data for solar elevation angles less than 5° were excluded to avoid obstructions caused by buildings and trees. The histograms reveal a bimodal distribution, characteristic for solar measurement data, with a distinct peak representing the transmittance of the sky under nearly cloud-free conditions. In this example, the peaks are at eCLT values of 0.94 and 0.92, respectively, indicating modest differences in the clear-sky transmittance between the first and last year of the monitoring period. Snow cover may shift the location of the peak, which allows an estimation of the regionally effective surface albedo. The location and width of the peak is slightly dependent on the presence of a thin cloud layer obscuring the sun, or on mixed sky conditions where the sun is unobscured while some parts of the sky have scattered clouds, but otherwise serves as a robust measure of the clear-sky transmittance because minor reductions of the direct beam become partly compensated by minor increases in the diffuse sky component.

To better identify the location of the clear-sky peak, the histograms were fitted with a bi-modal probability density distribution (PDF) consisting of two Beta-distributions, using the method by Assunção et al., 2003. A threshold of eCLT > 0.85 was set to separate the cloud-free peak from all-sky cases when estimating the relative sunshine hours per month.

The resulting eCLT value at the clear-sky peak of the histograms (Figure 15) for all months and years for e.g. station Landvik (LAN 58N) shows a pattern where winter months (October-March) exhibit pronounced downward linear trends and marked interannual variations. Trends in summer months (April-September) are on the other hand within ±0.4% per decade, corresponding to about ±1% change over the 28-year monitoring period.

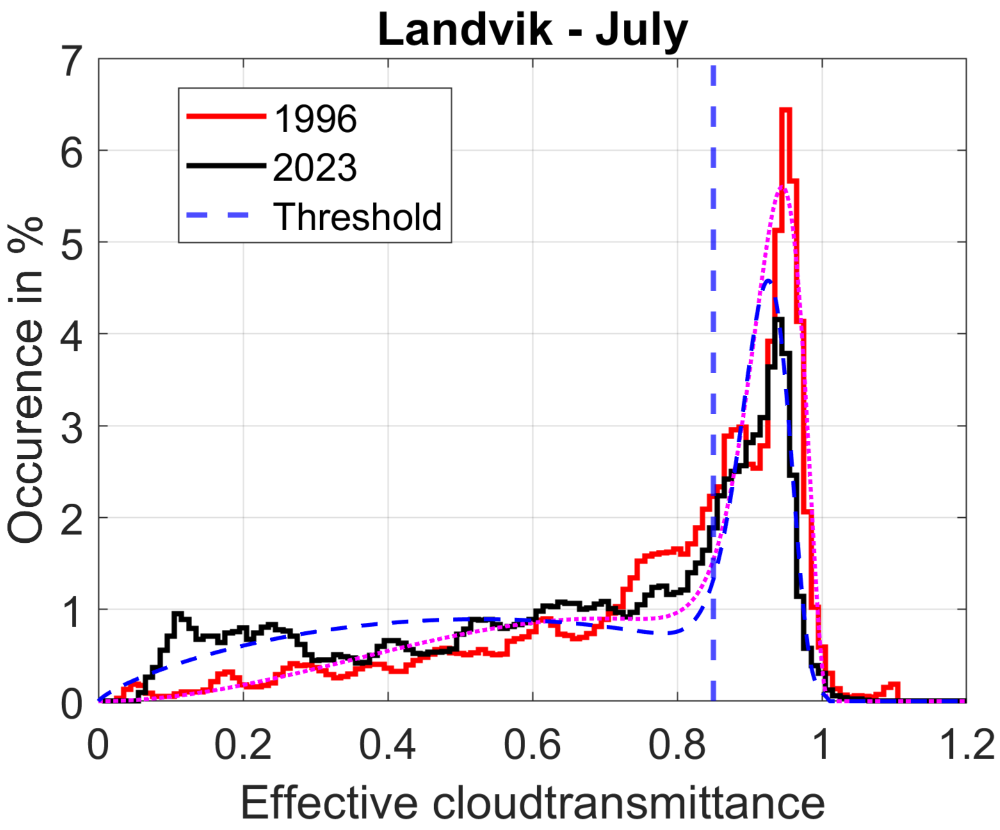

Figure 14 Histogram of hourly mean effective cloud transmittance (eCLT) in July in 1996 and 2023 at Landvik (LAN, 58N). The peaks at 0.94 and 0.92 correspond to almost cloud-free conditions. The threshold for separating overcast and cloud-free conditions is set to 0.85. Dashed curves are probability density fitting functions. Data is based on the 380-channel of GUV instruments.

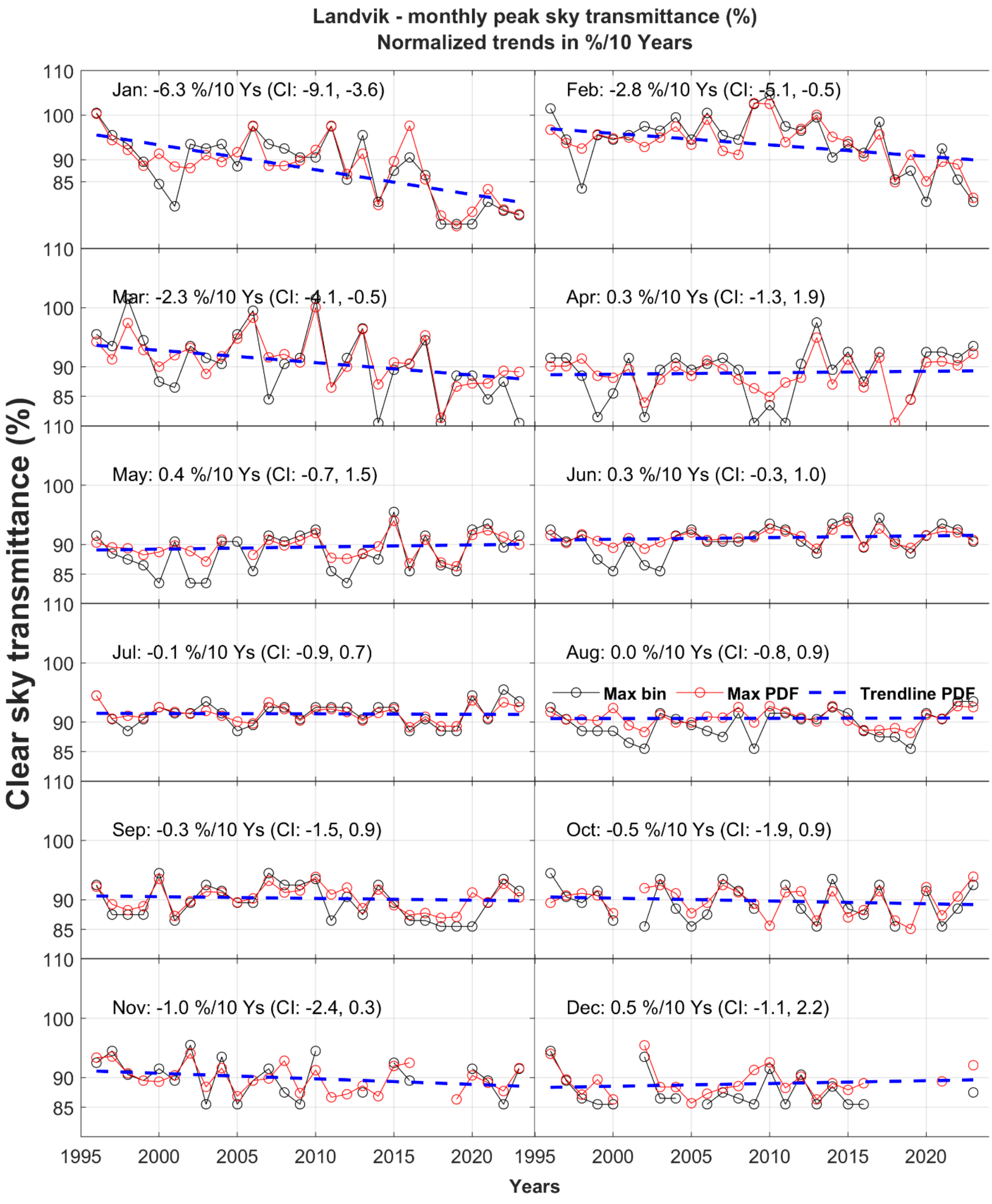

Figur 15 Histogram's peak locations representing nearly clear-sky conditions per year and month at Landvik (LAN, 58N). Black circles represent the histogram interval (bin) with the highest frequency of observations and red circles the peak of a probability density function (PDF) fitted to the histograms. Dashed blue line is a linear fit to the PDF-based peak locations (red circles). Subtitles show the decadal trend, with 95% confidence intervals in parenthesis. Missing data indicates months where a histogram peak could not be identified.

6.2 Trends in clear-sky transmittance

In this section, we focus on data gathered under cloud-free conditions to examine trends in atmospheric transparency through the clear-sky transmittance. Linear monthly trends in the eCLT value at the clear-sky peak for all stations (Figure 16) show that the southernmost station Landvik (LAN 58N) exhibits the most pronounced downward trends from January to March, with a maximum decrease of -6.3% per decade in January. The steep negative trend suggests long-term reductions in surface albedo, that could be interpreted as milder winters and increasingly more precipitation falling as rain rather than snow. Negative winter-trends are also seen for the northernmost station Ny-Ålesund (NYA 79N), with maxima in April (-1.3% per decade) and September (-1.4% per decade), which aligns with the general observations of earlier snowmelt in spring and delayed onset of snow accumulation in autumn in the Arctic. For the rest of the stations, winter months December-March exhibit weak positive trends.

In the summer months June-August the trends are also generally weak and positive (median 0.4% per decade) for the inland stations (KIS, 60N; OST, 60N; BLI, 60N), while trends for the coastal stations (LAN, 58N; BRG, 60N; TRH, 63N; and AND, 70N) range between -0.4% and 0.6% per decade, with a median value of 0.1% per decade. The generally very small and positive trends during summer months and snow-free conditions coincides with a declining trend in aerosol concentrations over Europe during the period since 2000 (Quaas et al. 2022). Mountain station Finse (FIN, 60N) exhibits a negative trend of -1.0 to -0.5% per decade during July and August. Finse is located near the Hardangerjøkulen glacier and may have experienced reduced surface albedo during summer months as result of accelerated deficit in area and mass balance of glaciers in mainland Norway since 2000 (Andreassen et al., 2020). Independently, a reduction in summer snow cover across the broader region surrounding the station may also have contributed to changes in surface albedo.

The observed trends in summer clear-sky transmittance from the UV data are small and of the same magnitude as differences in measured long-term drift between DSA and the manufacturer of the GUV instruments (BSI Inc). Independent data, e.g. on aerosols and snow cover, could be combined with the UV-data to further investigate trends in atmospheric transparency.

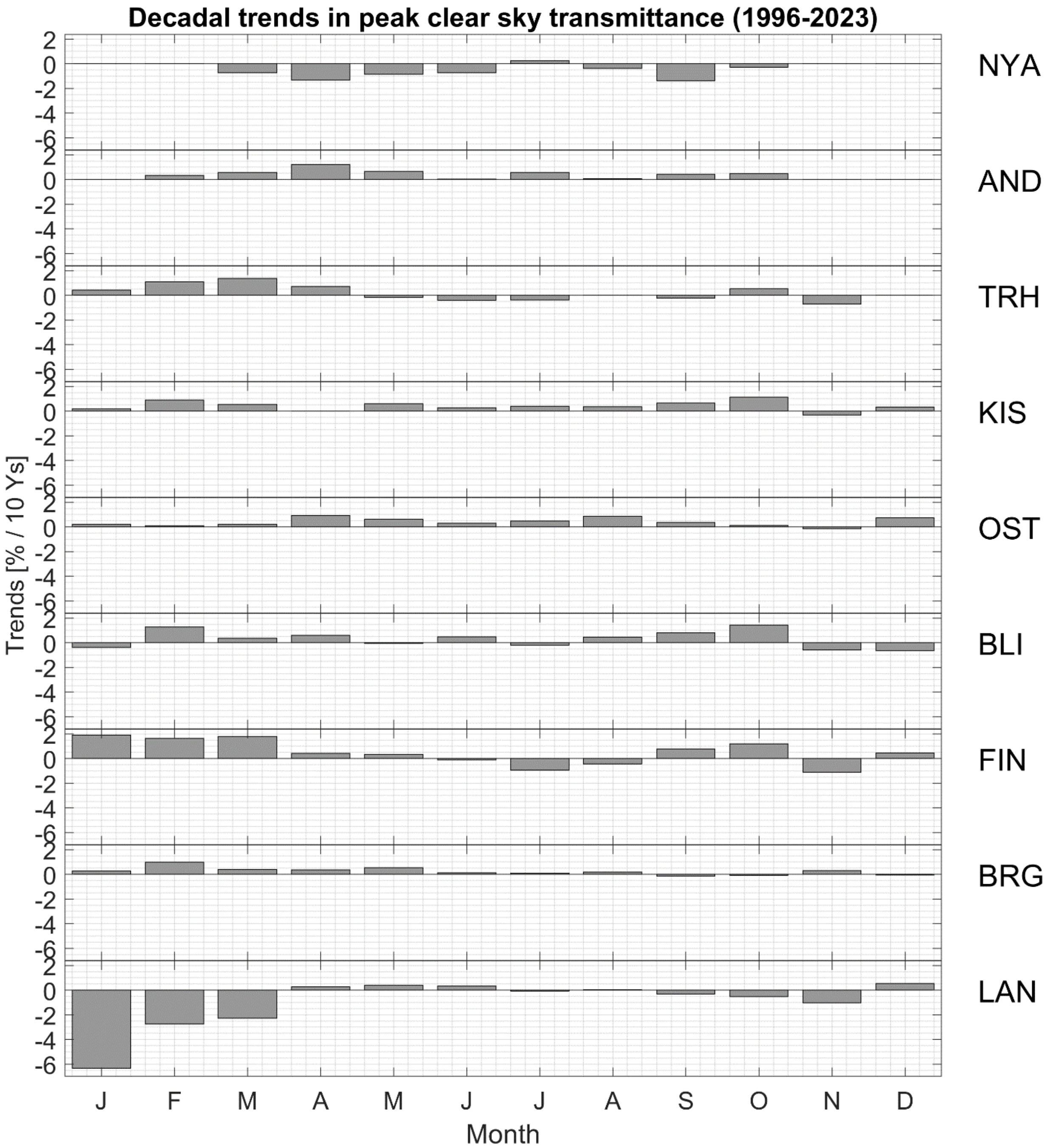

Figur 16 Monthly decadal trends in clear-sky transmittance at different stations for the period the stations have been monitoring. July and August are snow-free with exception of NYA and FIN, located near glaciers. Operation period for most stations is 1996-2023, with exception of AND (2000-2023), OST (1999-2023), BLI (1996-2019) and FIN (2003-2023).

6.3 Boxplots of monthly mean effective sky transmittance

The previous section provided an overview of the decadal trends in monthly mean clear-sky transmittances across various stations. In this section, we present boxplots (see Figure 17) to illustrate the seasonal distribution of monthly mean clear-sky transmittances. These boxplots highlight seasonal variability among different stations and demonstrate influences from surface albedo variations. Comparing seasonal variations, Finse (FIN, 60N) and Ny-Ålesund (NYA, 79N), influenced by their arctic winter climates exhibit the largest span in clear-sky eCLT, whereas Bergen (BRG, 60N) and Landvik (LAN, 59N), influenced by their mild coastal climates exhibit the smallest span. Year-to-year fluctuations in the timing of spring snowmelt and autumn snow accumulation may result in larger variability during these transition months compared to other times of the year. The lowest sky transmittance and interannual variability appear around August, where glaciers also have reached their minimum extent.

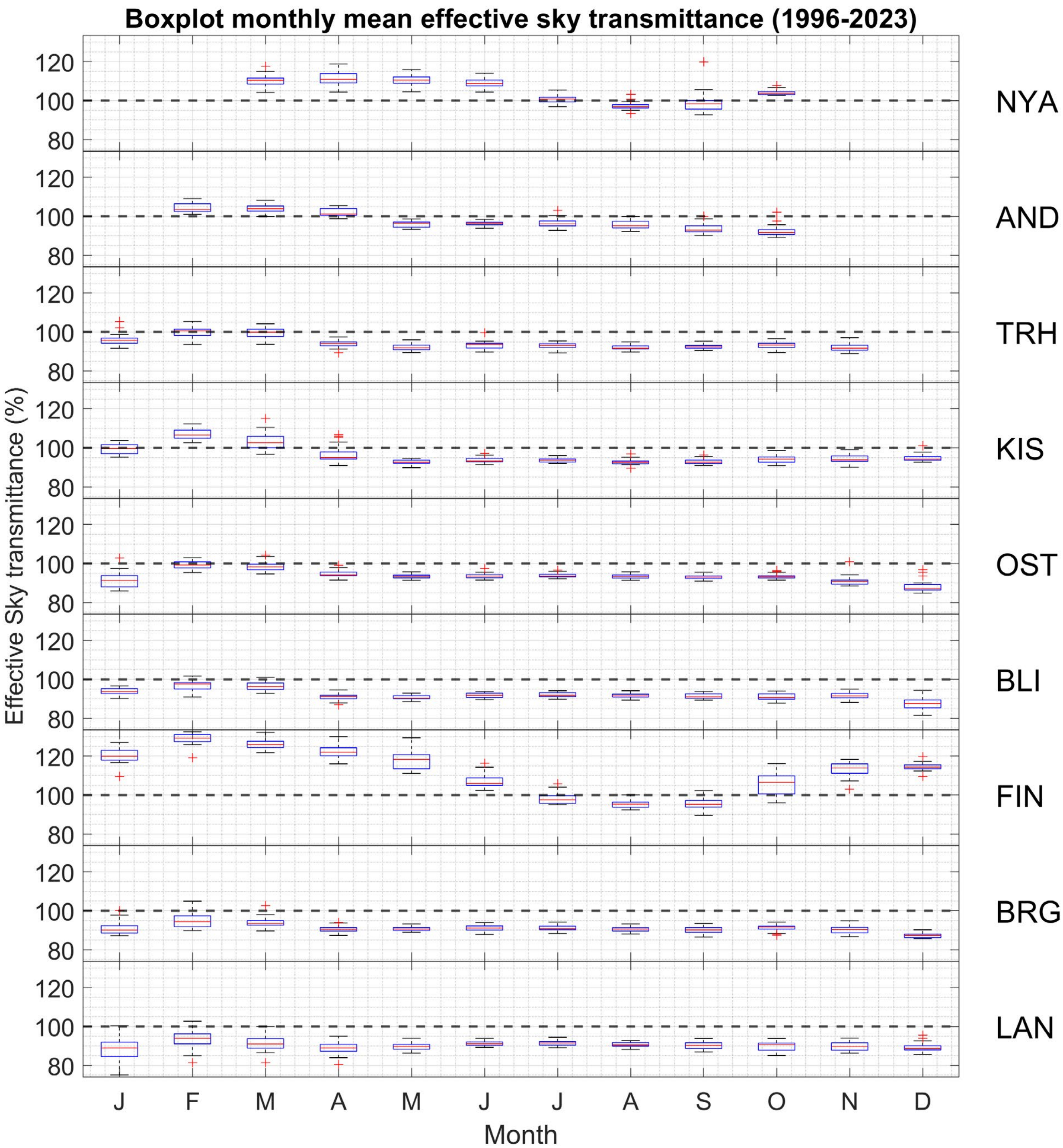

Figur 17 Boxplot of monthly mean clear-sky transmittance. Values are below 100% for snow-free conditions because the histogram peaks are influenced by stable, thin clouds and mixed sky conditions.

A comparison of the median monthly peak clear-sky transmittance (Figure 17) suggests that, for most stations, summer sky transmittance from June to August generally ranges between 91% and 93%, except for stations influenced by glaciers (FIN, 60N; NYA, 79N) and Andøya (AND, 69N), located on a mountain top island. The higher transmittance levels at Finse (FIN, 60N) and Ny-Ålesund (NYA, 69N) compared to lowland stations suggest enhanced surface irradiance from nearby glaciers and potentially lower aerosol loads due to their pristine locations. The elevated transmittance observed at Andøya (96%) may be influenced by similar factors, but in this case, it may involve cloud albedo contributing to a higher irradiance rather than surface albedo. From its observation station on top of the mountain station on Ramnan, located 380 meters above sea level, the instrument can observe the sky from above a layer of sea fog. The hypothesis is supported by frequent peaks in surface albedo during summer months, which can persist for 1-3 consecutive days—a phenomenon not observed at other network stations.

6.4 Surface albedo

In this section, we will derive surface albedo values from the clear-sky transmittances (Figure 17) and analyze seasonal distributions across the various stations. The transmittance data were first normalized to the lowest median monthly transmittance for the period July-September, where a minimum in seasonal albedo is expected. Unity transmittance now corresponds to the median summer albedo. A radiative transfer model (libRadtran) was used to create a look-up table for the enhancement in surface irradiance at 380 nm as a function of surface albedo. This table was normalized to the summer albedo value expected for each station, using the first quartile of surface albedo from OMI overpass observations during July to mid-September. Finse (FIN, 60N) exhibited the largest seasonal span in albedo values (Figure 18). A maximum surface albedo close to unity is observed in February, which then decreases to approximately 0.07 in August-September. The larger interquartile ranges in May and October highlight the interannual variability during the transitions between snowmelt and snow accumulation periods.

An overview of the derived surface albedo for all stations (Figure 19) illustrates how mountain stations Finse (FIN, 60N) and Arctic Ny-Ålesund (NYA, 79N) experience longer snow seasons and higher yearly surface albedo than other stations. Surface albedo zero (dashed lines) corresponds to non-reflective ground.

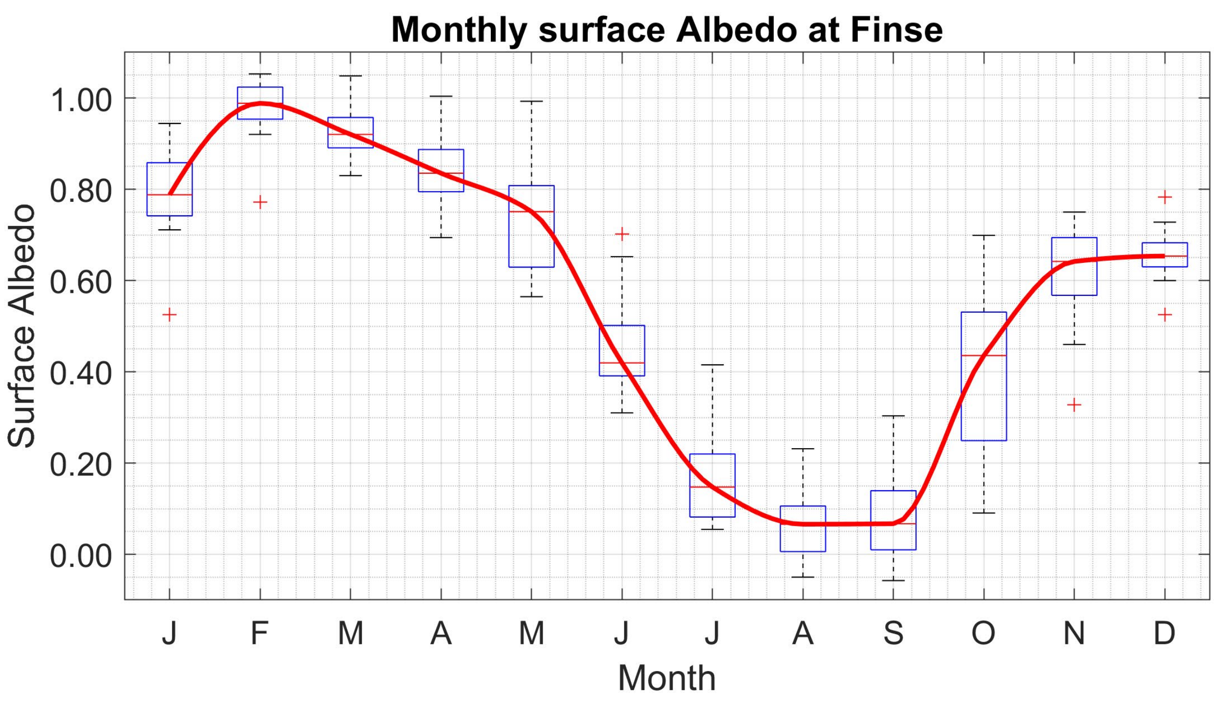

Figure 18 Boxplots of monthly mean surface albedo (380 nm) at Finse. Period 2003-2023. Red curve is the median for all years. Values are scaled to match the summer median surface albedo of satellite overpass data from the ozone monitoring instrument (OMI).

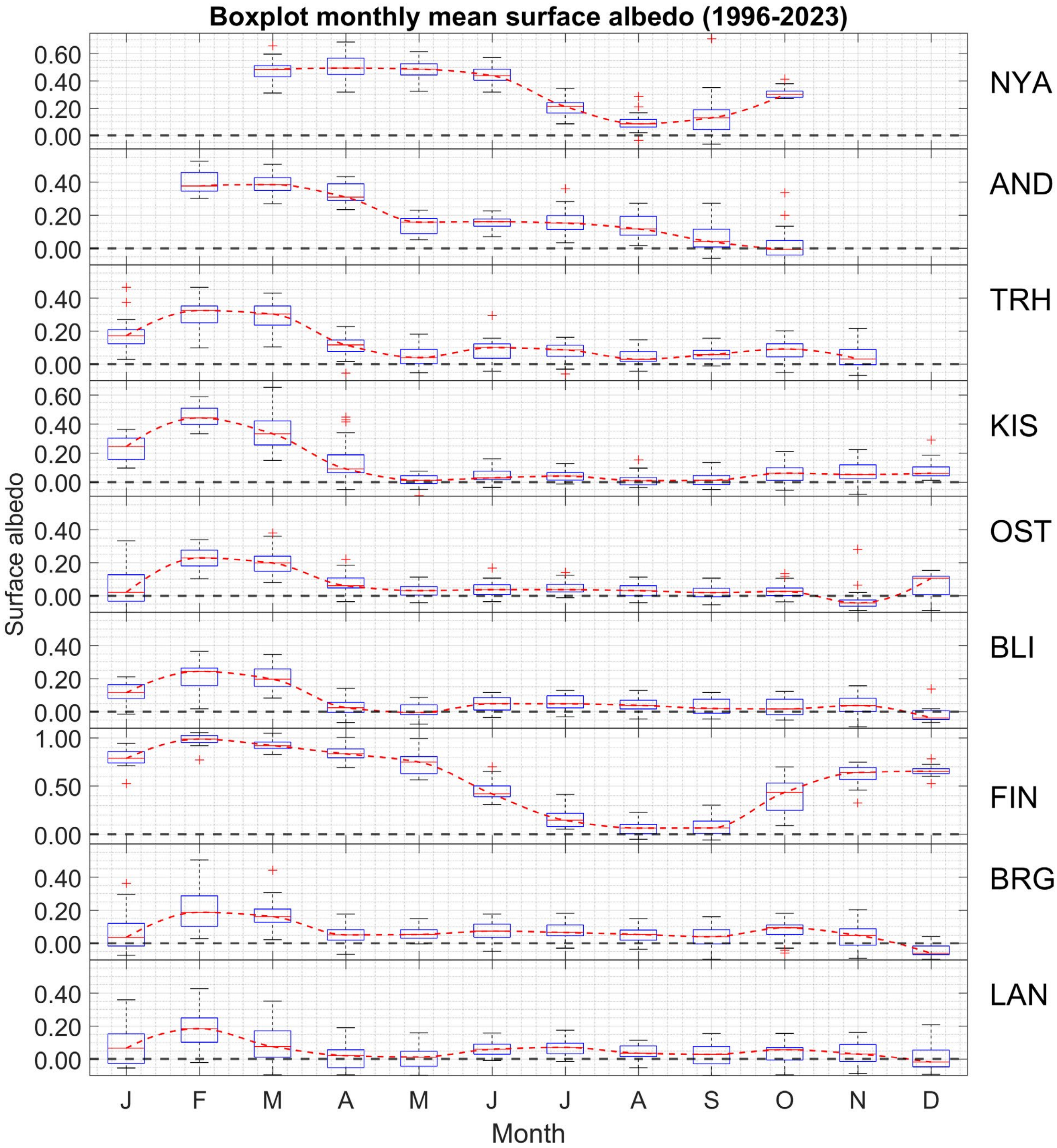

Figure 19 Boxplot of monthly mean surface albedo for all stations and period the stations have been monitoring. Note that the y-scales are different among different stations.

6.5 Trends in relative sunshine duration

The histograms of monthly effective cloud transmittance, eCLT, also allow for an assessment of relative sunshine durations (or cloud occurrence rate) and their associated trends. Monthly relative sunshine duration is estimated as the fraction of total sampling hours that exceed the threshold for clear-sky conditions (see Figure 14), eCLT > 0.85. For Landvik (LAN 58N), variations and trends in sunshine duration (Figure 20) closely follow the variations and trends in monthly mean eCLT at noon (Figure 12). This suggests that the yearly and monthly trends at Landvik observed over the past three decades (Figure 4,

Figure 12 and Figure 20) are primarily associated with an increase in the occurrence of cloud-free conditions. Additionally, there is a downward trend in regional winter surface albedo for this station, possibly linked to increased precipitation as rain during the winter season, and as discussed, a possible though statistically not significant increase in atmospheric transparency for most stations in the network (Figure 16).

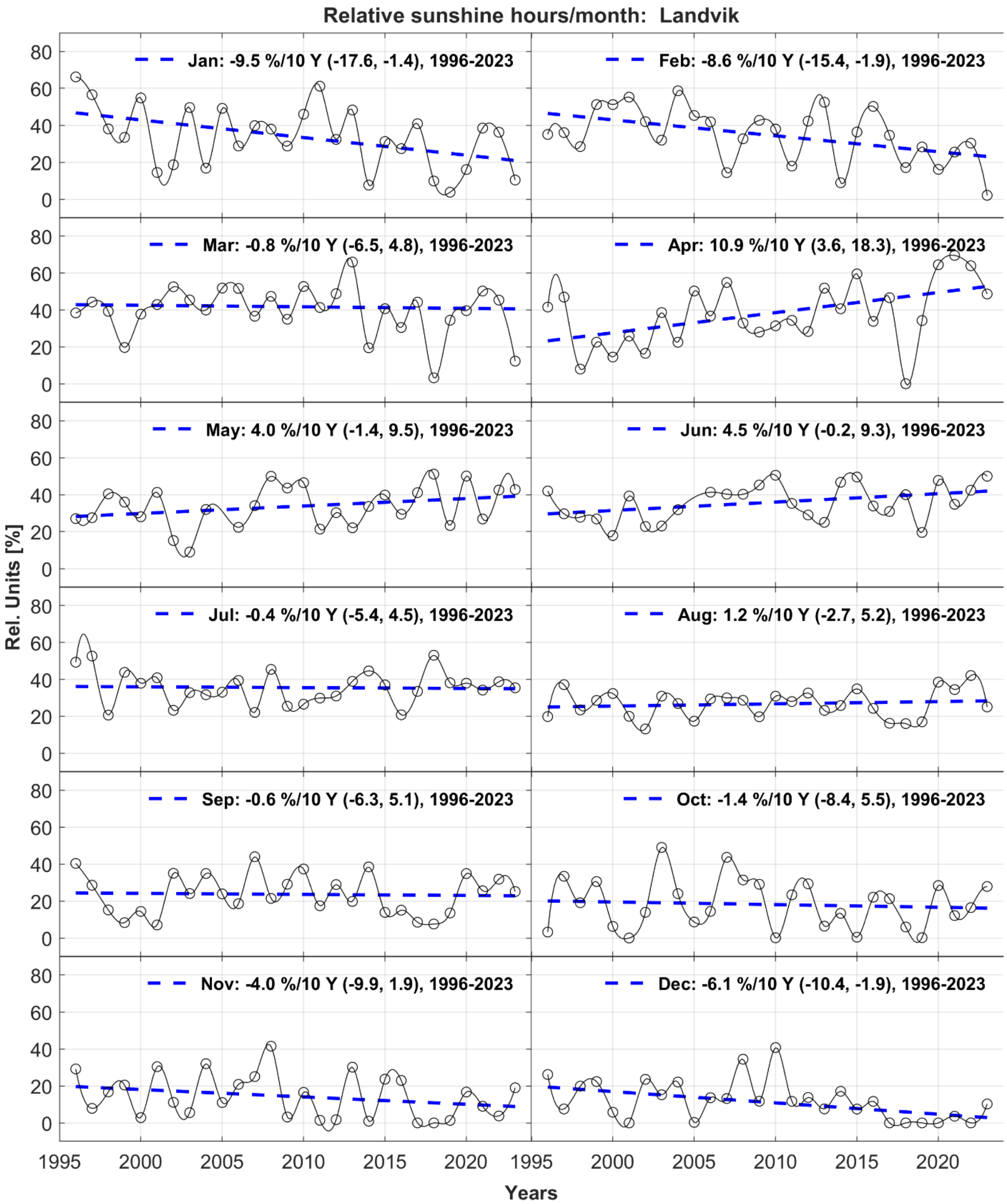

Figur 20 Variations in relative sunshine duration at Landvik (LAN, 58N), defined as the monthly fraction of hourly eCLTs exceeding the threshold for cloud-free conditions, relative to all-sky cases (see Figure 16). Legends denote linear decadal trend, confidence interval and period of yearly data. For comparison with trends in in noon monthly mean eCLT see Figure 14.

7 Linear correlations with climate systems

Previous chapters have investigated trends in the direct drivers of surface irradiance (clouds and aerosols, total ozone and surface albedo). These direct drivers are influenced by atmospheric circulation systems, coupled with ocean systems, that modulate wind, temperature, cloud and precipitation patterns, with a period that may differ from the yearly solar cycle. In the current chapter we will explore linear correlations between monthly mean surface UV doses and some large-scale circulation systems that may influence the cloudiness, surface albedo and TOC in Europe, including Norway.

7.1 Correlations between monthly mean UV-doses and NAO/AO indices

We will start with the North Atlantic Oscillation (NAO) (Hurrell et al., 2003) and the Arctic Oscillation (AO) (Spaeth and Birner, 2022; Thompson and Wallace 1998), which are indicators of the cyclonic activity in the North Atlantic and Arctic Oceans and adjacent continents. Data of NAO and AO indices were supplied by the Climate Prediction Center at NOAA. Looking at monthly tabulated data, NAO and AO indices are correlated (Jan 1995 to Dec 2023: A time series linear model (TSLM) of the Arctic Oscillation (AO) as a function of the North Atlantic Oscillation (NAO) showed a strong relationship, with an R^2 of 0.36 (adjusted $R^2 = 0.36$), $F(1, 346) = 197$, $p < 2.2 \times 10^{-16}$. We also observe that temperature and precipitation measured locally at the UV-monitoring station (data downloaded from https://seklima.met.no/) correlates with NAO/AO indices (Appendix 11.4, Figure 41), and that measured UV-A doses exhibit moderate to strong correlations with the locally measured temperature and precipitation (Appendix 11.4, Figure 42). Over the UV-monitoring period, the NAO has predominantly remained in a positive phase during winter months (1990‑2020) and in a negative phase during summer months (May‑August) from 2000 to 2020 (Appendix 11.3, Figure 40). The coupling between surface UV radiation and macroscale circulation patterns like NAO and AO was first studied by Čížková et al. (2018), analyzing UV measurement data from Hradec Králové (Czech Republic). Their results suggested that days with high E-UV doses occur most likely during the positive phase of NAO, when the subtropical high-pressure system located near the Azores islands extends its influence toward central Europe.

In the first step of examining linear correlations, we compare time series of UV-A dose variations (expressed as relative deviations of monthly means from the long-term monthly average) with the NAO and AO indices. To capture potential lagged responses, we treat the indices as drivers and apply a time shift to align them with the UV-A response before performing linear cross-correlation. All time series are smoothed using a 3- or 6-month running mean.

To assess how proximity to the ocean influences cloud climatology, we select a coastal station (BRG, 60N) and an inland station (KIS, 60N), located approximately 500 km east of the coast (Figures 21-24).

Bergen (BRG, 60N) exhibits peaks and troughs in UV-A that are distinctively anticorrelated with peaks and troughs in NAO indices and, even more strongly, with the AO indices, suggesting a strong connection between the winter cyclonic activity over the Atlantic and Arctic Oceans and local cloud cover at this coastal station (low-pressure associated with more clouds and vice versa). In contrast, these patterns are less pronounced for Kise (KIS, 60N), where peaks and troughs exhibit phase shifts, with a predominantly positive and statistically significant correlation, reflecting the combined effects of oceanic and inland, continental cloud climates.

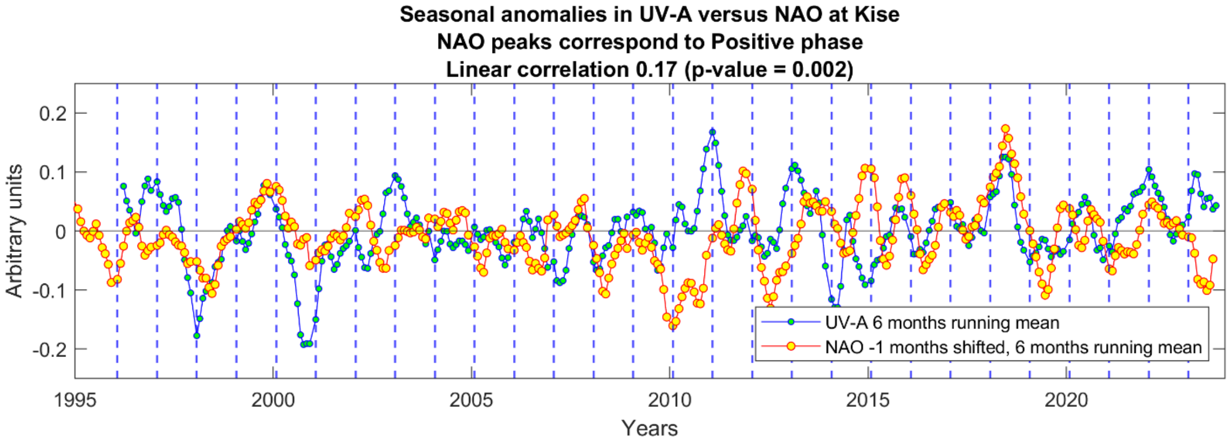

Figure 21 Seasonal anomalies in surface UV-A doses and the North Atlantic Oscillation (NAO) at station Kise (KIS, 60N). NAO data has been shifted -1 month and both time series smoothed applying 6 months running mean.

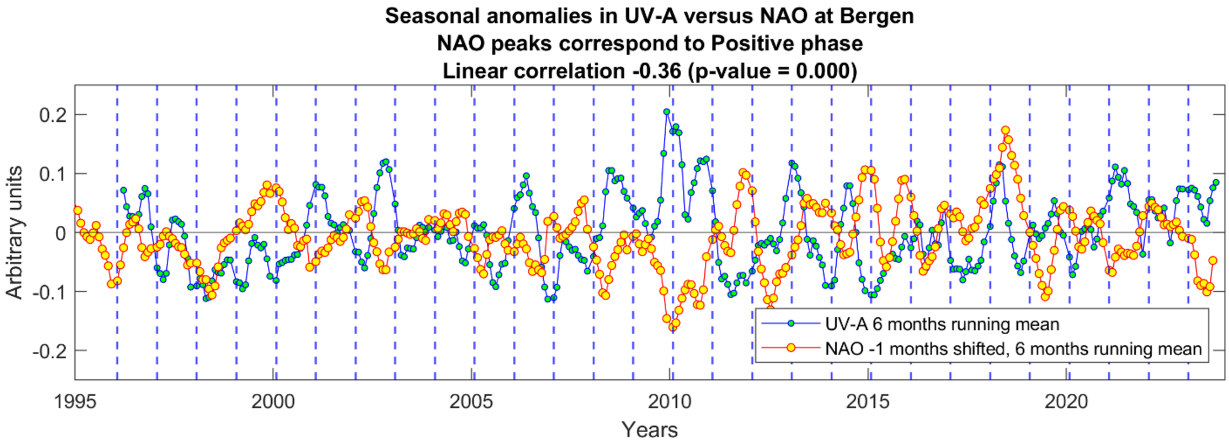

Figure 22 Same as the above figure, but for the coastal station Bergen (BRG, 60N).

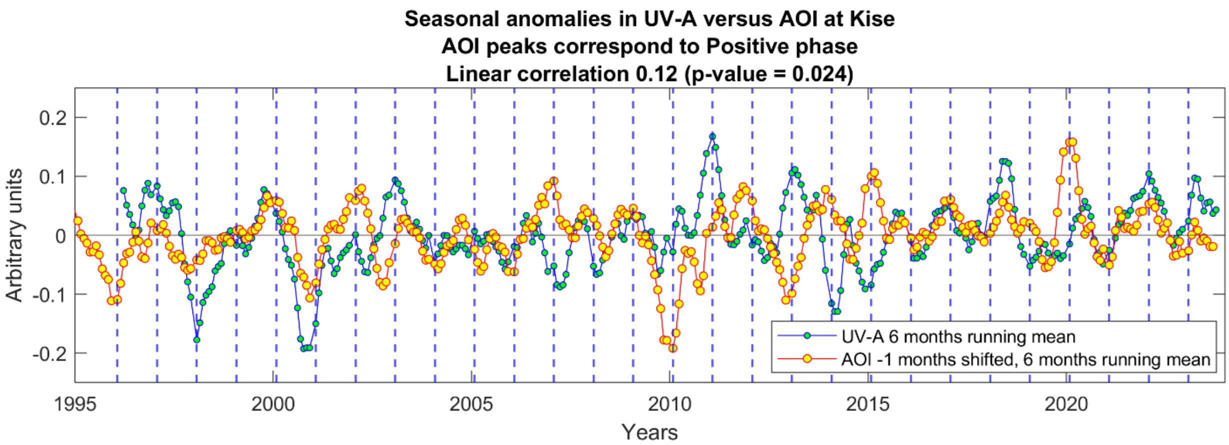

Figure 23 Seasonal anomalies in surface UV-A doses and the Arctic Oscillation (AO) at station Kise (KIS, 60N). AO data has been shifted -1 month and both time series smoothed applying 6 months running mean.

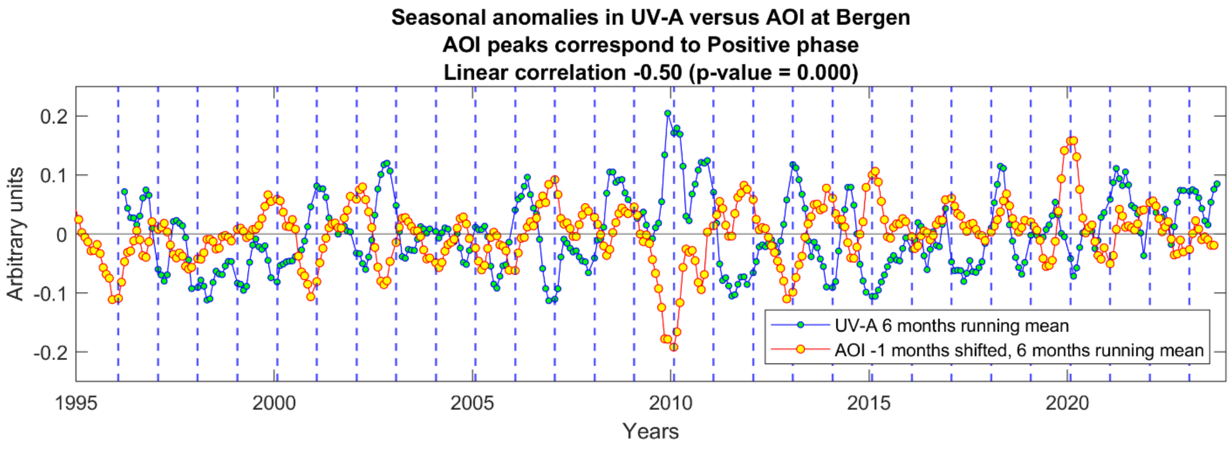

Figure 24 Same as the above figure, but for the coastal station Bergen (BRG, 60N).

In the next step, we examine seasonal patterns in the linear correlations between monthly E-UV doses and NAO/AO indices across different locations (Figure 25). The two coastal stations, Bergen (BRG 60) and Trondheim (TRH, 60N), exhibit strong negative correlations during winter (September-March), whereas the other stations only show weak negative correlations during winter months. A marked shift is seen during summer months (April-August): the three inland stations (BLI, OST, KIS, 60N) and the southernmost station (LAN, 58N) exhibit positive, moderate to strong correlations, in contrast to the two northernmost stations (AND, 69N, NYA, 79N) which continue to exhibit the negative, moderately strong correlations for winter months. The coastal station Bergen (BRG, 60N) and mountain station Finse (FIN, 60N) show only weak correlations of E-UV doses with NAO/AO indices during summer months, whereas the coastal station Trondheim (TRH, 63N) exhibits a transition between the positive summer correlations of inland stations and the negative summer correlations of stations in the north. The meridional pattern seen in summer correlations align with the meridional pattern seen in pairwise correlations in yearly E-UV and UV-A doses, which may also be expected considering that yearly E-UV doses are predominantly affected by the cloud climatology of summer months.

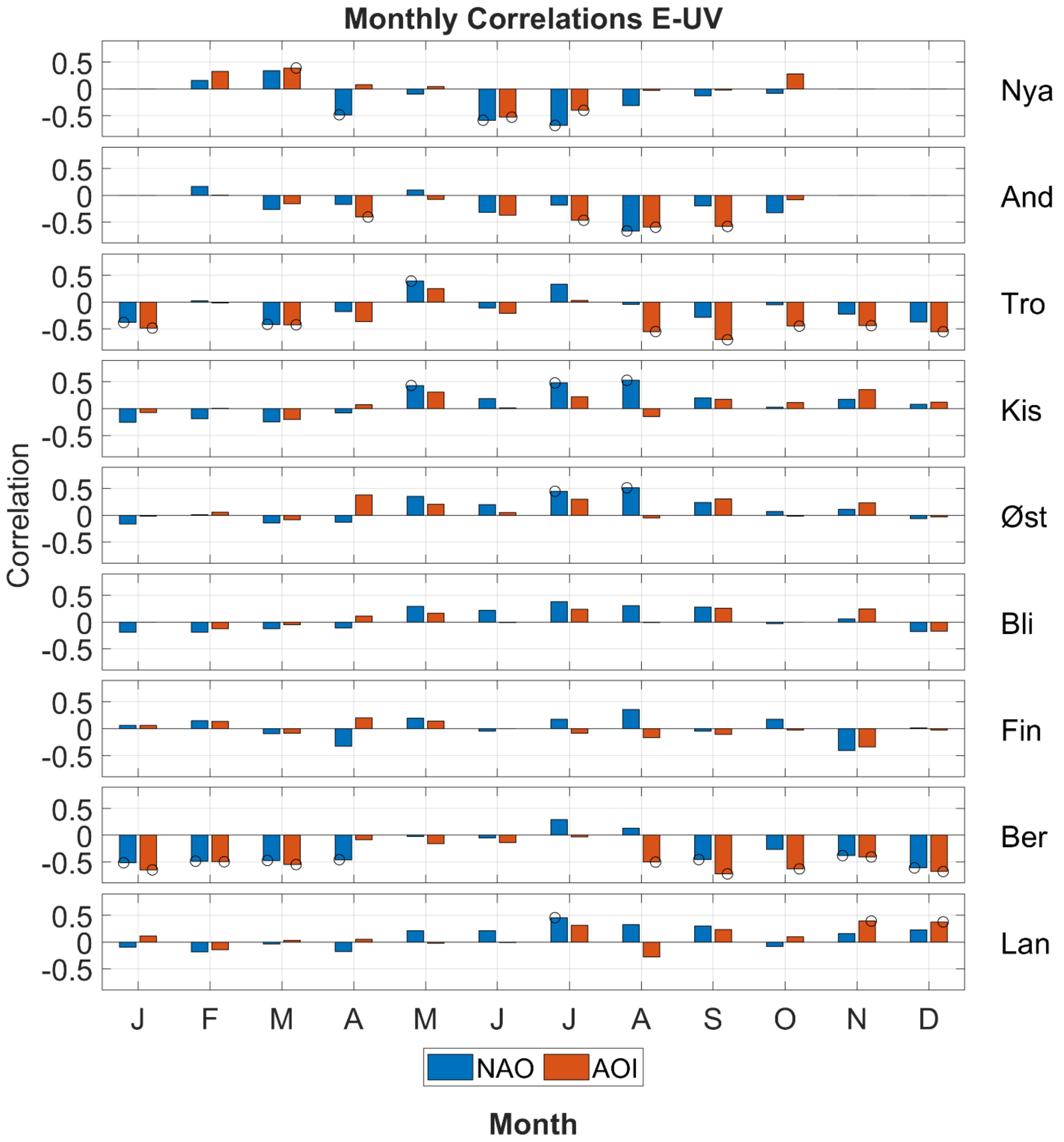

Figure 25 Correlations between monthly E-UV doses and the North Atlantic Oscillation (NAO) and the Arctic Oscillation (AO). Circles mark linear correlations that are statistically significant at the 95% confidence level.

7.2 Correlations between TOC and the QBO

In this section, we examine the correlation between the Quasi-Biennial Oscillation (QBO) and Total Ozone Column (TOC), using satellite overpass data from TOMS and OMI, as well as surface UV doses measured at different UV stations. For this analysis, we utilized the QBO 30 mb zonal wind at the equator, calculated as a zonal average by the Physical Sciences Laboratory (NOAA). We start with comparing TOC data for Kise (KIS, 60N) and anomalies in QBO (figure 26). The QBO data were shifted 6 months to align the two series, which may be interpreted as a time lag between alternations of the QBO wind directions above equator and changes in ozone transport to higher latitudes. Correlations between QBO and TOC overpass data at Kise (KIS, 60N) indicate that the easterly (negative) phase of the QBO is associated with enhanced TOC and enhanced efficiency of transport of ozone rich air from the equator to higher latitudes, and vice versa for the westerly (positive) phase of QBO. Both time series exhibit an oscillation with a period of approximately

28 months, while the TOC data also reveal a shorter oscillation, closely aligned with the 12-month annual solar cycle.

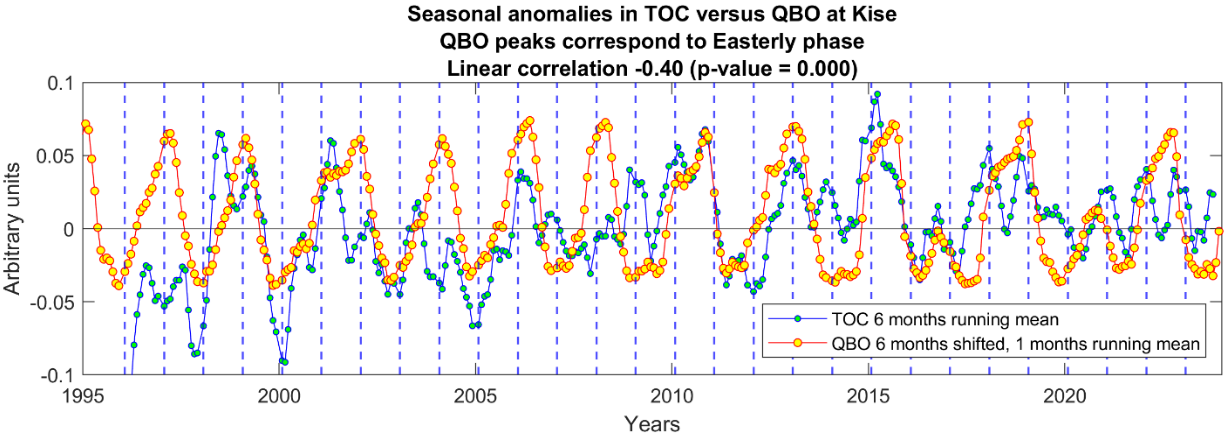

Figure 26 Anomalies in monthly mean total ozone, TOC (from monthly period means), based on TOMS and OMI satellite overpass data for Kise (KIS, 60N), versus the Quasi-Biennial Oscillation (QBO) zonal wind speeds in the tropical stratosphere. QBO data was shifted 6 months and scaled. The QBO in the plot has been inverted (signs flipped) for better visibility. TOC data was smoothed using a 6-month running mean. The period of stratospheric TOC variations generally aligns with variations in the QBO.

7.3 Correlations between monthly mean E-UV doses and QBO

Comparing surface E-UV and UV-A doses at Kise (KIS, 60N) with QBO (Figure 27 and 28), the peaks and troughs in surface data exhibit a cycle length close to the 12-month yearly cycle, compared with the approximately 28-month cycle of the QBO and TOC. In previous chapters we have shown that surface UV over the monitoring period is primarily affected by tropospheric weather systems (clouds), while QBO and TOC are components of stratospheric circulation. The impacts of QBO on weather systems in the troposphere is indirect and varies with the QBO phase.

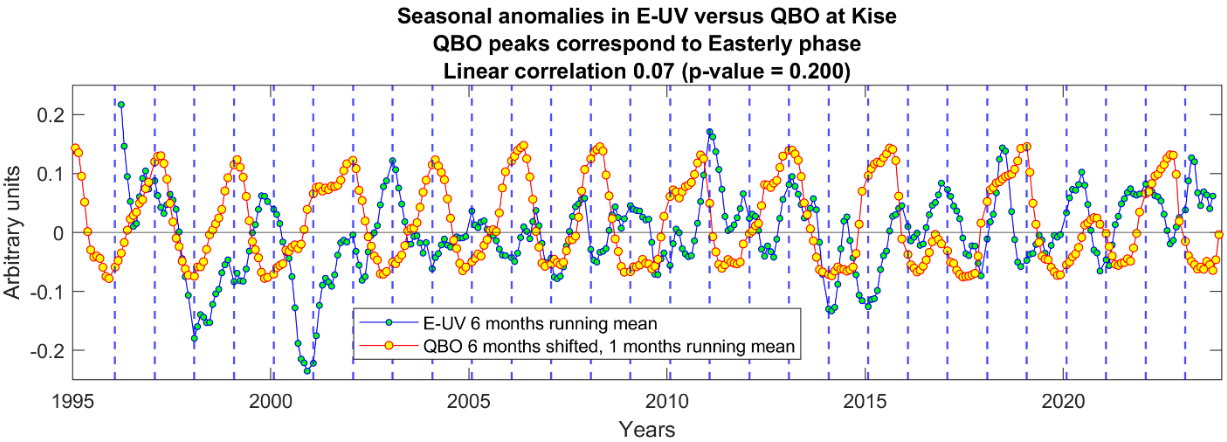

Figure 27 Anomalies in monthly mean surface E-UV doses (from monthly period means) at Kise (KIS, 60N), versus the QBO. QBO data was smoothed, scaled and inverted (signs flipped). E-UV data was smoothed using a 6-month running mean. The period of surface E-UV is shorter than that of QBO, aligning more closely with the yearly solar cycle.

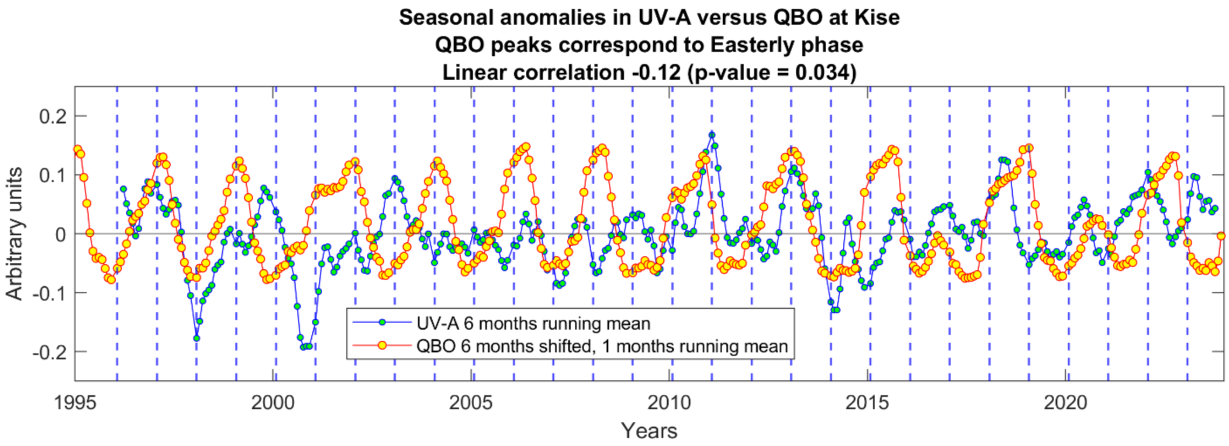

Figure 28 Same as figure above, but for UV-A at Kise (KIS, 60N).

7.4 Correlations of monthly mean E-UV dose with TOC

Surface E-UV is primarily influenced by solar elevation, clouds, aerosols, TOC, and surface albedo. These factors can have different impacts at an Arctic location like Svalbard compared to a station in southern mainland Norway. During the winter months, Ny-Ålesund (NYA, 79N) is typically within the polar vortex, which restricts the influx of ozone-rich air from the tropics. In contrast, Kise (KIS, 60N) usually remains outside the vortex, except during periods when the vortex is exceptionally strong and extensive or during the seasonal vortex breakup. Time series of TOC anomalies from satellite overpass data (Figure 29 and 30) reveal that Ny-Ålesund exhibits much stronger seasonality than Kise. Additionally, some winters, such as 1997/98, 2010/11, and 2019/20, show exceptionally low TOC at the Arctic location. Concurrent surface E-UV anomalies show distinct anticorrelations with TOC at both locations, with a stronger relationship observed at Ny-Ålesund than at Kise.

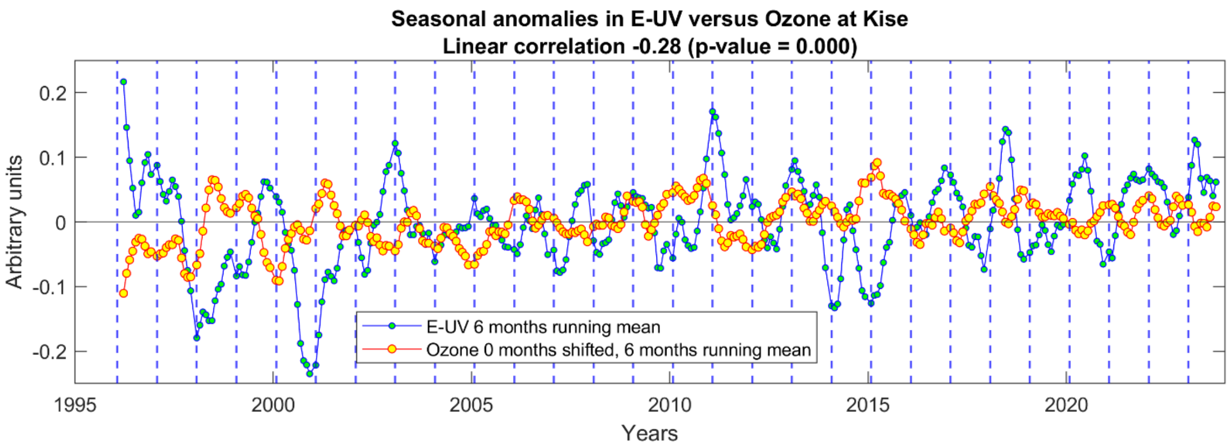

Figure 29 Anomalies in surface E-UV at Kise (KIS, 60N) and anomalies in TOC from satellite overpass data (TOMS and OMI).

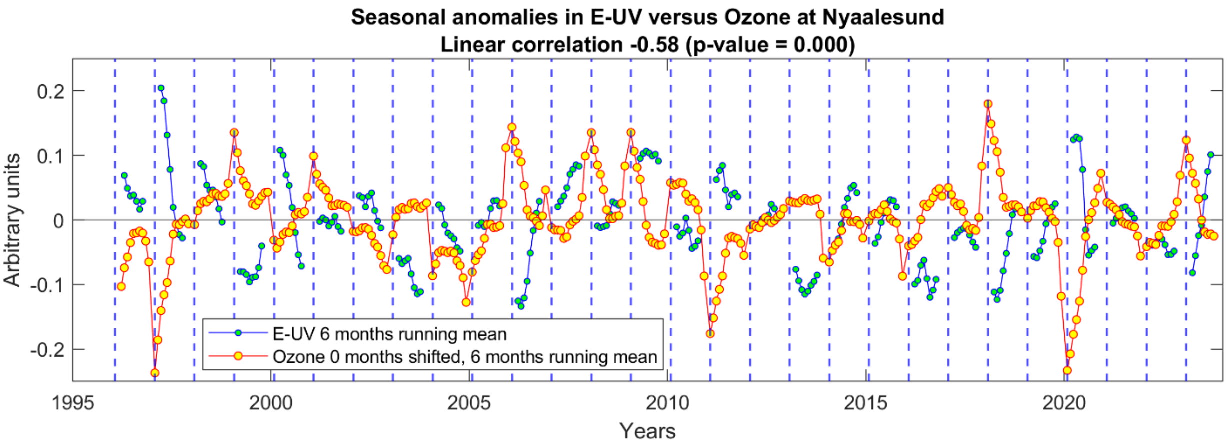

Figure 30 Anomalies in surface E-UV at Ny-Ålesund (NYA, 79N) and anomalies in TOC from satellite overpass data (TOMS and OMI).

7.5 Correlations of monthly mean UV-doses with variations in solar activity

The Solar Cycle is represented by the F10.7 cm solar radio emissions as a proxy for solar activity, which affects solar energetic particles (like protons and electrons) and modulates cosmic rays reaching the Earth. Energetic particles and cosmic rays may reach the lower stratosphere and upper troposphere in polar regions, ionizing air molecules. It is debated if variations in the solar activity may alter the production of cloud condensation nuclei, potentially affecting the cloud cover in polar regions (Carslaw et al., 2002; Seppälä et al., 2014). There are no evident correlations of monthly mean UV doses with the solar activity in the Norwegian network data at any lag times (Figure 31): any such correlation is likely small compared with the dominating effects of tropospheric circulations (clouds).

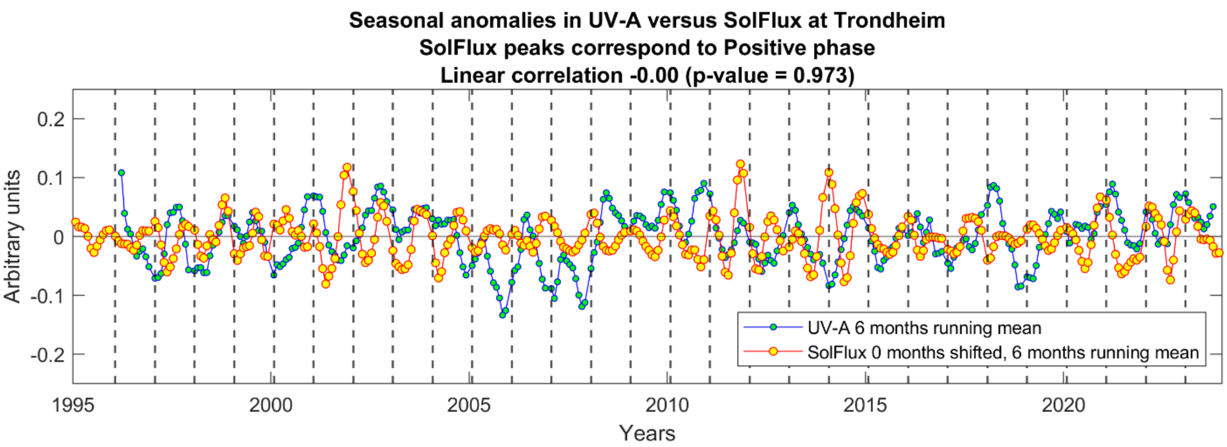

Figure 31 Anomalies in surface UV-A at Trondheim (TRH, 63N) and variations in solar activity.

7.6 Correlations with ENSO

The El Niño Southern Oscillation (ENSO) is a climate pattern in the equatorial part of the Pacific Ocean that influences weather worldwide. There are no evident correlations between the ENSO and surface E-UV and UV-A doses (Figure 32). The years 1997 and 1998 had an exceptionally strong transition in El Niño/La Niña phases and many of the southern stations in the network concurrently showed a large span in the relative deviation of E-UV and UV-A doses between these years. Other years of such exceptionally strong ENSO transitions were 2015 and 2016. However, these years do not show a similarly large span in relative deviations of yearly doses. Potentially disentangling traces of ENSO transitions in the UV-data would require further work and a longer lasting data set, considering the complex interplay of both direct and indirect drivers of surface UV.

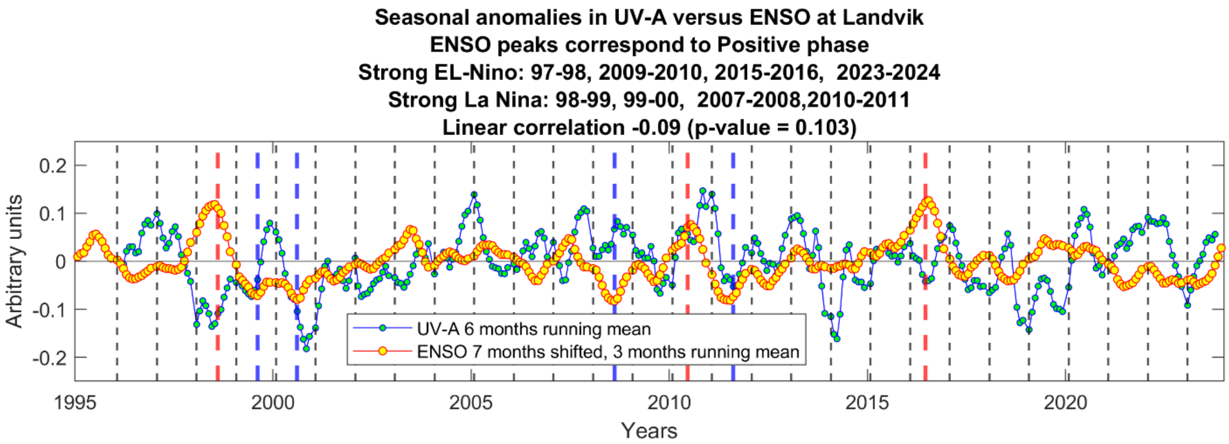

Figur 12 Anomalies in surface UV-A at Landvik (LAN, 58N) and ENSO at the equatorial Pacific Ocean. ENSO data has been time-shifted forward by 7 months. Dashed red lines indicate strong and very strong El-Niño events and blue lines moderate or strong La Niña events, time-shifted 7 months.

7.7 Correlations with Arctic Sea ice area

Arctic Sea ice area is the area of the Arctic Sea and adjacent seas that is covered by snow and ice. The area influences the radiation balance between incoming solar radiation and the amount reflected into space, affecting the overall radiation budget. Changes in summer sea-ice area may be coupled with e.g., summer NAO and AO. Over the monitoring period of the UV-network, arctic sea ice area and volume has drastically declined (Figure 33). Since 2007, ice that survives multiple summers is greatly reduced. There are no evident and consistent correlations between Arctic Sea ice area and surface E-UV and UV-A doses. Sea ice area might act as an indirect driver of UV-levels for most of the stations in the network (through effects on circulation systems), while for Ny-Ålesund (NYA, 79N) it can also be a direct driver on clouds and surface albedo. For this northernmost station (Figure 35), monthly mean UV-A doses are positively correlated with sea ice area during spring and October, and negative, but weakly correlated in summer/early autumn (June-September).

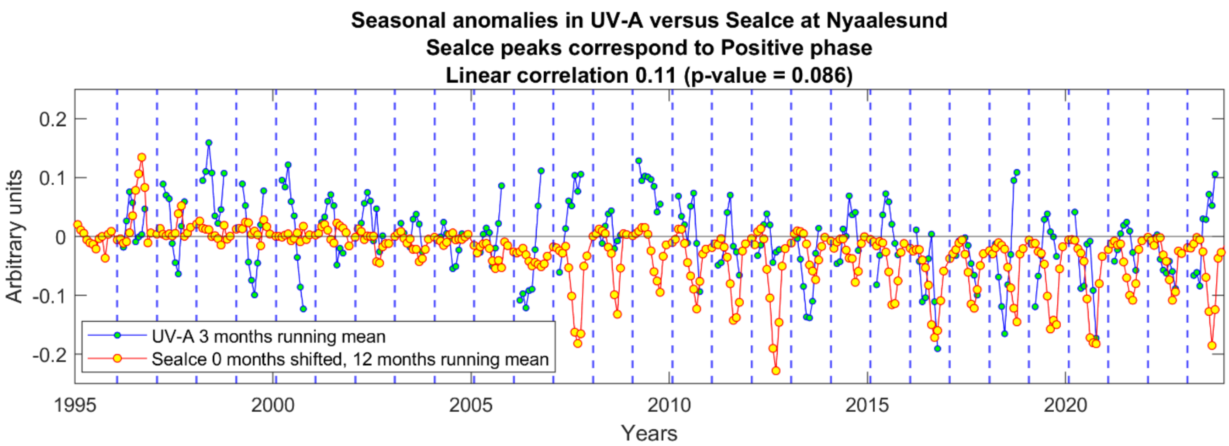

Figure 33 Anomalies in monthly mean surface UV-A doses in Ny-Ålesund and anomalies in Arctic Sea ice area. The minima in yearly sea ice anomalies occur mostly in September.

7.8 Station-specific seasonal correlations with surface UV

The previous section showed timeseries of some stratospheric and tropospheric circulation indicators and surface UV and TOC observations at a few UV-network locations. QBO showed a strong correlation with TOC whereas the correlation with surface UV through its influence on tropospheric cloud formation is harder to distinguish due to the different periods of the yearly solar cycle and the QBO. The correlation between solar activity and surface UV doses were also very weak. Therefore, we have excluded QBO and solar activity from further analysis and instead focused on NAO, AO, ENSO, and Arctic Sea ice as the main indirect drivers of observed surface UV variations.

Monthly correlations between these climate indices and E-UV and UV-A doses (Figures 34 and 35) show that NAO and AO (see also Figure 25) exhibit strong/moderate correlations with surface UV doses. During winter months, NAO and AO are negatively correlated with coastal stations (BRG, 60N and TRH, 63N), indicating that higher NAO/AO values during winter months, typically associated with low-pressure systems over the northern Atlantic, are linked to reduced surface UV doses. A meridional shift occurs in summer. In southern Norway, stations with continental climates (OST, 60N; KIS, 60N; LAN, 58N) exhibit positive correlations with the summer NAO, indicating that higher NAO values are associated with high-pressure systems and increased surface UV doses. Conversely, the two Arctic stations (AND, 69N, and NYA, 79N) show negative correlations with the summer NAO, suggesting that higher NAO values correspond to increased low-pressure activity in the Arctic, leading to greater cloud cover and reduced UV doses.

TOC shows a strong negative correlation with E-UV doses across all stations and months. Wavelengths in the UV-A range, which are only minimally affected by ozone absorption, still show negative correlations with TOC for most stations and months. These observations align with a well-known dynamic phenomenon where strong high- or low-pressure systems raise or lower the tropopause (the boundary layer between the stratosphere and troposphere), which affects the ozone concentration in the lower stratosphere (Steinbrecht et al., 1998). High-pressure conditions are typically linked to reduced ozone concentrations and to sunnier conditions, whereas low-pressure conditions tend to increase ozone levels and bring more clouds, effectively reducing UV-A doses. An exception is March month, exhibiting positive correlations of UV-A doses with TOC in Trondheim and Andøya, possibly coinciding with alterations in pressure systems associated to the seasonal weakening and breakup of the Arctic polar vortex.

The correlations between ENSO and Arctic Sea ice variations with E-UV and UV-A doses vary across stations and months, with some statistically significant correlations emerging sporadically. For instance, UV doses in May and July at stations in southern Norway show a negative correlation with strong El Niño winters, whereas the summer NAO is positively correlated with UV doses. Similarly, the coastal stations Bergen (BRG, 60N) and Trondheim (TRH, 63N) exhibit comparable patterns of UV-A and sea ice variations from the September minimum to late autumn, as do also UV-A and NAO, suggestion also an association between sea-ice extent and NAO.

In summary, indirect drivers, direct drivers and surface UV doses form a complex system. A deeper understanding of this system requires a longer UV monitoring period and models incorporating concurrent and interacting drivers rather than the initial exploration of one-to-one correlations shown here.

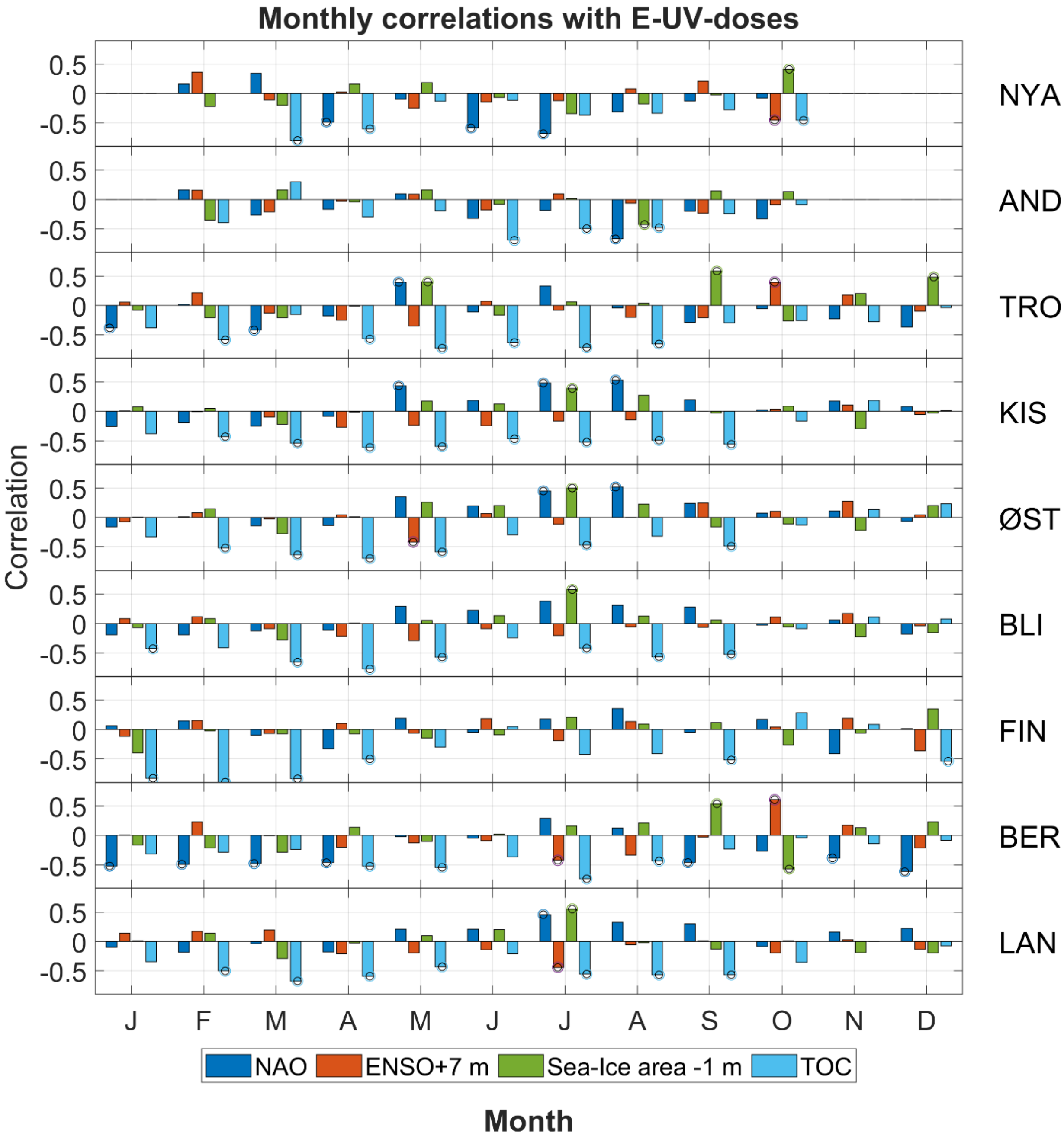

Figure 34 Correlations between E-UV, total ozone (TOC), and factors affecting global circulations (North Atlantic Oscillation, NAO, Arctic sea-ice area and the El Niño Southern Oscillation, ENSO). Circles mark linear correlations that are statistically significant at the 95% confidence level.

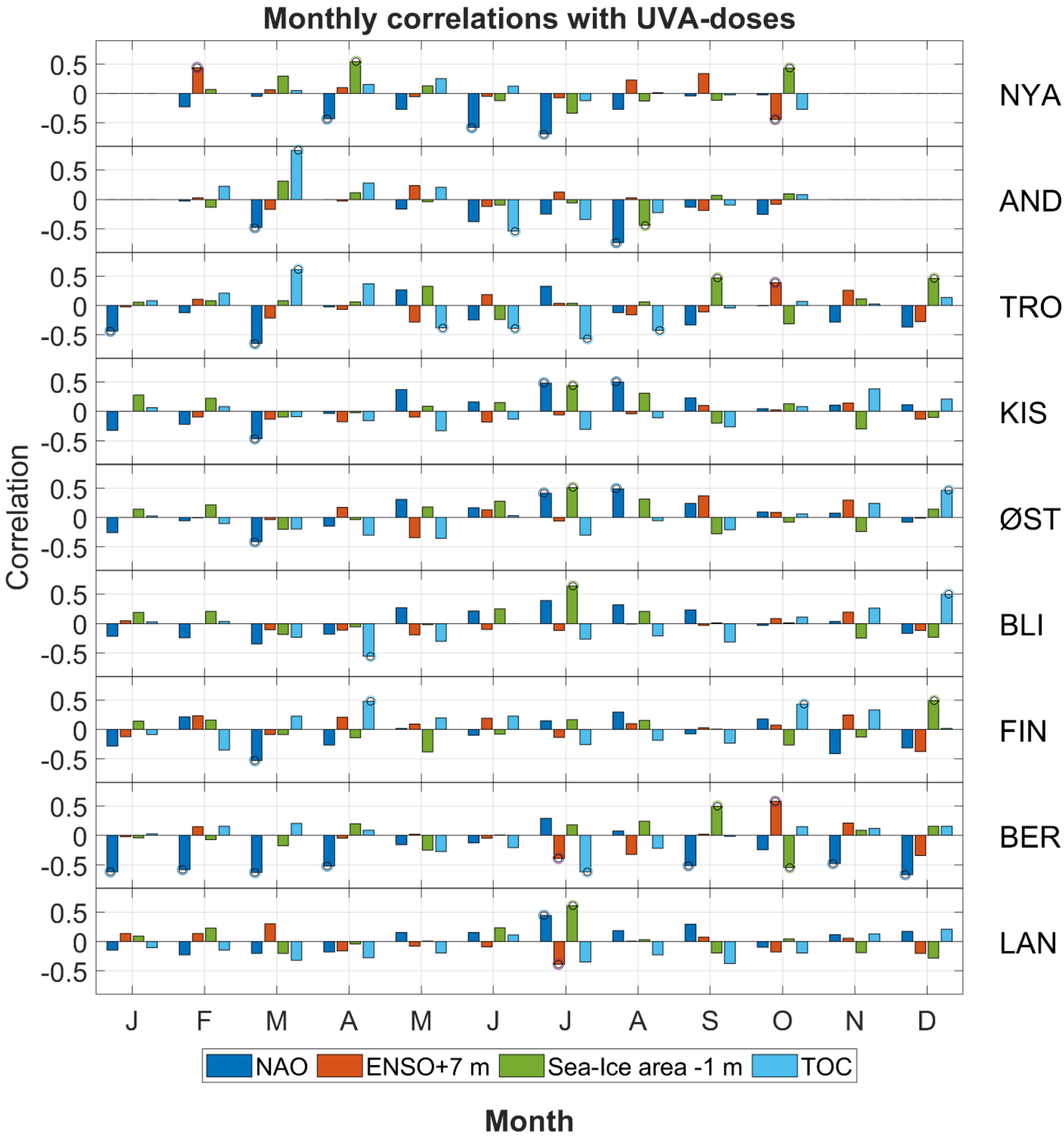

Figure 35 Correlations between UV-A, total ozone (TOC), and factors affecting global circulations (North Atlantic Oscillation, NAO, Arctic sea-ice area, and the El Niño Southern Oscillation, ENSO). Circles mark linear correlations that are statistically significant at the 95% confidence level.

8 Closing remarks

Data from nearly 30 years of UV monitoring have provided valuable information on variations in surface UV levels that are relevant to public health as well as to environmental and climate studies.

We see increases in yearly UV doses by +2% to +4% per decade at stations in southern Norway, diminishing northwards to -1.5% per decade at Svalbard. The trends are more pronounced on a monthly scale, with increases of up to +10% per decade in April in southern Norway and decreases of around -5% per decade in spring at Svalbard. The primary factors influencing surface UV levels include total ozone column (TOC), surface albedo, aerosols, and cloud cover.

During spring, as the polar vortex undergoes its seasonal breakup, daily variations in TOC can cause fluctuations in daily E-UV doses of several percent, sometimes reaching several tens of percent. However, the long-term influence of TOC trends on yearly UV doses is minimal, with an estimated impact of less than 0.5% per decade for the period 1996–2023, based on satellite data. This suggests that international agreements on phasing out ozone-depleting substances have been successful in preventing significant long-term reductions in TOC.

Surface albedo data retrieved from GUV instruments has allowed assessments of the magnitude and shifts in timing of snow melt and accumulation. The influence of surface albedo trends on yearly UV doses is small for lowland stations, estimated to less than 0.5% per decade. However, due to the much longer snow season in mountainous southern Norway (FIN, 60N) and Svalbard (NYA, 79N), lasting nearly eight months a year, the impact of surface albedo trends is more pronounced at these locations, with contributions of approximately +1% per decade in mountainous regions and -1% per decade in Svalbard to the overall trend in yearly E-UV doses.

Analyses of the distribution of summer hourly mean clear-sky transmittance suggest a possible +1% to +2% increase in the UV-A sky transmittance over the nearly 30-year monitoring period. However, these estimates are uncertain, and the results indicate that the influence of aerosol load trends on E-UV trends is very small.

The most influential driver of surface UV is changing cloudiness, observed as a brightening (sum of thinner clouds or reduced cloud fraction) from March to June in southern Norway, accompanied by an increase in relative sunshine duration. In contrast, a dimming (sum of thicker clouds or enhanced cloud fraction) is observed in the Arctic during spring. Cloud patterns are influenced by global and regional circulation systems. Among the circulation systems influencing cloud climatology in northern Europe, including Svalbard, the NAO and AO play a dominant role, acting as key indicators of cyclonic activity over the North Atlantic and Arctic Ocean.

During winter, the coastal stations Bergen (BRG, 60N) and Trondheim (TRH, 63N) exhibit a strong negative correlation between NAO/AO and surface E-UV and UV-A doses, suggesting that higher NAO/AO values, typically associated with storm activity and cloud cover, lead to reduced surface UV radiation. A meridional (south-north) pattern is seen during summer months. Stations in southern Norway with continental climates (LAN,58N, KIS 60N, OST and BLI, 60N) see an increase in summer E-UV and UV-A doses with high summer NAO, indicating sunnier conditions. Conversely, at arctic locations (AND, 69N, NYA, 79N), high summer NAO is associated with reduced E-UV and UV-A doses, suggesting low-pressure activity in the Arctic, leading to greater cloud cover and reduced UV doses.

The QBO, a wind pattern originating in the equatorial stratosphere, influences surface UV doses in Norway by modulating stratospheric ozone transport and strength of the tropospheric jet streams. Its impact on cloud climatology is observed through biennial, approximately 28 months, variations in eCLT and sunshine duration. Because the QBO and the Earth's yearly solar cycle have similar but not identical periodicities, their combined influence produces a beat-like modulation in surface UV levels over time. We also investigated linear correlations between surface UV doses and fluctuations in circulation drivers like the ENSO, solar activity and Arctic Sea ice area. The correlations were weak and spurious, suggesting complex interactions. A deeper understanding of the system would require models incorporating concurrent and interacting drivers as well as longer time series of both satellite- and ground-based observations.

Thirty years represents a short period for solar observations, especially considering that natural climate cycles span decades and centuries. Nonetheless, the observed trends in surface UV radiation, their underlying drivers, and the anticipated changes in circulation systems highlight the importance of continued monitoring for decades to come.

The Norwegian network stations are currently undergoing upgrades to continue UV monitoring for still more decades, with new instruments being gradually introduced to operate alongside the existing older instruments, enabling an overlap period for continuity and comparison. The new instruments monitor UV radiation as well as radiation in the visible and near infrared part of the solar spectrum. This expanded spectral range facilitates a more comprehensive understanding of how surface solar radiation interacts with climate change to affect health and ecosystems.

Solar UV-monitoring data from various global locations, including those in Norway, can contribute valuable insights to this worldwide effort to assess the influences of natural and man-made factors on climate, and provide data for policymaking mitigating detrimental effects for society and the environment.

8.1 Future work

- Continue solar UV monitoring and long-term trend assessments, with a particular focus on spring, when outdoor activity increases, and fair-skinned individuals face a higher risk of UV exposure.
- Ensure the high quality and reliability of measurement data and dose products.
- Ensure easy access to online UV measurement data to support public awareness, preventive health measures, and scientific research.
- Develop sun protection guidance for specific risk groups based on real-sky observations and modeling.
- Evaluate the effectiveness of shading structures and personal sun protection strategies in minimizing UV exposure.
- Develop conversion factors to translate long-term UV monitoring data—typically measured on horizontal surfaces—into estimates for tilted surfaces, enabling more accurate assessments of personal UV exposure.
- Provide UV monitoring data that supports research across health, environmental, and climate sciences, including studies on the combined impacts of UV radiation and global environmental and climate change.
- Support remote sensing validation efforts by providing ground-based UV monitoring data for satellite product verification.

9 Acknowledgements

We express our gratitude to Helse- og omsorgsdepartementet (HOD) og Klima- og miljødepartementet (KLD) for their financial support, which has made the continuous monitoring of solar UV radiation in Norway possible.

We are grateful for the partnership of Miljødirektoratet through their financial support of NILUs ozone and UV-monitoring stations.

We would also like to acknowledge the group of experts from Norwegian research institutions and universities, including the Norwegian Society for Photobiology and Photomedicine (NOFFOF). This consortium laid the groundwork for recognizing the importance of solar UV radiation monitoring.

Special thanks to the Nordic UV and Ozone Group (NOG), for hosting yearly meetings of fruitful cooperation in UV and ozone monitoring over more than 30 years, bringing together scientists from all of Europe.

On behalf of DSA and NILU, we express our gratitude to the institutions hosting the UV network locations and to the dedicated staff for the continuous support over many years, performing daily inspections and providing technical support. Their contributions have ensured high quality and reliability of the measurements over the past 30 years. Special thanks go to:

- Norwegian Institute of Bioeconomy Research (NIBIO) at Landvik and Kise, represented by Lars Havstad and Hugh Riley,
- Geophysical Institute, University of Bergen (UIB), represented by Anak Bhandari,
- Department of Physics, University of Oslo (UIO), represented by Arne Dahlback,
- Department of Physics, Norwegian University of Science and Technology (NTNU), Trondheim, represented by Vedran Furtula and Osvaldo Trigueiro Neto,
- Finse Alpine Research Station, represented by Erika Leslie and Jens Ådne Rekkedal Haga,
- Former Auroral Observatory, University of Tromsø, which hosted the instrument before its relocation to Andøya,
- ALOMAR Observatory, Andøya Space, represented by Reidar Lyngra,
- Norwegian Polar Institute for hosting the UV instrument at Ny-Ålesund.

Our thanks also go to Arne Dahlback from the Department of Physics, University of Oslo, for his pioneering work in integrating multiband filter radiometer measurements with radiative transfer modeling. His results held great importance for the choice of instrumentation and implementation of the network.

We also extend our special thanks to former colleagues at DSA, including Oddbjørn Mikkelborg, Børre Knutsen, and Tommy N. Aalerud, for building the UV network's IT infrastructure at DSA, and the support from the new IT team at DSA. Additionally, we are grateful to the IT team at NILU for enabling seamless sharing and backup of measurement data between DSA and NILU.

We acknowledge the valuable assistance of ChatGPT-4o, an AI technology that has served as a patient discussion partner, helping to interpret observations and enhance language for improved readability. Details on the use of AI are provided at the end of this acknowledgement.

Thanks to all institutions providing ancillary data enabling reconstruction of measured UV data for quality control of UV measurements and for filling gaps in measurements. Special thanks go to:

- The Swedish Meteorological and Hydrological Institute (SMHI), providing UV data with their STRÅNG model,
- Agrometeorology Norway (LMT), at NIBIO for access to total radiation data at the UV network locations,
- Norwegian Meteorological Institute (MET.no) for access to total radiation, cloud cover, temperature, and precipitation data at the UV network locations,
- Alfred Wegener Institute - Research Unit Potsdam for total radiation data in Ny-Ålesund,
- Geophysical Institute, UIB, for total radiation data in Bergen and clear-sky modelled data at all stations,
- Department of Geosciences, University of Oslo, providing total solar radiation data from the Finse Eco-Hydrological Observatory, through the program Land-Atmosphere Interactions in Cold Environments – LATICE,
- NASA for providing access to satellite based total ozone data,
- National Oceanic and Atmospheric Administration (NOAA) for oceanic and atmospheric circulation data,
- Swedish University of Agricultural Sciences, Svartberget Field-station in Vindeln for total ozone column data for the period 1995-1996 when satellite data are missing,
- Finnish Meteorological Institute in Sodankylä for total ozone column data for the period 1995-1996 when satellite data are missing.

Lastly, we would like to thank the team at Biospherical Instruments, San Diego, with special recognition to Germar Bernhard, for their ongoing support and technical services, which have kept the instruments operational long after replacement parts were no longer available.

9.1 Use of ChatGPT-4o in this report

The use of AI technologies requires open and transparent acknowledgement on how and why it has been used in academic work [Acknowledging use of AI | Academic Skills Kit | Newcastle University]

The use of AI in preparing the summary report for the Norwegian UV-monitoring network has primarily been as follows:

- Serving as a starting point to gather basic information on climate systems and interactions, influences on surface solar radiation, statistical terms and definitions before exploring relevant scientific literature through google search. Example prompts: "how can lifting of air masses over mountains lead to increased concentrations of ozone at higher elevations?" "what is the difference between AO and NAO?"

- Language refinements as by a virtual, native speaker familiar with the scientific topic: Improvements of draft paragraphs provided by the author, spell checks, use of correct grammar and synonyms, to improve readability and provide a concise language.

- Discussing observations and results:

  Data has been analyzed by the authors – without any use of AI. The conclusions in this report have also been based on our own analysis. However, AI has been helpful in discussing results. Two examples of questions provided to the AI are:
  1. "what makes August have an influence on TOC that is different from the other months in Norway and Svalbard, considering circulations?"
  2. "There is more strange things concerning north and south trends and correlations between anomalies in UVA and climate factors. I note that for stations between 58 and 63 North April has exceptional high increases in UVA and June also high UVA anomalies. At stations North, Andøya 70N and Svalbard 78N, there are strong negative trends in UVA

these two months. What make such big differences north and south in April and June? I also note that anomalies in sea-ice extent are small these months, and there is small reductions in precipitations in these months in the south, and more pronounced increases in precipitation at Andøya and Svalbard. how do you interprete these results? can precipitation really explain these big differences in UVA anomalies? Other factors not considered?»

A reply from AI to the latter question is: "To interpret these results comprehensively, one would need to consider a multi-faceted approach that includes detailed atmospheric data, cloud cover statistics, aerosol concentrations, and ozone levels, alongside the meteorological factors already considered. While precipitation trends offer some clues, they're just one piece of the broader climatic puzzle affecting UVA radiation patterns. Further, in-depth studies would be necessary to disentangle these complex relationships and ascertain the primary drivers behind the observed UVA anomalies."

10 References

10.1 Master and doctoral theses

1. Jensen, C. A. (1997). Spektrale målinger av ultrafiolett stråling i Trondheim. Dataanalyse og kvalitetskontroll. Master thesis, Norwegian University of Science and Technology.
2. Thorseth, T. M. (2000). Solar ultraviolet irradiance measurements, instrumentation, intercomparison, and interpretations. Doctoral thesis, Norwegian University of Science and Technology.
3. Carlson, T. (2005). UV-stråling i Norge. Satelittestimater, modellestimater og bakkemålinger. Master thesis, University of Bergen.
4. Sjølingstad, B. (2007). Reconstruction of UV radiation: UV exposure of the Arcto-Atlantic cod egg population, 1957-2005. Master thesis, University of Bergen.
5. Medhaug, I. (2007). Reconstruction of UV-radiation and its potential implications on development of skin cancer. Master thesis, University of Bergen.
6. Bhattarai, B. K. (2007). Factors affecting solar ultraviolet radiation. Doctoral thesis, Norwegian University of Science and Technology.
7. Sharma, R. R. (2012). Study of satellite and ground UV Index: Climatology and effects of geophysical parameters. Doctoral thesis, Norwegian University of Science and Technology.
8. Karset, I.H.H. (2013). UV-stråling: Modellering av skyers og bakkealbedoens effekt, samt analyse av langtidsendringer på Blindern og Svalbard. Master thesis, University of Oslo.
9. Rønneberg, S. (2016). Feasability of using phototherapy with sunlight for treatment of neonatal jaundice in low-income countries. Master thesis, Norwegian University of Science and Technology.
10. Nedrebø, S. (2017). Use of market ready light dosimeters for patients with erythropoietic protoporphyria disorder. Master thesis, University of Bergen.

10.2 Scientific publications

11. Aalerud, T. et al (2006). StrålevernRapport 2006:4 Østerås: Statens strålevern.
12. Andreassen, L.M., Elvehøy, H., Kjøllmoen, B., Belart, J.M.C. (2020). Glacier change in Norway since the 1960s – an overview of mass balance, area, length, and surface elevation changes. Journal of Glaciology; 66(256):313-328. doi:10.1017/jog.2020.10
13. Assunção, H., Escobedo, J. & Oliveira, A. Modelling frequency distributions of 5 minute-averaged solar radiation indexes using Beta probability functions (2003). Theor Appl Climatol 75, 213–224. https://doi.org/10.1007/s00704-003-0733-9
14. Bais, A. F., McKenzie, R.L., Bernhard, G., Aucamp, P.J., Ilyas, M., Madronich, S., Tourpali, K. (2015). Ozone depletion and climate change: impacts on UV radiation. Photochem Photobiol Sci. 2015 Jan;14(1):19-52. doi: 10.1039/c4pp90032d. PMID: 25380284.
15. Baldwin, M. P., Gray, L. J., Dunkerton, T. J., Hamilton, K., Haynes, P. H., Randel, W. J., Holton, J. R., Alexander, M. J., Hirota, I., Horinouchi, T., Jones, D. B. A., Kinnersley, J. S., Marquardt, C., Sato, K., & Takahashi, M. (2001). The quasi-biennial oscillation, Rev. Geophys., 39(2), 179–229, doi:10.1029/1999RG000073.

16. Bernhard, G. & Seckmeyer, G. (1997). Measurements of spectral solar UV irradiance in tropical Australia. J. Geophys. Res., 102, 8719-8730. Doi:10.1029/97JD00072

17. Bernhard, G., Dahlback, A., Fioletov, V., Heikkilä, A., Johnsen, B., Koskela, T., Lakkala, K., and Svendby T. (2013). High levels of ultraviolet radiation observed by ground-based instruments below the 2011 Arctic ozone hole. Atmos. Chem. Phys., 10573-10590, doi: 10.5194/acp-13-10573.

18. Bernhard G., Arola, A., Dahlback, A., Fioletov, V., Heikkilä, A., Johnsen, B., Koskela, T., Lakkala, K., Svendby, T., & Tamminen, J. (2015). Comparison of OMI UV observations with ground-based measurements at high northern latitudes. Atmos. Chem. Phys., 15, 7391-7412.

19. Bernhard G. H., Fioletov V., Gross J.-U., Ialongo I., Johnsen B., Lakkala K., Manney G. L., Müller R., and Svendby, T. (2020). Record-Breaking Increases in Arctic Solar Ultraviolet Radiation Caused by Exceptionally Large Ozone Depletion in 2020. Geophys. Res. Letters. 10.1029/2020GL090844. https://agupubs.onlinelibrary.wiley.com/doi/10.1029/2020GL090844.

20. Bernhard, G. H., Fioletov, V. E., Grooß, J.-U., Ialongo, I., Johnsen, B., Lakkala, K., Manney, G. L., Müller, R., and Svendby, T. (2023). Ozone and UV Radiation [In: State of the Climate in 2022]. Bull Amer Meteor Soc, 104 (9), s308-s310, https://doi.org/10.1175/2023BAMSStateoftheClimate.1.

21. Butler, A. H., Lee, S. H., Bernhard, G. H., Fioletov, V. E., Grooß, J.-U., Ialongo, I., Johnsen, B., Lakkala, K., Müller, R., Svendby, T., and Ballinger, T. J. (2024): The Arctic [In: State of the Climate in 2023]. Bull Amer Meteor Soc, 105 (8), s285-s287, https://ametsoc.net/sotc2023/SoCin2023_FullReport.pdf.

22. Calbó, J., Pagès, D., & González, J.-A. (2005), Empirical studies of cloud effects on UV radiation: A review, Rev. Geophys., 43, RG2002, doi:10.1029/2004RG000155.

23. Carslaw, K. S, Harrioson, R. G., & Kirkby, J. (2002). Cosmic rays, clouds, and climate. Science 298, 1732, DOI: 10.1126/science. 1076964.

24. Čížková, K., Láska, K., Metelka, L., and Staněk, M. (2018). Reconstruction and analysis of erythemal UV radiation time series from Hradec Králové (Czech Republic) over the past 50 years, Atmos. Chem. Phys., 18, 1805–1818, https://doi.org/10.5194/acp-18-1805-2018.

25. Commission Internationale de l’Eclairage (1987): McKinlay A.F., Diffey B.L. A reference action spectrum for ultraviolet induced erythema in human skin. CIE Research Note, CIE-Journal, Vol. 6, No.1, 17-22.

26. Commission Internationale de l'Éclairage. (1997). *CIE 125-1997: Standard Erythema Dose - A Definition.* Vienna: CIE Central Bureau.

27. Commission Internationale de l’Eclairage (1998). Erythema Reference Action Spectrum and Standard Erythema Dose. CIE S007E-1998. CIE Central Bureau, Vienna, Austria.

28. Commission Internationale de l’Eclairage (2006). Action spectrum for the conversion of 7-DH7 to previtamin D3 in human skin (CIE 174:2006). International Commission on Illumination.

29. Commission Internationale de l’Eclairage (2016). Photocarcinogenesis Action Spectrum, (Non-Melanoma Skin Cancers, NMSC) (ISO/FDIS 28077:2016E). International Commission on Illumination.

30. Dahlback, A. (1996). Measurements of biologically effective UV doses, total ozone abundances, and cloud effects with multichannel, moderate bandwidth filter instruments, Appl. Optics, 35, 6514–6521.

31. DeLuisi, J., Theisen, D., Augustine, J., Disterhoft, P., Lantz, K., Weatherhead, E., Hodges, G., Cornwall, C., Petropavlovskikh, I., & Stevermer A. (2022). On the correspondence between surface UV observations and TOMS determinations of surface UV: a potential method for quality evaluating world surface UV observations. Ann. Geophys. [Internet]. 2003Dec.25 [cited 2022Aug.26];46(2). Available from: https://www.annalsofgeophysics.eu/index.php/annals/article/view/3403

32. Dong, B., Sutton, R. T., and Wilcox, L. J. (2022). Decadal trends in surface solar radiation and cloud cover over the North Atlantic sector during the last four decades: drivers and physical processes. *Clim Dyn* **60**, 2533–2546 (2023). https://doi.org/10.1007/s00382-022-06438-3

33. Douglass, A.R., Newman, P.A, Solomon, S. (2014). The Antarctic ozone hole: An update. Physics Today, 67, 42-48, https://doi.org/10.1063/PT.3.2449, 2914.

34. Eckhardt, S., Stohl, A., Beirle, S., Spichtinger, N., James, P., Forster, C., Junker, C., Wagner, T., Platt, U., and Jennings, S. G. (2003). The North Atlantic Oscillation controls air pollution transport to the Arctic, Atmos. Chem. Phys., 3, 1769–1778, https://doi.org/10.5194/acp-3-1769-2003.

35. Emde, C., Buras-Schnell, R., Kylling, A., Mayer, B., Gasteiger, J., Hamann, U., Kylling, J., Richter, B., Pause, C., Dowling, T., & Bugliaro, L. (2016). The libRadtran software package for radiative transfer calculations (version 2.0.1), Geosci. Model Dev., 9, 1647–1672, https://doi.org/10.5194/gmd-9-1647-2016.

36. Farman, J.C., Gardiner, B.G., and Shanklin, J.D. (1985). Large Losses of Total Ozone in Antarctica Reveal Seasonal ClOx/NOx Interaction, Nature, 315, 207-210, doi:10.1038/315207a0.

37. Feister, U. & Grewe, R. (1995). Spectral albedo measurements in the UV and visible region over different types of surfaces. Photochemistry and Photobiology. 62. 736 - 744. 10.1111/j.1751-1097.1995.tb08723.x.

38. Flint, S. D. & Caldwell, M. M. (2003). A biological spectral weighting function for ozone depletion research with higher plants, Physiologia Plantarum, 117,137-144. Data downloaded from: http://uv.biospherical.com/Version2/doserates/Flint.txt

39. Gröbner, J., Schreder, J., Kazadzis, S., Bais, A. F., Blumthaler, M., Görts, P., Tax, R., Koskela, T., Seckmeyer, G., Webb, A. R., & Rembges, D. (2005). Traveling reference spectroradiometer for routine quality assurance of spectral solar ultraviolet irradiance measurements. Appl. Opt. 44, 5321-5331

40. Hannevik, M. et al (1998). StrålevernRapport 1998:10. Østerås: Statens strålevern.

41. Hall, R., Erdélyi, R., Hanna, E., Jones, J.M. and Scaife, A.A. (2015), Drivers of North Atlantic Polar Front jet stream variability. Int. J. Climatol, 35: 1697-1720. https://doi.org/10.1002/joc.4121

42. Hanssen-Bauer, I., Førland, E.J., Hadde-Freeland, I., Hisdal, H., Lawrence, D., Mayer, S., Nesje, A., Nilsen, J.E. Ø., Sandven, S., Sandø, A.B., Sorteberg, A., & Ådlandsvik, B (2017). Climate in Norway 2100 – a knowledge base for climate adaptation. Norwegian Environment Agency (Miljødirektoratet), ISSN 2387-3027. Accessed May 03, 2024. www.miljodirektoratet.no/M741.

43. Hunter, J.H., Taylor, J.H., & Moser, H.G. (1979). Effect of ultraviolet irradiation on eggs and larvae of the northern anchovy, Engraulis mordax, and the pacific mackerel, Scomber japonicus, during the embryonic stage. Photochemistry and Photobiology, 29, 325-338, 1979. Data downloaded from: http://uv.biospherical.com/Version2/doserates/Hunter.txt

44. Hurrell, J.W., Kushnir, Y., Ottersen, G. and Visbeck, M. (2003). An Overview of the North Atlantic Oscillation. In The North Atlantic Oscillation: Climatic Significance and Environmental Impact (eds J.W. Hurrell, Y. Kushnir, G. Ottersen and M. Visbeck). https://doi.org/10.1029/134GM01

45. Hülsen, G., Gröbner, J., Nevas, S., Sperfeld, P., Egli, L., Porrovecchio, G., & Smid, M. (2016). Traceability of solar UV measurements using the Qasume reference spectroradiometer. Appl. Opt. 55, 7265-7275

46. Johnsen, B. et al (2002). StrålevernRapport 2002:4. Østerås: Statens strålevern.

47. Johnsen B., Kjeldstad B., Aalerud T.N., Nilsen L.T., Schreder J., Blumthaler M., Bernhard G., Topaloglou C., Meinander O., Bagheri A., Slusser J.R. and Davis J. (2008). Intercomparison and harmonization of UV index measurements from multiband filter radiometers, JGR Volume 113, doi:10.1029/2007JD009731.

48. Johnsen, B. et al (2011). StrålevernRapport 2011:2 Østerås: Statens strålevern.

49. Karpechko A.Yu., Backman L., Thölix L., Ialongo I., Andersson, M., Fioletov, V., Heikkilä, A., Johnsen, B., Koskela, T., Kyrölä, E., Lakkala, K., Myhre, C. L., Rex, M., Sofieva, V.F., Tamminen, J., Wohltmann, I. (2013). The link between springtime total ozone and summer UV radiation in Northern Hemisphere extratropics. JGR Volume 118, Issue 15, pp 8649–8661, doi: 10.1002/jgrd.50601.

50. Keim U, Gandini S, Amaral T, Katalinic A, Holleczek B, Flatz L, Leiter U, Whiteman D, Garbe C (2021). Cutaneous melanoma attributable to UVR exposure in Denmark and Germany. Eur J Cancer. 2021 Dec;159:98-104. doi: 10.1016/j.ejca.2021.09.044. Epub 2021 Nov 3. PMID: 34742161.

51. Knight J, Scaife A, Bett PE, et al. (2020). Predictability of European Winters 2017/2018 and 2018/2019: Contrasting influences from the Tropics and stratosphere. Atmos Sci Lett. 2021; 22:e1009. https://doi.org/10.1002/asl2.1009

52. Knudsen, B. M., Jønch-Sørensen, H., Eriksen, P., Johnsen, B. and Bodeker, G. E. (2005). UV radiation below an Arctic vortex with severe ozone depletion. Atmos. Chem. Phys., 5, 1–7.

53. Kosmopoulos, P. G., Kazadzis, S., Schmalwieser, A. W., Raptis, P. I., Papachristopoulou, K., Fountoulakis, I., Masoom, A., Bais, A. F., Bilbao, J., Blumthaler, M., Kreuter, A., Siani, A. M., Eleftheratos, K., Topaloglou, C., Gröbner, J., Johnsen, B., Svendby, T. M., Vilaplana, J. M., Doppler, L., Webb, A. R., Khazova, M., De Backer, H., Heikkilä, A., Lakkala, K., Jaroslawski, J., Meleti, C., Diémoz, H., Hülsen, G., Klotz, B., Rimmer, J., and Kontoes, C. (2021). Real-time UV index retrieval in Europe using Earth observation-based techniques: system description and quality assessment, Atmos. Meas. Tech., 14, 5657–5699, https://doi.org/10.5194/amt-14-5657-2021.

54. Koepke, P., Schmalwieser, A.W., Backer, H. De, Bais, A., Curylo, A., Eerme,K., Feister, U., Johnsen, B., Junk, J., Kazantzidis, A., Krzyscin, J., Lindfors, A., Olseth, J.A., Outer, P. den, Pribullova, A., Slaper, H., Staiger, H., Verdebout, J., Vuilleumier, L. and Weihs, P. (2007). Comparison of algorithms and input data for modelling solar ultraviolet radiation in the past. Geophysical Research Abstracts, Vol. 9, 08259.

55. Lakkala, K., Kujanpää, J., Brogniez, C., Henriot, N., Arola, A., Aun, M., Auriol, F., Bais, A. F., Bernhard, G., De Bock, V., Catalfamo, M., Deroo, C., Diémoz, H., Egli, L., Forestier, J.-B., Fountoulakis, I., Garane, K., Garcia, R. D., Gröbner, J., Hassinen, S., Heikkilä, A., Henderson, S., Hülsen, G., Johnsen, B., Kalakoski, N., Karanikolas, A., Karppinen, T., Lamy, K., León-Luis, S. F., Lindfors, A. V., Metzger, J.-M., Minvielle, F., Muskatel, H. B., Portafaix, T., Redondas, A., Sanchez, R., Siani, A. M., Svendby, T., and Tamminen, J. (2020). Validation of

the TROPOspheric Monitoring Instrument (TROPOMI) surface UV radiation product, Atmos. Meas. Tech., 13, 6999–7024, https://doi.org/10.5194/amt-13-6999-2020.

56. Lawrence, Z. D., Perlwitz, J., Butler, A. H., Manney, G. L., Newman, P. A., Lee, S. H., & Nash, E. R. (2020). The remarkably strong Arctic stratospheric polar vortex of winter 2020: Links to record-breaking Arctic Oscillation and ozone loss. Journal of Geophysical Research: Atmospheres, 125, e2020JD033271. https://doi.org/10.1029/2020JD033271

57. Lindfors, A., Kaurola, J., Arola, A., Koskela, T., Lakkala, K., Josefsson, W., Olseth, J. A., and Johnsen B. (2007). A method for reconstruction of past UV radiation based on radiative transfer modeling: Applied to four stations in northern Europe, J. Geophys. Res., 112, D23201, doi:10.1029/2007JD008454.

58. Magnus, K. (1973), Incidence of malignant melanoma of the skin in Norway, 1955–1970. Variations in time and space and solar radiation. Cancer, 32: 1275-1286. https://doi.org/10.1002/1097-0142(197311)32:5<1275::AID-CNCR2820320537>3.0.CO;2-8

59. McKinlay, A. F. and Diffey, B. L. (1987). A reference action spectrum for ultraviolet induced erythemal in human skin. CIE Research Note, 6(1), 17-22

60. Molina, M., Rowland, F. (1974). Stratospheric sink for chlorofluoromethanes: chlorine atom-catalysed destruction of ozone, Nature, 249, 810–812, https://doi.org/10.1038/249810a0.

61. Neale, R. E., Lucas, R. M., Byrne, S. N., Hollestein, L., Rhodes, L. E., Yazar, S., Young, A. R., Berwick, M., Ireland, R. A., & Olsen, C. M. (2023). The effects of exposure to solar radiation on human health. Photochemical & photobiological sciences: Official journal of the European Photochemistry Association and the European Society for Photobiology, 22(5), 1011–1047. https://doi.org/10.1007/s43630-023-00375-8

62. Nilsen, L.T., Johnsen, B., Komperød, M., Christensen, T., Hannevik, M. (2015). UV exposure of the Norwegian population. From sun and sunbeds. StrålevernRapport 2015:7. Østerås: Norwegian Radiation Protection Authority. Language: Norwegian.

63. Nilsen, L.T., Saxebøl, G., Kofstadmoen, H., Espetvedt, S.L., Sørensen, I.L., Nøkleby, H., Robsahm, T.E., Husaas, E., Husby, M.L. (2019). National UV- and skin cancer strategy. DSA-rapport 2019:02, Østerås: Norwegian Radiation and Nuclear Safety Authority. Language: Norwegian.

64. Norvang. L. T. et al. (2000). StrålevernRapport 2000:4. Østerås: Statens strålevern.

65. Oslo Economics (2018). Samfunnskostnader forbundet med hudkreft (Societal costs associated with skin cancer). Notat utarbeidet for Statens strålevern. Oslo Economics, 17. september 2018. Available at https://dsa.no/publikasjoner?aar=2018. Downloaded 03.02.2025.

66. Paek, H., Yu, J.-Y. & Qian, C. (2017). Why were the 2015/2016 and 1997/1998 extreme El Niños different? Geophys. Res. Lett., 44, 1848–1856, doi:10.1002/2016GL071515.

67. Petkov, B.H, Vitale, V., Di Carlo, P., Hansen, G.H., Svendby, T.M., Laska, K., Sobolewski, P.S., Solomatnikova, A., Pavlova, K., Johnsen, B., Posyniak, M.A., Elster, J., Mazzola, M., Lupi, A., & Verazzo, G. (2022). The extreme Arctic ozone depletion in 2020 as was observed from Svalbard. https://doi.org/10.5281/zenodo.5751922 Chapter 4 in Feldner J, Hübner C, Lihavainen H, Neuber R, Zaborska A (eds) 2022: SESS report 2021, Svalbard Integrated Arctic Earth Observing System, Longyearbyen. https://sios-svalbard.org/SESS_Issue4

68. Petkov, B. H., Vitale, V., Di Carlo, P., Drofa, O., Mastrangelo, D., Smedley, A. R. D., et al. (2023). An unprecedented Arctic ozone depletion event during spring 2020 and its impacts

across Europe. Journal of Geophysical Research: Atmospheres, 128, e2022JD037581. https://doi.org/10.1029/2022JD037581

69. Quaas, J., Jia, H., Smith, C., Albright, A. L., Aas, W., Bellouin, N., Boucher, O., Doutriaux-Boucher, M., Forster, P. M., Grosvenor, D., Jenkins, S., Klimont, Z., Loeb, N. G., Ma, X., Naik, V., Paulot, F., Stier, P., Wild, M., Myhre, G., and Schulz, M. (2022). Robust evidence for reversal of the trend in aerosol effective climate forcing, Atmos. Chem. Phys., 22, 12221–12239, https://doi.org/10.5194/acp-22-12221-2022.

70. Rousi, E., Fink, A. H., Andersen, L. S., Becker, F. N., Beobide-Arsuaga, G., Breil, M., Cozzi, G., Heinke, J., Jach, L., Niermann, D., Petrovic, D., Richling, A., Riebold, J., Steidl, S., Suarez-Gutierrez, L., Tradowsky, J. S., Coumou, D., Düsterhus, A., Ellsäßer, F., Fragkoulidis, G., Gliksman, D., Handorf, D., Haustein, K., Kornhuber, K., Kunstmann, H., Pinto, J. G., Warrach-Sagi, K., and Xoplaki, E. (2023). The extremely hot and dry 2018 summer in central and northern Europe from a multi-faceted weather and climate perspective, Nat. Hazards Earth Syst. Sci., 23, 1699–1718, https://doi.org/10.5194/nhess-23-1699-2023.

71. Saxebøl, G. (1990). Nordisk nettverk for UV-stråling (eng. Nordic Network for UV-Radiation). Presentation at the Scientific meeting on Norwegian Biophysics and Medical Physics/Technology, Kongsvoll Fjellstue, 29-31 March 1990.

72. Saxebøl, G. (2000). UVH—A proposal for a practical unit for biological effective dose for ultraviolet radiation exposure. Radiat. Prot. Dosim. 2000, 88, 261.

73. Schmalwieser et al. (2017). UV Index monitoring in Europe, Photochem. Photobiol. Sci., 16, 1349-1370, https://doi.org/10.1039/C7PP00178A.

74. Schmalwieser, A.W. (2020). Possibilities to estimate the personal UV radiation exposure from ambient UV radiation measurements. Photochem Photobiol Sci 19, 1249–1261, https://doi.org/10.1039/d0pp00182a

75. Seckmeyer, G., Bais, A., Bernhard, G., Blumthaler, M., Johnsen,B., Lantz, K., and McKenzie, R. (2010). Instruments to Measure Solar Ultraviolet Radiation – Part 3: Multi-channel filter instruments, Global Atmosphere Watch Report, World Meteorological Organization, Geneva, Switzerland, https://www.wmo.int/pages/prog/arep/gaw/documents/GAW190_TD_No_1537_web.pdf (last access:10 February 2016), 2010

76. Setlow, R. B. (1974). The wavelengths in sunlight effective in producing skin cancer: a theoretical analysis. P. Natl. Acad. Sci. USA 71, 3363-3366.

77. Seppälä, A., Matthes, K., Randall, C.E. et al. (2014). What is the solar influence on climate? Overview of activities during CAWSES-II. Prog. in Earth and Planet. Sci. 1, 24. https://doi.org/10.1186/s40645-014-0024-3.

78. Skaland, R. G., Colleuille, H., Andersen, A. S. H., Mamen, J., Grinde, L., Tajet, H. T. T., Lundstad, E., Sidselrud, L. F., Tunheim, K., Hanssen-Bauer, I., Benestad, R., Heiberg, H., & Hygen, H. O. (2019). Tørkesommeren 2018. METinfo 14/2019. Oslo, utgitt 4. januar 2019

79. Spaeth, J. and Birner, T. (2022). Stratospheric modulation of Arctic Oscillation extremes as represented by extended-range ensemble forecasts, Weather Clim. Dynam., 3, 883–903, https://doi.org/10.5194/wcd-3-883-2022.

80. Staiger, H., Outer, P. den, Bais, A., Feister, U., Johnsen, B., and Vuilleumier, L. (2008). Hourly resolved cloud modification factors in the ultraviolet. Special Issue: One century of solar ultraviolet research Atmos. Chem. Phys., 8, 2493–2508. www.atmos-chem-phys.net/8/2493/2008/

81. Stenehjem, J.S., Veierød, M.B., Nilsen, L.T., Ghiasvand, R., Johnsen, B., Grimsrud, T.K., Babigumira, R., Støer, N.C., Rees, J.R., Robsahm,T.E. (2018A). Anthropometric factors and Breslow thickness: Prospective data on 2570 cutaneous melanoma cases in the population-based Janus Cohort. Br J Dermatol. 2018; 179(3); 632-641. doi: 10.1111/bjd.16825.

82. Stenehjem, J.S., Veierød, M.B., Nilsen, L.T., Ghiasvand, R., Johnsen, B., Grimsrud, T.K., Babigumira, R., Rees, J.R., Robsahm, T.E. (2018B). Anthropometric factors and cutaneous melanoma: Prospective data from the population-based Janus Cohort. Int J Cancer. 2018 Feb 15;142(4):681-690. doi: 10.1002/ijc.31086.

83. Stenehjem, J.S., Støer, N.C., Ghiasvand, R., Grimsrud, T.K., Babigumira, R., Rees, J.R., Nilsen, L.T., Johnsen, B., Thorsby, P.M., Veierød, M.B., Robsahm, T.E. (2020). Prediagnostic serum 25-hydroxyvitamin D and melanoma risk. Sci Rep. 2020 Nov 18;10(1):20129. doi: 10.1038/s41598-020-77155-2. PMID: 33208828; PMCID: PMC7676247.

84. Stenehjem JS, Støer NC, Ghiasvand R, Grimsrud TK, Babigumira R, Rees JR, Nilsen LT, Johnsen B, Thorsby PM, Veierød MB, Robsahm TE (2022). Prediagnostic serum 25-hydroxyvitamin D and leptin in relation to melanoma-specific death and overall death. Pigment Cell Melanoma Res. 2022 Mar;35(2):280-284. doi: 10.1111/pcmr.13026. Epub 2022 Jan 10. PMID: 34978150.

85. Steinbrecht, W., Claude, H., Köhler, U. & Hoinka, K. P. (1998). Correlations between tropopause height and total ozone: Implications for long-term changes, J. Geophys. Res., 103(D15), 19183–19192, doi:10.1029/98JD01929.

86. Svendby, T. M., Johnsen, B., Kylling, A., Dahlback, A., Bernhard, G., Hanse, G. H., Petkov, B., and Vitale, V. (2021). GUV long-term measurements of total ozone column and effective cloud transmittance at three Norwegian sites, Atmos. Chem. Phys., 21, 7881–7899, 2021 https://doi.org/10.5194/acp-21-7881-2021

87. Svendby, T. M., Fjæraa, A. M., Schultze, D., Bäcklund, A., and Johnsen, B. (2024). Monitoring of the atmospheric layer and natural ultraviolet radiation. Annual Report 2023. (NILU 20/2024). Kjeller.

88. Tan, K. C., Lim, H. S., & Jafri. M. Z. m. (2018). Study on solar ultraviolet erythemal dose distribution over Peninsular Malaysia using Ozone Monitoring Instrument. Egypt. J. Remote Sens. Space Sci. 21, pp. 105-110. https://doi.org/10.1016/j.ejrs.2017.01.001

89. Thompson, D. W., and Wallace, J. M. (1998). The Arctic oscillation signature in the wintertime geopotential height and temperature Fields. GRL, 25,9, pp. 1297-1300. https://agupubs.onlinelibrary.wiley.com/doi/epdf/10.1029/98GL00950

90. Turner J, Parisi AV. (2018). Ultraviolet Radiation Albedo and Reflectance in Review: The Influence to Ultraviolet Exposure in Occupational Settings. *International Journal of Environmental Research and Public Health*; 15(7):1507. https://doi.org/10.3390/ijerph15071507

91. Witthuhn, J., Deneke, H., Macke, A., Bernhard, G. (2017). Algorithms and uncertainties for the determination of multispectral irradiance components and aerosol optical depth from a shipborne rotating shadowband radiometer. Atmos. Meas. Tech., 10, 709–730, doi:10.5194/amt-10-709-2017.

92. WHO (2002). Global solar UV index. A practical guide. World Health Organization.

93. WMO (2008). Johnsen B et al. (2008). Intercomparison of global UV index from multiband filter radiometers: Harmonization of global UVI and spectral irradiance. GAW report no. 179 / WMO/TD-No. 1454. Geneve: World Meteorological Organization.

94. WMO (2011). Annual Bulletin on the Climate in WMO Region VI - Europe and Middle East. Accessed [02.05.2024]. https://www.dwd.de/EN/ourservices/ravibulletinjahr/archiv/bulletin_2011.pdf?__blob=publicationFile&v=4.

95. Xie, L., Macken, A., Johnsen, B., Norli, M., Skogan, O.A.S., Tollefsen, K.E. (2022). The MicroClimate Screen – A microscale climate exposure system for assessing the effect of CO2, temperature and UV on marine microalgae. Marine Environmental Research 179. https://doi.org/10.1016/j.marenvres.2022.105670

96. Zerefos, C. S., Fountoulakis, I., Eleftheratos, K., & Kazantzidis, A. (2023). Long-term variability of human health-related solar ultraviolet-b radiation doses from the 1980s to the end of the 21st century. Physiological Reviews, 103(3), 1789-1826. https://doi.org/10.1152/physrev.00031.2022

10.3 Data resources

- Data from the Norwegian UV-monitoring network: https://github.com/uvnrpa
- Total ozone data is provided by the NASA Goddard Space Flight Center.
- TOMS, Total ozone, daily, gridded data: https://ozonewatch.gsfc.nasa.gov/data/eptoms/
- OMI, Total ozone, daily, gridded data: https://ozonewatch.gsfc.nasa.gov/data/omi/
- OMI, Total ozone, overpass data:

  https://gs614-avdc1-pz.gsfc.nasa.gov/pub/data/satellite/Aura/OMI/V03/L2OVP/OMUVB/
- Ground-based total ozone for the period satellite-based observations are missing (1995-96) is accessed through the World Ozone and Ultraviolet Radiation Data Centre: https://woudc.org/data/stations/, applying measurements from stations Oslo (60N), Vindeln (Sweden 64N) and Sodankylä (Finland 67N)
- Temperature, precipitation, total solar radiation, and cloud cover data for the UV-station locations are provided by the Norwegian Meteorological Institute (MET.no) https://seklima.met.no/ and by the Norwegian Institute of Bioeconomy Research (NIBIO) https://lmt.nibio.no/
- Time series of hourly mean CIE-weighted UV data for estimating cloud modification factors are provided by the Swedish Meteorological and Hydrological Institute (SMHI) through the STRÅNG mesoscale model for solar radiation, https://strang.smhi.se/
- Time series of total solar radiation for estimating cloud modification factors for the Baseline Surface Radiation Network (BSRN) Station Ny-Ålesund station are provided by the Alfred Wegener Institute - Research Unit Potsdam, PANGAEA, https://doi.org/10.1594/PANGAEA.150000 and https://doi.org/10.1594/PANGAEA.914927
- Time series of total solar radiation for estimating cloud modification factors in Bergen is provided by the Geophysical Institute at the University of Bergen, through the web-based API https://veret.gfi.uib.no/taarn/
- Time series of clear-sky modelled solar radiation for stations in Norway were provided by Jan Asle Olseth† at the University of Bergen
- Time series of total solar radiation for estimating cloud modification based on the Finse Eco-Hydrological Observatory is provided by Norbert Pirk (norbert.pirk@geo.uio.no)

- Time-series of the Quasi-biennial Oscillation is provided by the Physical Sciences Laboratory – NOAA. Data downloaded from https://psl.noaa.gov/data/correlation/qbo.data
- Time-series of the North-Atlantic Index (NAO) is provided by the Climate Prediction Center – NOAA. Data downloaded from https://psl.noaa.gov/data/correlation/nao.data
- Time-series of the Arctic Oscillation Index (AO) is provided by the Climate Prediction Center – NOAA. Data downloaded from https://www.cpc.ncep.noaa.gov/products/precip/CWlink/daily_ao_index/monthly.ao.index.b50.current.ascii.table
- The 10.7cm Solar Flux Data is provided as a service by the National Research Council of Canada. Data is downloaded from https://psl.noaa.gov/data/correlation/solar.data
- The Niño 3.4 SST Index is provided by the Physical Sciences Laboratory – NOAA. Data is downloaded from https://psl.noaa.gov/gcos_wgsp/Timeseries/Nino34/
- Monthly sea ice extent and area data files is provided by The National Snow and Ice Data Center - NOAA. Data is downloaded from https://nsidc.org/data/seaice_index/data-and-image-archive

11 Annex

11.1 Quality and traceability of data products

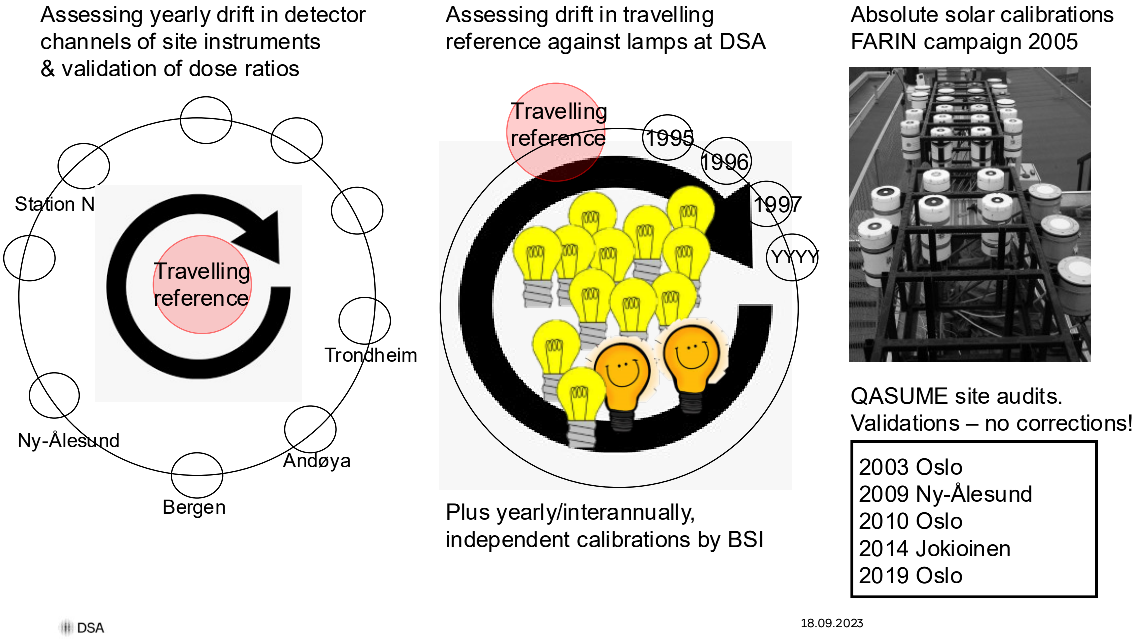

Figure 36 Calibration chain of the Norwegian UV-monitoring network. Left: Yearly site visits with the travelling reference instrument operating side-by-side the local instruments to assess long term drift in responsivity of station instruments. Center: Assessing long term drift in the travelling reference instrument, applying calibrated quartz tungsten lamps – performed 4-5 times a year. Interannual calibrations by the manufacturer Biospherical Instruments, inc. (San Diego) for an independent evaluation of long-term drift of the travelling reference Right: Absolute solar calibrations performed in the FARIN international intercomparison campaign in 2005. Solar intercomparisons against the QASUME World reference spectroradiometer, WRC/PMOD.

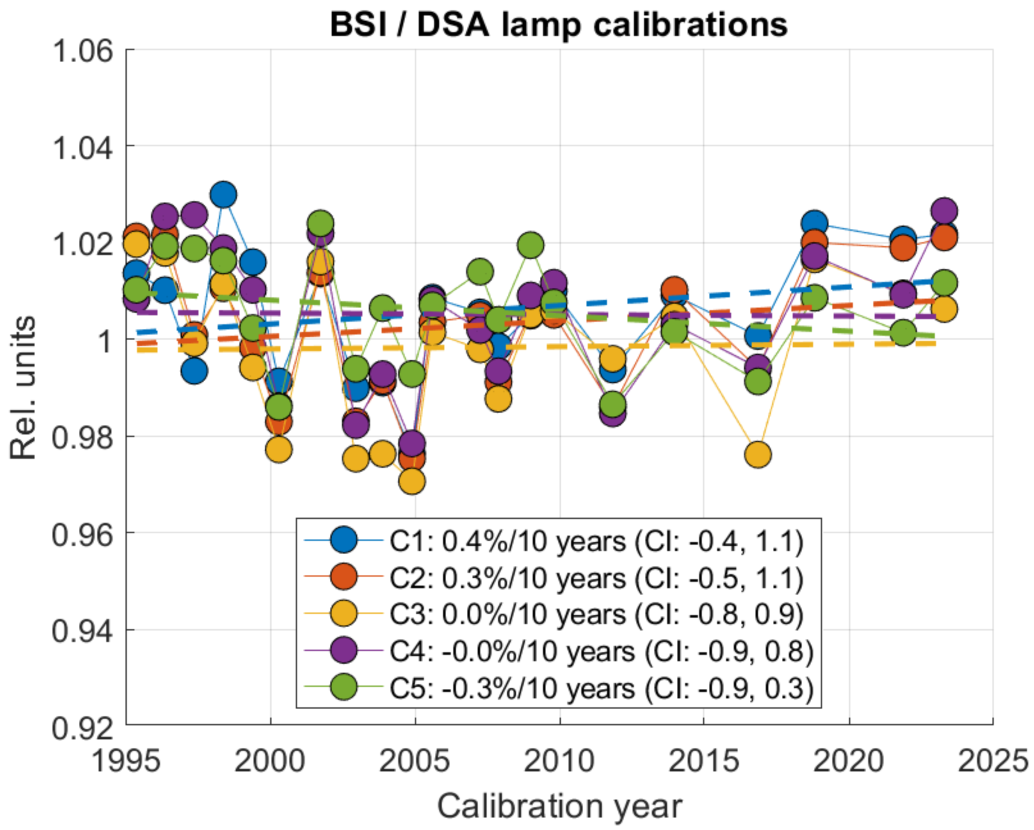

Figure 37 Ratio in scale factors [V/W/m^2/nm]) for individual detector channels (C1-C5) of the travelling reference GUV, as obtained from the manufacturer BSI's own calibration certificates after interannual lamp measurements in San Diego, relative to scale factors determined from lamp measurements at DSA before and after shipments to BSI. The linear fits indicate consistent and stable irradiance scales over the years the travelling reference instruments has been operating in the Norwegian UV-monitoring network.

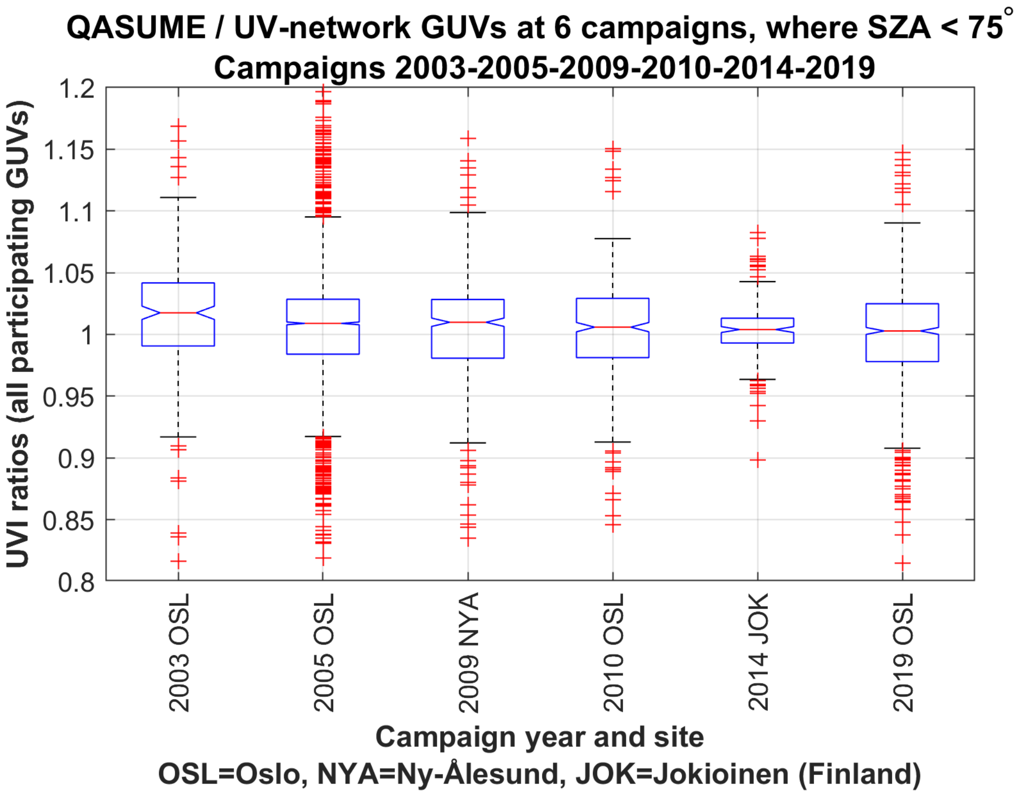

Figure 38 boxplots (median and interquartiles) of ratios in UVI of QASUME reference data relative to UVI of groups of GUV-instruments participating in six intercomparison campaigns.

11.2 Continuity in measurements and gap filling

UV-measurements are recorded as one-minute averages. Figure 26 presents an overview of measurement up-times at the respective stations. Up-time is defined here as the percentage of samples successfully acquired from sunrise to sunset over a full year, relative to an ideal instrument operating without interruptions. In the period 2000-2023 there have been only small gaps in measurements. An exception is year 2005, where all instruments were participating in the 6 weeklong FARIN-campaign at Østerås (OST, 60N). Gaps in 1995 and 1996 were due to initial preparations and quality control before the instruments were installed at their respective locations. Notes about Østerås (OST, 60N), Bergen (BRG, 60N) and Finse (FIN, 60N): Østerås (OST, 60N) had large gaps in measurements up to 1999, as this station initially was established for calibration purposes only and therefore did not have a permanently installed GUV instrument. From 1999, a new GUV instrument was purchased and installed at Østerås (OST, 60N), providing continuous measurements. In 1998, an incidence with water intrusion inside the GUV-instrument operating in Bergen (BRG, 60N) resulted in loss of measurements while the instrument was serviced by the manufacturer in San Diego. Up to 2002, measurements at Finse (FIN, 60N) were performed with a Solar Light model 501, broadband meter, which frequently suffered data communication problems and loss of data when the storage capacity was exceeded. From 2002, a new GUV instrument was permanently installed at Finse (FIN, 60N). Finally, two of the instruments have been transferred to new locations: From Tromsø (TSO, 69N) to Andøya (AND, 69N) in 2000, and from Blindern (BLI, 60N) to Kjeller (KJE, 60N) in 2019. This was necessary to ensure still continuous measurements and regular attendance by local personnel.

Missing measurements have been complemented with a gap filling method, providing complete period means of hourly, daily, monthly, and yearly doses. Each data file on https://github.com/uvnrpa contains rows of period means of quality-controlled dose rates and integrated doses, with a column flagging the uptime of measurements in each interval. The gap-filling is based on the libRadtran radiative transfer model (Embde et al., 2016), providing clear-sky irradiances for the location, solar elevation angle and total ozone amount. A seasonal correction is applied, matching modelled irradiances with measured real-sky irradiances, to account for the typical seasonal variation in surface albedo and aerosol amount. Finally, the modelled clear-sky irradiances are multiplied with cloud modification factors (CMF). These CMFs are primarily based on local pyranometer instruments measuring total solar radiation but also based on synoptic observations of total cloud coverage in okta values. At one station (FIN, 60N), CMF has also been retrieved from the SL-501 broadband UV-instrument.

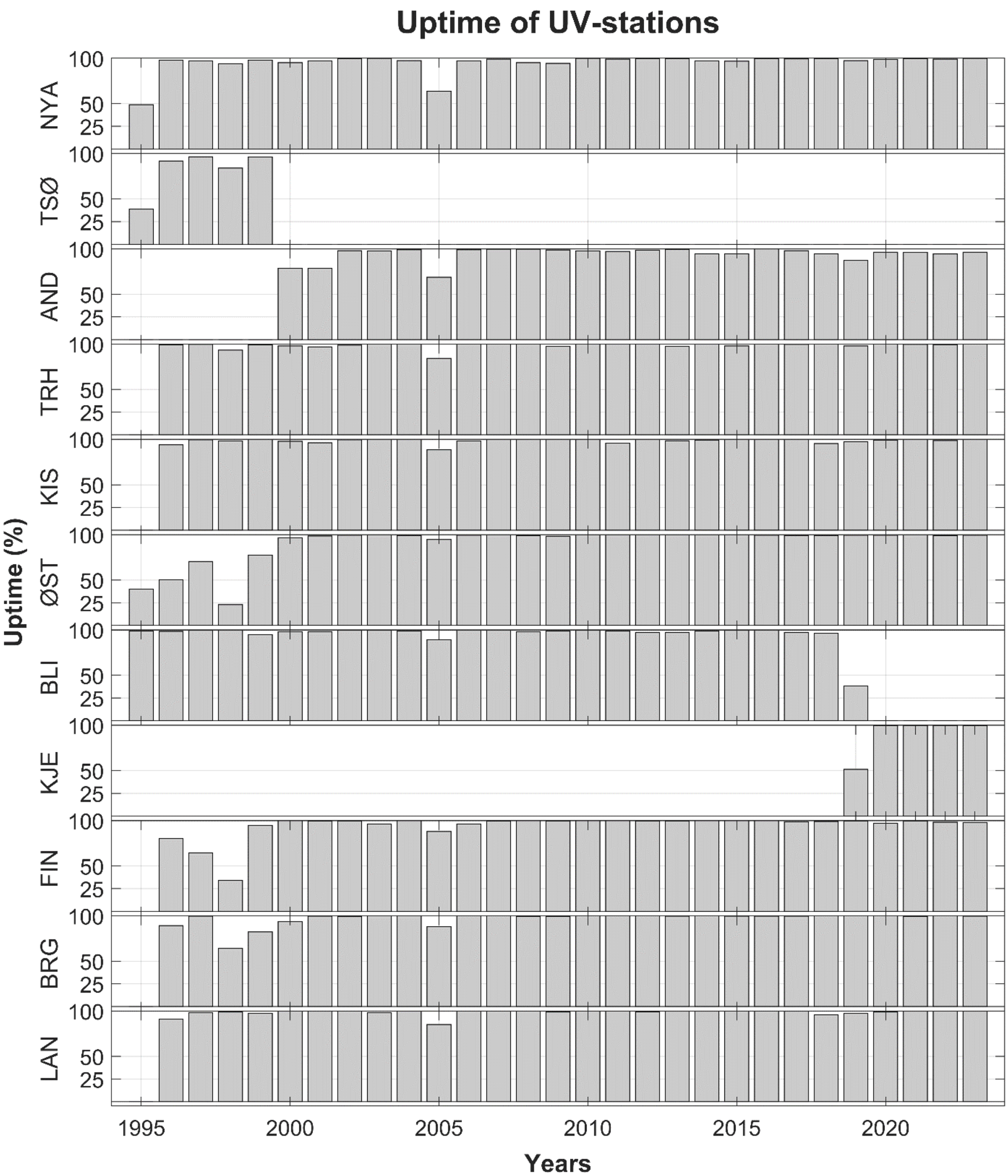

Figure 39 Uptime (continuity in measurements) per year for each station. Discontinuities in 1999/2000 and 2019 are due to transfer of instruments to new locations: From Tromsø (TSO, 69N) to Andøya (AND, 69N) and Blindern (BLI, 60N) to Kjeller (KJE, 60N), respectively. Reduced uptimes in 2005 were a result of the FARIN intercomparison campaign, during which instruments were temporarily relocated from their home sites to the DSA, the host of the campaign.

11.3 North Atlantic Index and long-term variations

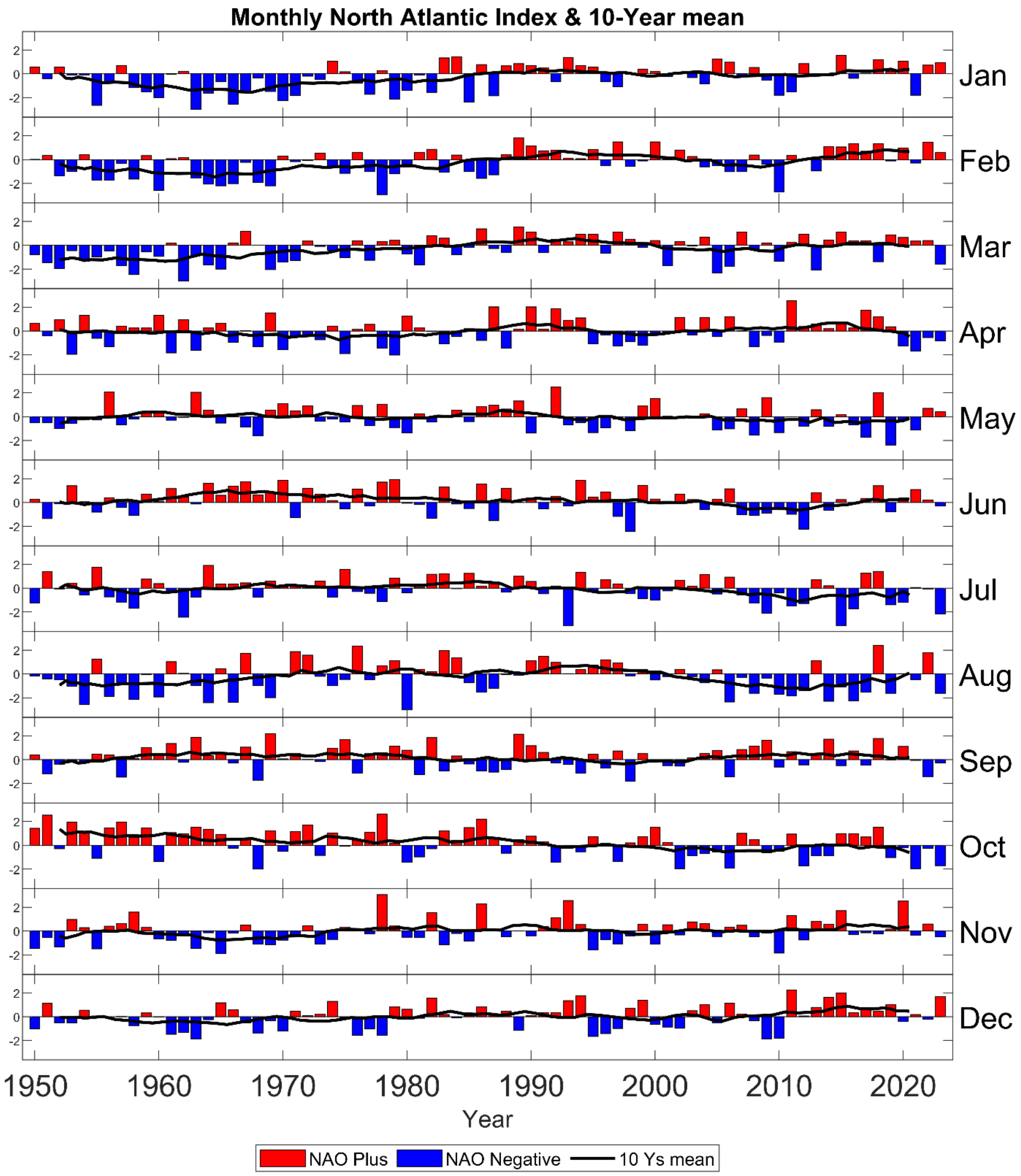

Figure 40 Monthly mean North Atlantic Index and 10-year means. Data sourced from https://psl.noaa.gov/data/correlation/nao.data

11.4 Monthly correlations between NAO, temperature and precipitation

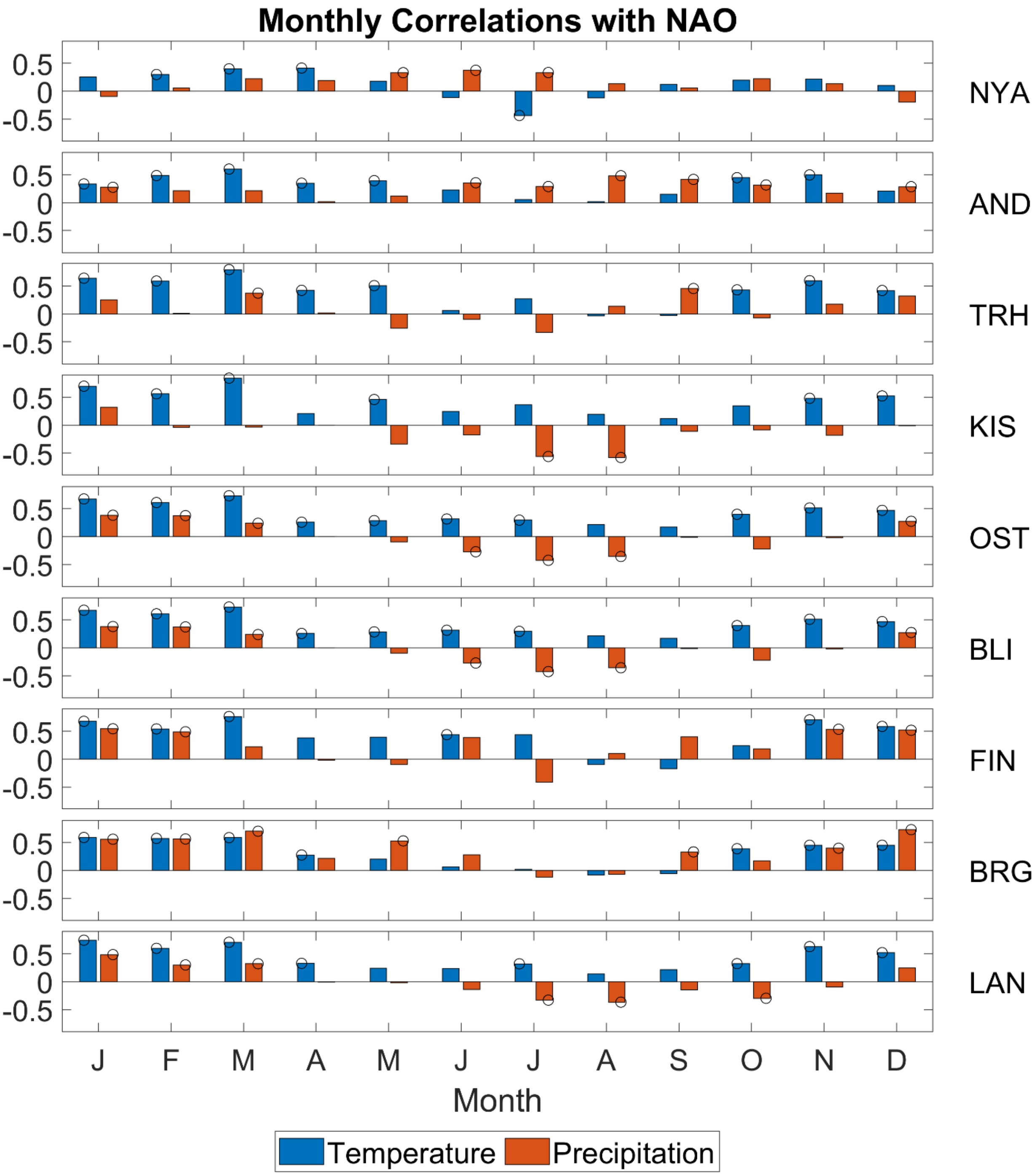

Figure 41 Correlations between NAO and temperature and precipitation. Circles mark linear correlations that are statistically significant at the 95% confidence level. Data from section 8.

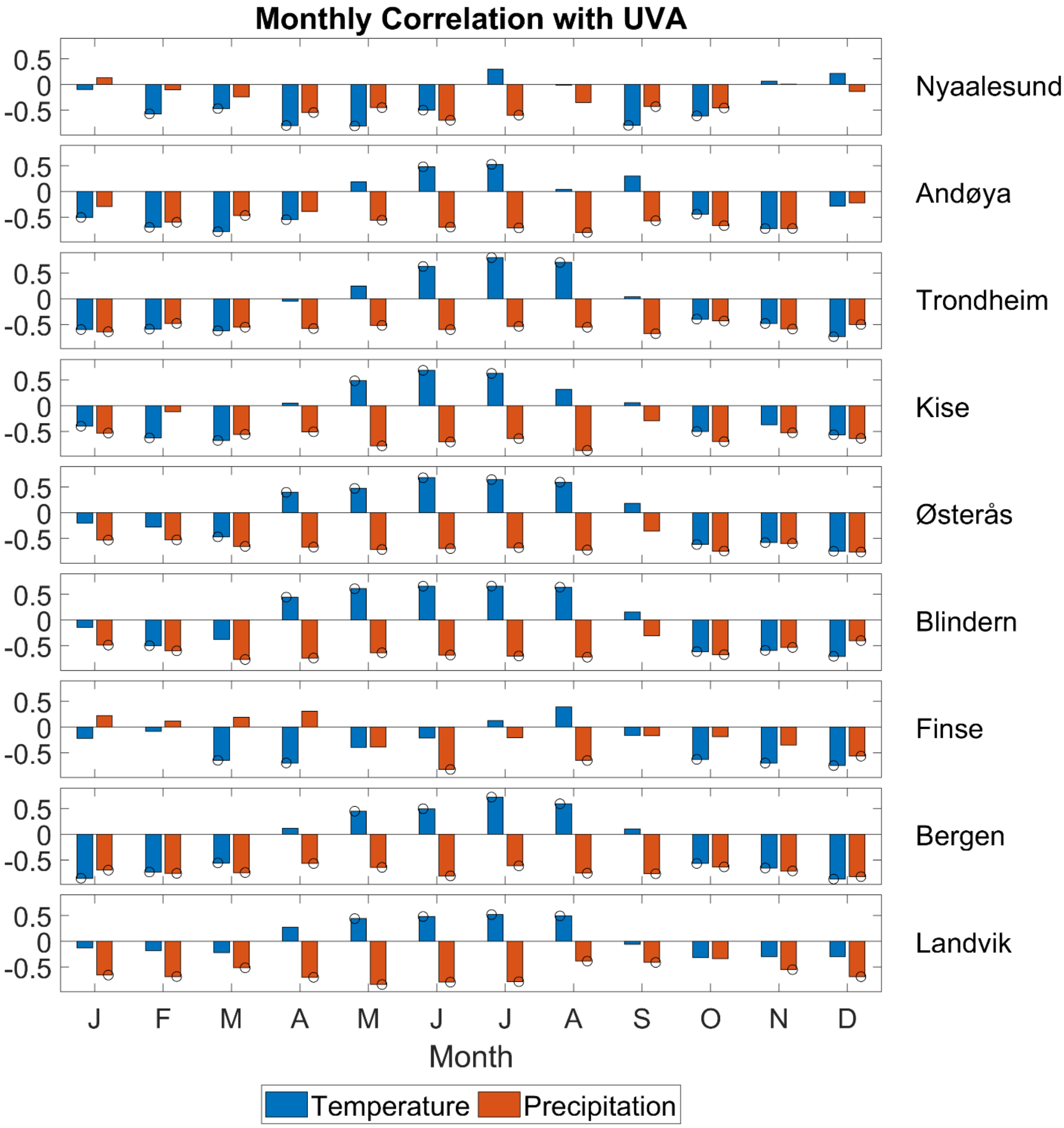

Figure 42 Correlations between monthly mean UV-A doses and temperature and precipitation. Circles mark linear correlations that are statistically significant at the 95% confidence level.

11.5 Drivers and trends in yearly doses with Robust regression fit

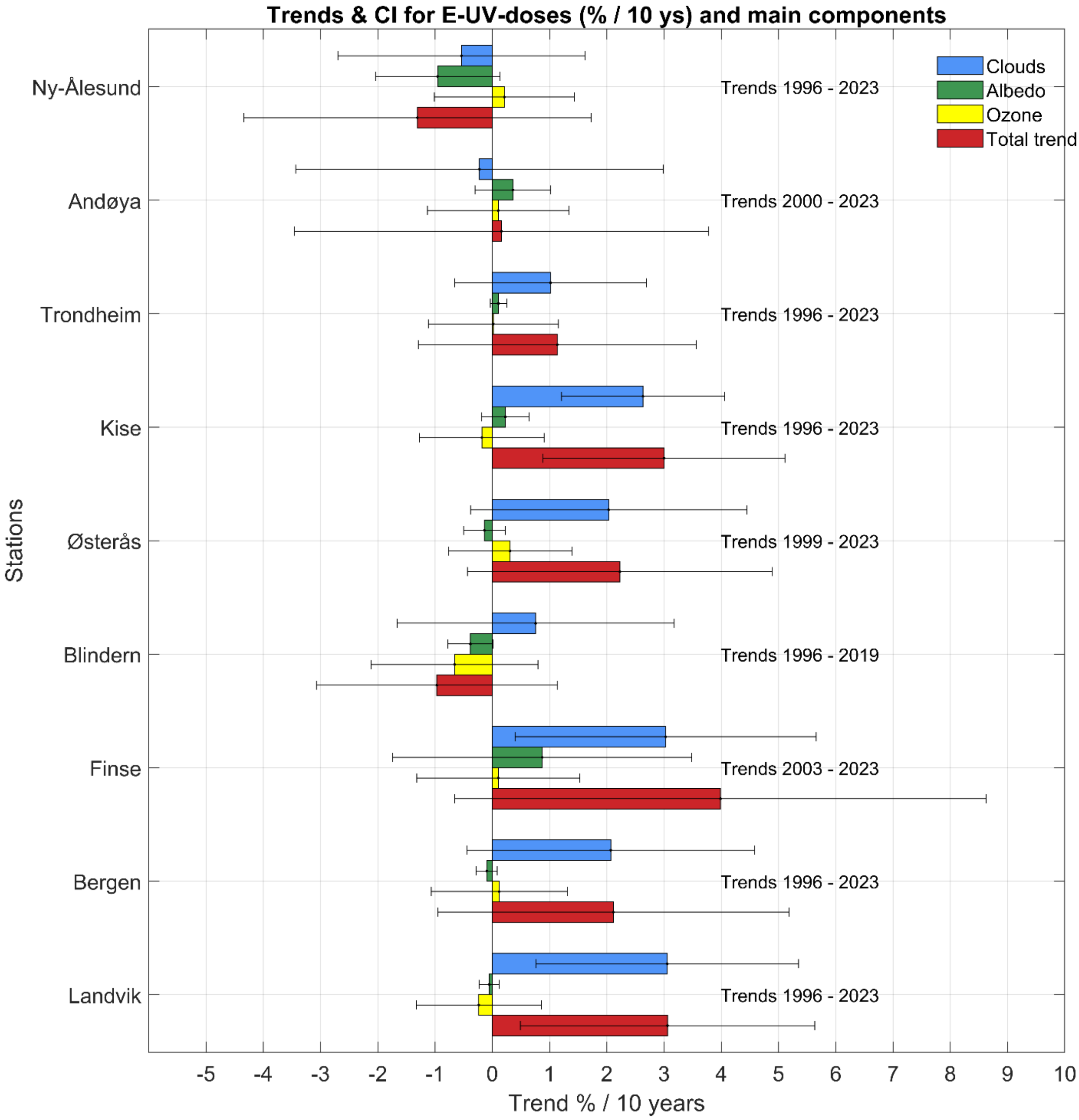

Figure 43 Same as Figure 9 (Trends in E-UV and components), but linear trends and confidence intervals are based on Robust Fit to highlight different sensitivity to outliers in the data set.

11.6 UV Index and hourly integrated erythemal dose

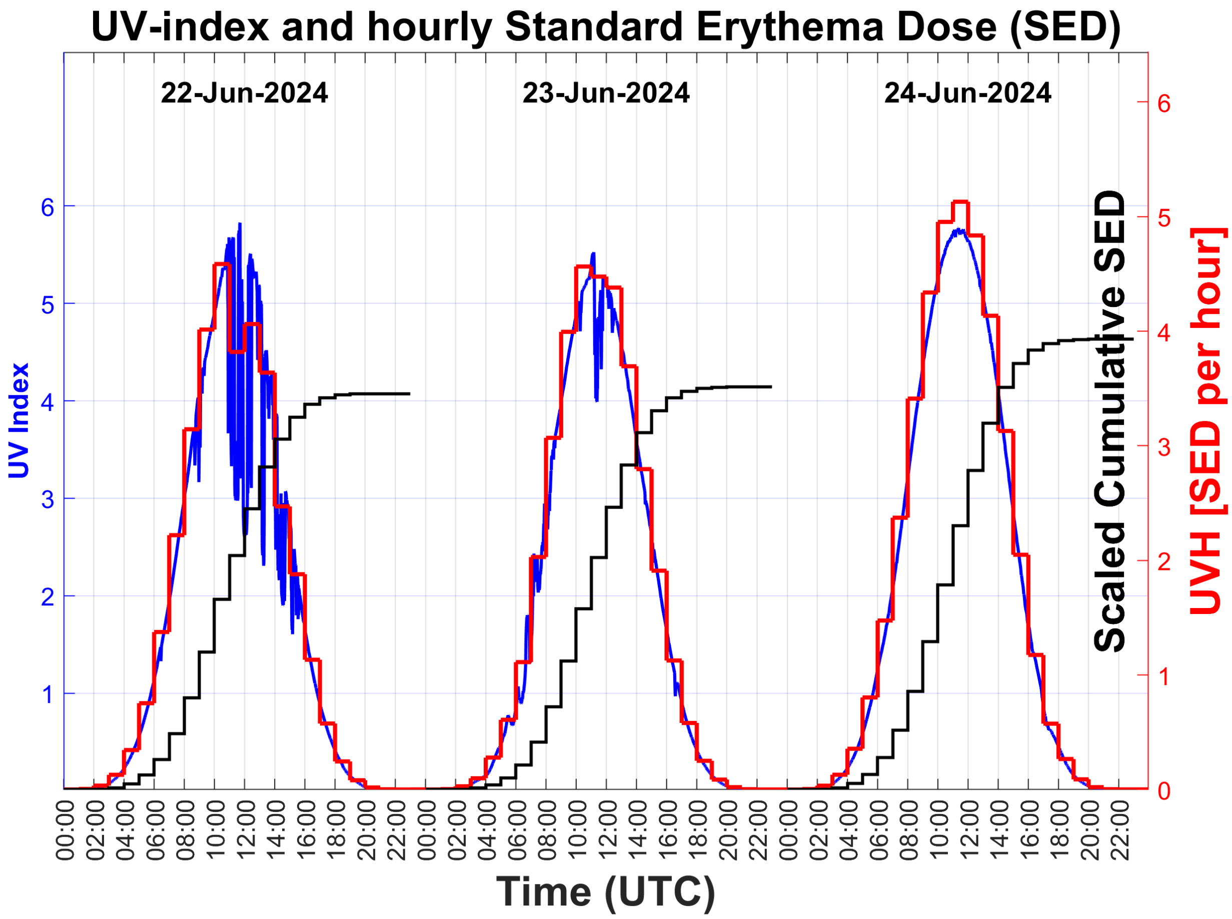

Figure 44 UV Index, UVH (UV index hour) in hourly standard erythema dose (SED) and scaled cumulative doses for three summer days at Østerås (OST 60N). The cumulated doses per day corresponds to about 39 SED, or 3900 J/m2.

11.7 Solar calibration platform at DSA

Figure 45 The solar calibration facilities at the roof of the DSA-building. The instrumentation includes the NRP-spectroradiometer and travelling reference GUV instrument participating in QASUME intercomparisons.

ISSN 0804-4910

dsa@dsa.no
+47 67 16 25 00
dsa.no

1 DSA-rapport 01-2025
Overvaking av radioaktivitet i luft 2024

2 DSA Report 02-2025
Ukrainian Regulatory Threat Assessment 2024

3 DSA Report 03-2025
Three Decades of UV-monitoring in Norway: Trends and Drivers

DSA

Norwegian Radiation and
Nuclear Safety Authority